Genetic Selection of Cardiomyocytes and Pacemaker Cells Derived From Human Embryonic Stem Cells

Jay Alexander Gantz

A dissertation
submitted in partial fulfillment of the
requirements for the degree of

Doctor of Philosophy

University of Washington

2013

Reading Committee:

Michael A. Laflamme, Chair

Michael Regnier

Luis F. Santana

Program Authorized to Offer Degree:

Department of Bioengineering

University of Washington

Abstract

Genetic Selection of Cardiomyocytes and Pacemaker Cells Derived From Human Embryonic Stem Cells

Jay Alexander Gantz

Chair of the Supervisory Committee:
Associate Professor Michael A. Laflamme
Departments of Pathology and Bioengineering

Cardiomyocytes derived from human pluripotent stem cells are poised to transform heart disease treatment. However, current methods to produce stem cell-derived cardiomyocytes result in a mixture of cardiac phenotypes that is neither well controlled nor completely understood. Before safe and effective cardiac cell therapies can transition from the lab to the clinic, the consequences of phenotype heterogeneity need to be further studied.

Improved genetic tools to label, track, and isolate specific cell types from heterogeneous differentiating populations are needed to understand the timing and identity of the signals that control stem cell differentiation. Traditional genetic manipulation methods do not translate well to human pluripotent cells. While viral methods have been useful, they are limited by random copy number and insertion site(s), insertional mutagenesis, transgene or endogenous gene silencing, and limited transgene capacity. To overcome these drawbacks, we used zinc finger nuclease gene targeting technology to create a novel line of “stoplight” human embryonic stem cells. “Stoplight” cells can be used to permanently mark and purify a subpopulation of differentiating cells based on the activation of a user-specified genetic promoter. We isolated near-homogenous populations of fluorescently marked undifferentiated cells and used the

putative pan-striated muscle MCK/CK7 promoter to isolate a nearly homogeneous population of stem cell-derived cardiomyocytes using the “stoplight” cell line.

Next, we used the “stoplight” cells to isolate and characterize two subpopulations of stem cell-derived cardiomyocytes that activate either the chicken GATA6 or MLC2v promoter during differentiation. We measured the automaticity, beating rate, action potentials, net ion currents and immunophenotype of these two populations and demonstrate they are distinct from each other. Our data suggest the populations represent putative early stage AV nodal (cGATA6) or ventricular (MLC2v) cardiomyocytes. Characterization of the bulk automaticity and beating rates of purified cGATA6 and MLC2v cardiomyocyte aggregates revealed significant differences that highlight the influence of subtype purity on bulk electrical behavior. Aggregates of cGATA6 cells beat significantly faster and maintained automaticity better than aggregates of MLC2v or admixed cardiomyocytes. In the past, stem cell-derived cardiomyocyte subtypes could only be studied as single cells; our data suggest the “stoplight” cell line is an ideal platform to study stem cell-derived cardiomyocyte subtypes and highlight the importance of subtype purity in bulk automaticity.

As a whole, these studies highlight the importance of selecting subpopulations of differentiating cells. Genetically modified cells, such as the “stoplight” cell line, are a crucial stepping-stone to finding the signaling molecules and/or cell surface markers that will translate these subpopulations to clinical use. Safe cardiac cell therapies demand a detailed understanding of the automaticity of transplanted cells. Subtype purity has a dramatic effect on bulk automaticity and will be a critically important consideration in future therapeutics.

Table of Contents

List of Figures

List of Tables

List of Abbreviations

ACTN2	Alpha-actinin 2
APA	Action potential amplitude
APD50	Action potential duration at 50% repolarization
APD90	Action potential duration at 90% repolarization
AV	Atrioventricular
AVB	Atrioventricular bundle
AVCS	Atrioventricular conduction system
AVN	Atrioventricular node
BMP	Bone morphogenic protein
CAG	CMV early enhancer/chicken beta-actin promoter
cAMP	Cyclic adenosine monophosphate
CCS	Cardiac conduction system
cGATA6	Chicken GATA6
CK7	Muscle creatine kinase promoter variant CK7
Cre	Cre recombinase
EB	Embryoid body
EF1α	Elongation factor-1 alpha
ESC	Embryonic stem cell
GFP	Green fluorescent protein
H7	Human embryonic stem cell line H7
HCN	Hyperpolarization-activated cyclic nucleotide gated
hESC	Human embryonic stem cell
hESC-CM	Human embryonic stem cell-derived cardiomyocyte
hiPSC	Human induced pluripotent stem cell
hMSC	Human mesenchymal stem cell
HR	Homologous recombination
I_f	Funny current
I_{K1}	Cardiac inward-rectifying potassium current
I_{KACh}	Acetylcholine-activated inward-rectifying potassium current
iPSC	Induced pluripotent stem cell
LBB	Left bundle branch
MDP	Maximum diastolic potential
MEF	Mouse embryonic fibroblast
mESC	Mouse embryonic stem cell
MLC2v	Myosin light chain 2v
mTmG	Myristoylated tdTomato myristolated eGFP

NHEJ	Non-homologous end joining
PCR	Polymerase chain reaction
PM	Pacemaker
RBB	Right bundle branch
ROCK	Rho-associated protein kinase
RUES2	Human embryonic stem cell line RUES2
SA	Sinoatrial
SAN	Sinoatrial node
SIRPA	Signal-regulatory protein alpha
SR	Sarcoplasmic reticulum
VCAM1	Vascular cell adhesion molecule 1
WT	Wild type
ZFN	Zinc-finger nuclease

Acknowledgements

I met Michael Laflamme a little over five years ago when I was a first-year medical student. He gave a fascinating talk at a local bioengineering conference and struck me as someone who would be a good mentor. Over the last five years, that hunch has been justified. Mike has been an insightful teacher and an astute mentor who has encouraged me to step outside my comfort zone while respecting my goals as a graduate student. His calm approach to honest science is one I aspire to emulate. Beyond Mike's leadership, the Laflamme lab has been a supportive and fun place to work and learn. Ben Van Biber patiently taught me the subtleties of working with stem cells and has been a colleague, friend and fishing buddy. Kara White Moyes, Scott Lundy, Dominic Filice and Chelsea Pagan, my fellow graduate students in the lab, have been partners in crime as we shared the slow and sometimes painful crawl toward graduation. Wei Zhong Zhu taught me how to patch clamp and always brightened my day with his unwavering smile and laugh. Wei Zhong also collected the cGATA6 data that was a driving force for my project. Amanda Vega created the MLC2v-CRE lentiviral vector and recorded most of the patch clamp data in this dissertation. Yuji Shiba always had words of encouragement. Yiheng Xie helped me get started in molecular biology. Finally, Jon Kim, Willi Obenza, Cody Horst and Serena Snyder kept our lab running smoothly.

The collaboration between the Laflamme Lab and Chuck Murry's lab has also been invaluable to my research. Chuck has been a second mentor to me in addition to serving on my Supervisory Committee. On more than one occasion Chuck helped me see the bigger picture when I was too focused on the details. Nathan Palpant, a post-doc in the Murry Lab, deserves special acknowledgement. Nathan took me under his wing when I first joined the Laflamme Lab and we worked closely together on the mTmG-2a-Puro project. Nathan taught me the bulk of what I know about molecular cloning. Hans Reinecke, Veronica Muskheli, John Mignone, Kareen Kreutziger, James Chong, James Fugate, Mark Saiget, Sarah Fernandes, Sharon Paige,

Elina Minami and Isa Werny were always happy to answer questions. Martha Lee merits particular mention for her tireless and effective work helping me navigate the more confusing aspects of a large university.

The UW Medical Scientist Training Program has provided me with an outstanding training environment. MSTP directors Marshall Horwitz, Larry Loeb, Mary-Claire King, Alec Clowes, and Julie Overbaugh have been a terrific source of support and guidance in my training. MSTP administrators Marcie Buckner, Julia Lawrence, Maureen Holstad, Kathy Hobson and Sandra Maddux have answered countless questions and continue to keep me on track in the program. In the Bioengineering Department, Dorian Varga was always my advocate and made sure I was doing the right thing at the right time.

I would also like to acknowledge my PhD Supervisory Committee. Professors Michael Laflamme, Charles Murry, Michael Regnier, Fernando Santana, and Bertil Hille listened to my proposals, suggested sensible alternatives, and respected my objectives as a graduate student. Thank you for your guidance.

Finally, I would like to thank my family and friends for their love and support. My wife, Aura, is the love of my life, my better half, and often my left hand. My parents, Bruce and Mary, have always supported my most outlandish pursuits. My two sisters, Ellen and Jessica, and their families; and my aunts, uncles, cousins and extended family members all deserve commendation for their unfaltering love and support when I explain that I am still in school. Lastly, my amazing friends, Andrew, Anna, Joe, Arjun, Russell, Dave, Jake, Rachel, Gabe, Emily, Alison, Becky, Jennie, Dylan, Kate, Bret, Kate, Steve, Becca, Lauren and Barbara, have made these past six years in Seattle some of the best in my life.

Dedication

I dedicate this work to my late grandfather, Robert Gantz. My grandfather is one of the most amazing people I have ever known. His thirst for life and ability to know and love those around him, despite occasional fundamental differences, are qualities we should all aspire to emulate.

Chapter 1: Introduction

Heart disease has been the leading cause of death in the United States for more than 100 years since it overtook tuberculosis in 1910 (*1*). Today, heart disease is responsible for nearly 24% of all American deaths (*2*). While most people typically associate death due to heart disease with the dramatic heart attacks seen on television and in movies, acute myocardial infarction is only responsible for one in five deaths caused by heart disease (*2*). Most often, heart disease-related deaths are attributed to multiple interrelated underlying causes. However, arrhythmias (disorders of heart rhythm initiation and/or propagation) contribute to more heart disease deaths than any other single factor. Despite pharmacologic, surgical and implantable device treatment options, four out of five deaths due to heart disease list arrhythmias as an underlying cause (*3*).

Cardiac Conduction System Development and Pacemaker Identification

The cardiac conduction system (CCS) consists of the sinoatrial node (SAN), the atrioventricular node (AVN), and the AV conduction system (AVCS), which is comprised of the AV bundle (AVB), the left and right bundle branches (LBB, RBB), and the Purkinje system. While CCS cells share some characteristics (generally smaller cells with poorly developed sarcomeres and few mitochondria), each part of the system has a unique molecular signature and developmental origin.

Similar to almost the entire cardiac system, the CCS is derived from mesoderm (*4*). The heart starts to beat approximately three weeks after fertilization and is the earliest functional organ in human embryonic development. The early heart is simply a tube formed from the cardiac crescent that contracts in a peristaltic wave. Contrary to classical models, recent data suggests that the early heart tube does not contain specialized regions that expand into adult

structures, but rather that new heart tissue is added to the heart tube from the surrounding mesoderm and specialized through local signaling (*5*–*7*). The fate of this newly added tissue is therefore dependent on its final location, not predetermined. This is an important concept to consider when engineering cardiac cell therapies from stem cells; perhaps specific cell populations, such as pacemaker cells or ventricular cells, will be able to be derived using a defined set of molecular cues instead of being selected from an admixed population.

The Sinoatrial Node

The embryonic heart tube initiates automaticity from its venus pole and maintains this pattern of venus to arterial contraction from development until death. The SAN develops in cardiomyocytes added to the venus pole of the heart (*8*). The transcription factors that drive SAN development are mostly of the T-box family. Most cells in the heart tube are exposed to factors such as Tbx5 and Tbx20 that are important for working myocardium (chamber myocardium of the atria or ventricles) development. Tbx2 and Tbx3 are transcriptional repressors that inhibit the working chamber program and are found in all CCS cells including the SAN. SAN cells also express the Shox2 transcription factor, a repressor of the otherwise ubiquitous cardiac transcription factor Nkx2.5. Finally, a study by Mommersteeg et al. demonstrates all SAN cells are further characterized by Tbx18 expression (*9*). The transcriptional program for the SAN can therefore be characterized as $Tbx2^{+}/Tbx3^{+}/Tbx18^{+}/Shox2^{+}/Nkx2.5^{-}$.

Cardiac electrophysiological behavior is determined by the expression of particular ion channels and gap junctions. The SAN has few gap junctions of low conductance (primarily of the connexin 45 isoform) and prominent hyperpolarization-activated cyclic nucleotide-gated (HCN) channels, chiefly HCN4 and HCN2 (*10*). Other markers in the developing SAN include

high levels of CD57 (HNK-1) and low levels of both Scn5a (Nav1.5 channel) and Nppa (ANF) (*11*).

The Atrioventricular Node

The AVN is the only conductive link between the atria and the ventricles. Similar to the SAN, Tbx2 and Tbx3 expression in the AVN represses the working chamber program (*11*). However, unlike the SAN, the AVN expresses Nkx2.5. The AVN is further differentiated from the SAN by a lack of Tbx18 expression. The AVN transcriptional program is characterized as $Tbx2^{+}/Tbx3^{+}/Tbx18^{-}/Shox2^{-}/Nkx2.5^{+}$.

The purpose of the AVN is to delay the action potential between the atria and ventricles. It is not surprising then that the AVN is similar to the SAN in its relative paucity of low conductance gap junctions, primarily of the connexin 45 isoform (*10*). The AVN also lacks significant Scn5a expression. Finally, the AVN exhibits robust automaticity (although at a slightly slower basal rate than the SAN) and expresses HCN4/HCN2.

The Atrioventricular Conduction System

Once an action potential exits the AVN into the AVB it is rapidly conducted through the LBB/RBB to the Purkinje network. This rapid conduction requires a different architecture from the SAN and AVN including an abundance of high conductance gap junctions. While the transcriptional program that controls the development of the AVCS is not as well understood as the SAN or AVN, the AVCS is known to be derived from ventricular myocardium (*12–14*). Rentschler et al. demonstrated that recombinant neuregulin-1β peptide induces a cardiac conduction system-like phenotype in mouse embryonic cardiomyocytes. In human cells, our group reported that neuregulin-1β treatment increases the ratio of working-type:nodal-type cardiomyocytes, a finding that is consistent with the conduction system origins of the AVCS (*15*).

The AVB/LBB/RBB are characterized by abundant connexin 40 and Scn5a expression, even in the presence of Tbx3, while the Purkinje network expresses a mix of connexin 40 and 43 and does not express Tbx3 (*16*). Automaticity in the AVCS diminishes distal to the AVN but remains at low levels; adult Purkinje fibers typically beat 15-30 times per minute in isolation. HCN channel expression correspondingly decreases distally with HCN4 the predominant isoform in humans (*10*).

Approaches to Transgenic Labeling of the Atrioventricular Conduction System

Seven transgenic models that label the developing atrioventricular conduction system have been reported in the mouse. Davis and colleagues reported the cGATA6|LacZ mouse, which uses the core chicken GATA6 promoter and 1.5 kb upstream regulatory sequence to mark the developing AV node and AV bundle (*17*). The CCS|LacZ mouse was reported by Logan and colleagues to mark nearly the entire developing cardiac conduction system (*18*), although it is now thought that the conduction system-specificity of the CCS|LacZ model is a function of where the transgene was inserted, not the transgene itself (*19*). MinK (KCNE1) is an important subunit in a variety of important pacemaking/conduction ion channels, including KCNQ1, HERG and HCN1-4. The mink|LacZ mouse was reported by Kupershmidt et al. to mark the proximal conduction system including the sinus node region and atrioventricular junction (*20*). The HOP|LacZ mouse reported by Chen and Ismat targets the LacZ transgene to the locus of the atypical homeodomain-only transcription factor HOP (*21*, *22*). Transgene expression is seen in the entire cardiac conduction system distal to, and including, the AV node. The cardiac troponin-I|LacZ model reported by Di Lisi et al. marks the developing AV canal and later the AV node and lower rims of both atria (*23*). The Cx40|EGFP mouse reported by Miquerol et al. shows EGFP expression in the coronary arteries, the atria, the AV node and the entire His-Purkinje system (*24*). Finally, a recent report details the Tbx3|Venus mouse where

the entire conduction system proximal to the Purkinje network, including the SA node, is marked with yellow fluorescent venus protein (*25*).

Our group used the chicken GATA6 promoter (-1.5/0.0/GATA6) reported by the Burch group as a putative marker of nodal cardiomyocytes derived from hESCs (*15*). We transduced early hESC-CMs with a lentivirus where the cGATA6 promoter drove EGFP expression and patch clamped on GFP^+ and GFP^- cells. 95% (20/21) of GFP-expressing cells demonstrated action potentials that were nodal-like, with a slow max AP upstroke velocity, faster spontaneous beating rate, and a more depolarized maximum diastolic potential. Only 10% (2/20) GFP-negative cells had a nodal-like action potential phenotype. We suspect these GFP-negative cells were most likely non-transduced as our lentiviral transduction efficiency was ~50%. These encouraging results using the cGATA6 promoter as a marker of nodal-like cells was the basis for choosing the cGATA6 promoter to mark and select nodal-like cells using the mTmG-2a-Puro cells in Chapter 3.

Cardiac Arrhythmias Remain a Significant Cause of Morbidity and Mortality

Disturbances in heart rhythm have been known to be medically significant for at least the last 2500 years, when Chinese physicians first estimated a patient's prognosis by counting the frequency of skipped heartbeats (*26*). Since then, significant progress has been made in understanding the development and propagation of cardiac contraction; today the heartbeat is understood to be orchestrated by a) the finely tuned differential expression of ion channels in cardiac muscle (*27*), and b) mechanisms that control the intracellular flow of calcium in cardiac myocytes (*28*). Despite this understanding, cardiac arrhythmias contribute to more deaths in the United States than chronic lower respiratory disease, stroke, accidents, and Alzheimer's disease (the third through sixth leading causes of death) combined (*29*).

Cardiac arrhythmias can be broadly categorized into bradyarrhythmias (an abnormally slow heart rate) and tachyarrhythmias (an abnormally fast heart rate). While both bradyarrhythmias and tachyarrhythmias are significant sources or morbidity and mortality, bradyarrhythmias are a far more common indication for an implantable cardiac pacemaker and will be the focus of the remainder of this section. Bradyarrhythmias are most often caused by pathology of either the sinoatrial (SA) node or the atrioventricular (AV) node and associated AV conduction system.

Sinoatrial Node Dysfunction

The SA node is a heterogeneous region of specialized cardiomyocytes surrounding the SA nodal artery in the crista terminalis at the junction of the superior vena cava and right atrium. An archetypal SA node myocyte is less structurally organized than the surrounding atrial myocardium with fewer myofibrils, poorly developed sarcoplasmic reticulum and few if any visible intercalated discs. The distinction between SA node myocytes and atrial myocytes becomes blurred toward the border of the SA node where cells exhibit structural and functional characteristics of both populations. Few intercellular gap junctions and large amounts of interstitial tissue within the SA node result in poor intranodal electrical coupling. This limited electrical coupling also exists between the SA node and surrounding atrial myocytes allowing the relatively small number of core SA node myocytes to remain electrically insulated from the surrounding atria. Electrical isolation between the more hyperpolarized atrial myocytes and SA node cells is critical for proper pacemaking function.

SA node dysfunction can result from both extrinsic and intrinsic etiologies. The most common extrinsic causes of SA node dysfunction are drugs and influences on the autonomic nervous system such as vasovagal stimulation. Extrinsic causes of SA node dysfunction are often reversible and can frequently be medically managed. In contrast, intrinsic causes of SA

node dysfunction are often irreversible and include injury due to disease (coronary artery disease, inflammatory myocarditis, etc.), heritable or de novo genetic mutation, and chest/cardiac trauma.

SA node dysfunction is frequently a silent pathology with no obvious symptoms. Indeed, even long SA node pauses are not necessarily symptomatic due to automaticity exhibited in other regions of the heart, such as the atrioventricular node and proximal ventricular conduction system. When symptoms such as hypotension, syncope, fatigue, and weakness do occur, they are often nonspecific and must be tightly correlated with electrocardiographic findings to make a definitive diagnosis of SA node dysfunction. An important characteristic of SA node dysfunction is its lack of association with increased mortality. Treatments for SA node dysfunction are therefore aimed at alleviating symptoms and include treating any underlying extrinsic causes, a chronic positive chronotropic drug regimen such as theophylline, or placement of a permanent electronic pacemaker.

Atrioventricular Node Dysfunction

Pacemaking activity from the SA node stimulates atrial contraction and is conducted through the atrial myocardium to the transitional zone of the atrioventricular (AV) node at the posterior-inferior aspect of the right atrium. The AV node is a heterogeneous structure that serves to delay the pacemaking impulse in order to allow completion of atrial contraction prior to ventricular activation. As the pacemaking impulse travels through the AV node, it traverses the atrioventricular boundary and gradually intertwines with the bundle of His (also called the AV bundle), the start of the infranodal ventricular conduction pathway. Once in the bundle of His, the pacemaking impulse is rapidly conducted to the right and left bundle branches, which ramify extensively to become the Purkinje fiber network that coordinates the pacemaking impulse throughout the ventricular myocardium.

The bradyarrhythmias associated with AV node dysfunction are most commonly a form of AV block where the pacemaking impulse partially or completely fails to reach the ventricles. Clinically important types of AV block include second degree type II and third degree, both of which are direct indications for an electronic pacemaker. For a full review of different types of AV block see (*30*). Similar to SA node dysfunction, AV block is frequently asymptomatic and has extrinsic and/or intrinsic etiologies. While partial AV block is often alleviated transiently by intravenous administration of a cholinergic antagonist (atropine) or β-adrenoreceptor agonist (isoproterenol), complete, or third degree, AV block is usually refractory to such treatments. In either symptomatic partial or complete AV block, the definitive treatment is placement of a permanent electronic pacemaker (*31*).

The Implantable Cardiac Pacemaker

Although medicine has crudely understood that the heartbeat and the flow of electricity are intimately related since at least the middle of the 1700s, it was not until the late 19th century that British physician John Alexander MacWilliam first comprehensively described an electrical model of cardiac pacing (*32*). In the early 20th century, physicians including Drs. Mark Lidwill and Albert Hyman developed rudimentary and only partially effective external electrical pacing devices, but the machines were bulky, utilized external electrodes that were painful to patients, and met with professional skepticism (see Figure 1.1A). The idea of an electrical pacemaking device was gradually accepted after 1952, when Dr. Paul Zoll maintained a patient's heartbeat with an external pacemaker for a sufficient amount of time that he was eventually able to return home (*33*). The pacemakers of the early 1950s, however, had serious drawbacks including size (often described as larger than a breadbox), and the requirement of AC wall power (see Figure 1.1B). Finally, in 1957, Earl Bakken invented a battery-powered, transistorized, wearable pacemaker (*34*). The transition from a small wearable pacemaker to a fully implantable device

occurred quickly and in 1958 a Swedish team led by Dr. Åke Senning implanted the first completely internal pacemaker (*35*) (for a similar device, see Figure 1.1C).

In the last 50 years, implantable cardiac pacemakers have enjoyed improved efficacy and safety. Atrial-synchronized devices in the 1960s provided more physiological pacing while rate-sensing devices in the early 1970s provided on-demand pacing only if the heartbeat was absent (*36*). By the 1980s pacemakers began to include more sophisticated microprocessors and more advanced battery chemistries. These advances facilitated the inclusion of movement and temperature sensors within the implanted device permitting rate-responsive pacing that could increase or decrease pacing to match the physiological needs of a patient's physical activity. More advanced battery chemistries, especially the transition to lithium-based batteries, extended the interval required between surgical battery changes. By the 1990s externally programmable devices routinely had multiple leads to pace both the atria and ventricles and could go a decade or more between battery changes (see Figure 1.1D).

Despite the sophistication of modern implantable electronic pacemakers, today's most complex devices continue to have significant drawbacks. Implantable electronic pacemakers require repeated battery replacement surgeries (approximately once per decade), are susceptible to exogenous electromagnetic interference (such as MRI), suffer from lead fracture, only nominally respond to intrinsic neurohormonal cues, can cause ventricular dyssynchrony, and cannot adapt to the changing size of a growing heart, making them particularly ill-suited for pediatric populations in which they are frequently used (*37*). Furthermore, almost 6% of pacemakers have to be removed due to foreign body infection (*38*). In light of these shortcomings, cell-based or so-called "biological pacemakers" are seen as a potential alternative to overcome these obstacles. Although there have been many approaches toward a biological pacemaker (see section: Potential Cell Sources for a Biological Pacemake*r*), an acceptable biological alternative

to electronic pacemakers remains to be developed and will have a significant impact on the treatment of heart rhythm disorders.

Potential Cell Sources for a Biological Pacemaker

A biological pacemaker does not have leads, does not require battery power, should respond to neurohormonal cues, should adapt to a growing heart, and should only require one placement procedure. It has the potential to be a transformative treatment alternative to electronic pacemakers (see section: The Implantable Cardiac Pacemaker). In light of these advantages, significant effort has been devoted toward engineering a biological pacemaker. Initial studies used transient gene therapy to increase the adrenergic sensitivity of existing pacemaker cells (*39*, *40*). Subsequent approaches modified non-pacemaker cardiac tissue through viral gene delivery (*41–48*), created so-called non-cardiac 'trigger cells' that form a two cell syncytium with otherwise quiescent cardiomyocytes to induce automaticity (*49–51*), or delivered spontaneously beating early differentiated human embryonic stem cell-derived cardiomyocytes (hESC-CMs) (*52*, *53*).

β_2-Adrenergic Receptor Overexpression

The earliest efforts to bioengineer better cardiac pacemaking attempted to increase the sympathetic sensitivity of existing pacemaking cells. A balance of sympathetic and parasympathetic stimulation of the SA and AV nodes normally maintains chronotropic control of the heart. Sympathetic adrenergic stimulation acts through β_1 and β_2 receptors, which, through a canonical G-protein coupled receptor pathway, activate adenylyl cyclase and increase the intracellular concentration of cAMP. Increased concentrations of cAMP act to both raise the sensitivity and kinetics of the hyperpolarized cyclic nucleotide-gated (HCN) family of ion channels, and increase the release of calcium from the sarcoplasmic reticulum (SR) via the

ryanodine receptor, the two central mechanisms that are thought to determine pacemaking rate. HCN channels change the heart rate by modulating the flux of the diastolic depolarization current (I_f), periodic calcium release from the SR depolarizes the cell by increasing the activity of the electrogenic sodium/calcium exchange pump (NCX); β-adrenergic signaling therefore increases heart rate by effecting greater depolarizing HCN and NCX currents.

Edelberg and colleagues reasoned that because the greatest density of β-adrenergic receptors was found in the sinus node and the connection between β-adrenergic signaling and I_f was understood, increasing the density of β-adrenergic receptors in the vicinity of the SA node might lead to a sustained increase in heart rate (*39*). This hypothesis was supported when plasmids expressing the β_2-adrenergic receptor were transiently transfected into murine right atria and an approximately 40% increase in endogenous heart rate was observed compared to control. The same group was able to show similar results in a porcine model three years later (*40*). However, in both studies, the authors acknowledged the limitations of transient transfection and explained that improved viral gene delivery strategies were needed to deliver a more permanent modulation of the cardiac pacemaker. Furthermore, increasing the sympathetic sensitivity of the SA node is unlikely to affect distal conduction pathologies.

Modification of Non-pacemaker Cardiomyocytes by Gene Delivery to Modulate Ionic Currents

Multiple groups pursuing a biological pacemaker acknowledged the aforementioned attempts to overexpress β-adrenergic receptors but decided to target non-pacemaking tissue for viral-mediated gene therapy in order to create pacemaking activity in otherwise quiescent myocardium. They recognized that a) many arrhythmias might fail to adequately respond to supplemental stimulation of the SA node, and b) the ability to activate pacemaking activity at different locations would allow targeted therapies for pathologies at multiple positions in the pacemaking/conduction system.

Miake and colleagues' first approach was rooted in cardiac development (see section: Cardiac Conduction System Development and Pacemaker Identification) (*41*). In early embryonic cardiac tissue, all cells possess intrinsic pacemaker activity. As development progresses and cardiomyocytes become specialized subtypes, each subtype develops a characteristic electrical signature. In the case of ventricular muscle, the myocardium becomes quiescent, largely because of the significant inward-rectifying potassium current, I_{K1}, which maintains diastolic hyperpolarization. Building on previous pharmacologic studies, they hypothesized that repression of the I_{K1} current would activate latent pacemaking activity. Indeed, when they expressed a dominant-negative form of the I_{K1} channel using an adenovirus injected into guinea-pig ventricular muscle, they observed spontaneous pacemaker-like beating activity that was not seen in controls.

The Rosen group took a different approach to creating pacemaking cells from quiescent myocardium. Instead of inhibiting the I_{K1} current, they chose to virally overexpress the HCN2 channel, a channel known to participate in endogenous pacemaking activity (*42*). They aimed to recruit additional pacemaking currents to cells that might otherwise display few. Furthermore, the study critiqued the report by Miake et al., noting that I_{K1} expression was known to be low in existing pacemaking tissue, the location that made the most sense for a targeted therapeutic. They tested their hypothesis by injecting HCN2-expressing adenovirus into the left atrium of a canine model. Spontaneous atrial rhythms were observed under vagal stimulation in all animals that received HCN2 virus, while control animals exhibited no spontaneous activity.

The Rosen group next moved to a more clinically relevant model to test HCN2 overexpression. They chose to overexpress HCN2 in the left bundle branch (LBB) of the ventricular conducting system and hypothesized they would see pacemaker-like escape rhythms upon vagal-induced heart block (*43*). Six of seven animals that received HCN2 adenovirus in the LBB exhibited left-sided escape rhythms at appropriate pacemaking rates

(>60 beats per minute) while four of six control animals demonstrated much slower escape rates of right-sided origin. This was the first demonstration of a biological pacemaker in the cardiac conduction system that could successfully pace the ventricular muscle.

Initial human trials of the safety and long-term efficacy of a biological pacemaker are expected to include tandem electronic and biological pacemaking. With this expectation the Rosen group transitioned to a model where experimental conditions included both adenoviral delivery of pacemaking channels to the LBB and a backup electronic pacemaker (*44*). With the additional rhythmic support of the electronic pacemaker they chose to induce complete AV block by radiofrequency ablation of the AV node rather than transient block induced by vagal stimulation. This is a more physiological model of AV block since vagal stimulation elicits a response along the entire SA/AV axis. Results were encouraging: shorter escape intervals and less electronic pacing was seen in dogs with HCN2 overexpression compared to electronically paced controls. Furthermore, upon intravenous administration of epinephrine, the HCN2 treated animals registered a significant increase in heart rate in a dose dependent manner when the control dogs with electronic pacemakers and LBB saline injections demonstrated no change.

Shortly after Bucchi and colleagues published their results, Ron Li's group experimented with combining overexpression of I_f channels and inhibition of I_{K1} (*54*). Lieu et al. demonstrated that viral overexpression of HCN channels in atrial muscle (where I_{K1} is weaker than in ventricular muscle) could in fact render an atrial cell non-physiologically depolarized while remaining quiescent. Upon administration of the I_f blocker ZD7288, these cells became spontaneous. Conversely, there were transduced quiescent cells that remained hyperpolarized. Administration of Ba^{2+}, an I_{K1} blocker, in these cells elicited automaticity. Furthermore, this automaticity ceased upon prolonged Ba^{2+} exposure and the cells exhibited a depolarized resting potential. These experimental results highlight the careful balance necessary to maintain automaticity between hyperpolarization-activated currents and inward-rectifying currents. This

balance uncovers the potential safety concern of I_f/I_{K1} mismatch that could easily occur in a setting where overexpression/inhibition is not tailored to the recipient cell's electrical baseline. Perhaps more importantly, this necessity for balance calls into question the likelihood that a viral gene therapy strategy, where expression heterogeneity is expected and extremely difficult to control, will become a realistic therapeutic option.

Despite these potential shortcomings, work on a translational biological pacemaker model using viral gene delivery has continued. In 2012 Cingolani et al. used off-the-shelf clinical equipment to deliver a combination of viral I_{K1} inhibition and HCN2 overexpression with a backup electronic pacemaker in a porcine model of AV block accomplished using targeted radiofrequency ablation (*46*). The experimental animals exhibited significantly less electronic pacemaker activation, a significantly higher mean heart rate, and appropriate anterograde ventricular activation through the His-Purkinje system that was not seen in control animals. As with all viral gene delivery studies, there was concern for unintended transduction outside the site of viral delivery. This study quantified the biodistribution of a GFP control adenovirus administered in an identical fashion. While recombinant adenovirus was found primarily in the heart, it was also detected at lower levels in the lungs, liver, spleen and kidney. These data are an important first step necessary to quantify the potential off-target biodistribution and toxicity in a viral injection model.

The Cingolani study also discusses the potential use of biological pacemakers as a temporary pacing measure in the event that an electronic pacemaker must be removed due to infection. There is a required period of antibiotic administration following pacemaker explantation during which patients should remain completely free of implanted hardware. Percutaneous temporary pacing devices used during this period are associated with the recurrence of infection upon reimplantation of a permanent device. While transcutaneous pacing is an option, it is often highly uncomfortable for patients. This is the ideal setting, then,

for the transient pacemaking activity reported with adenoviral administration of pacemaking genes.

While the I_{K1} inhibition and HCN2 overexpression data discussed above are encouraging, the model fails to achieve the ideal outcome of combining minimal dependence on electrical backup pacing with appropriate resting and sufficiently autonomically responsive beating rates. The pacing seen in the I_{K1} inhibition/HCN2 overexpression study was well below physiological levels. To overcome these drawbacks, Boink and colleagues coexpressed HCN2 with skeletal muscle sodium channel 1 (SkM1), a non-cardiac ion channel that has a more depolarized inactivation potential than the SCN5a cardiac sodium channel (*48*). The group reasoned that this would offer more availability of sodium channels during diastole and lead to a more negative threshold potential, essentially engineering the cells to be primed for increased beating rates. Combined HCN2/SkM1 animals displayed faster basal beating rates, lower escape time, less electronic pacing (0%), and higher maximal beat rates than either HCN2 or SkM1 alone, supporting the underlying hypothesis.

Reprogramming Non-pacemaker Cardiomyocytes Using Gene Delivery

The most recent attempt to create a biological pacemaker using gene delivery is a significant departure from the studies described above. Rather than expressing one or more genes that promote or inhibit ion channel activity, Kapoor et al. attempted to convert quiescent ventricular myocytes into pacemaker cells by transcription factor overexpression (*47*). Looking to the transcriptional regulators known to play a role in SA node development, the group used adenoviral vectors to overexpress Shox2, Tbx3, Tbx5, Tbx18 and Tbx20 in neonatal rat ventricular cardiomyocytes. Only Tbx18 transduced cultures demonstrated an increase in the percentage of spontaneously beating monolayer cultures compared to GFP control. When examined as single cells, Tbx18 transduced cells appeared to have transdifferentiated into SA

node-like cells with a more positive diastolic resting potential, a higher index of automaticity, higher spontaneous intracellular calcium oscillations, a 3.4 fold increase in HCN4 expression, higher intracellular concentrations of cAMP, and distinctive SA node-like morphology (smaller with more disorganized myofibrils) when compared to GFP transduced control cells.

Importantly, these findings translated to an in vivo model. Tbx18 adenovirus was injected into the cardiac apex of guinea pigs. Transient heart block was induced with intravenous methacholine three to five days later. All GFP control animals exhibited slow junctional rhythm with anterograde QRS polarity on ECG while five of seven animals injected with Tbx18 demonstrated retrograde QRS polarity and faster beating rates indicative of ectopic pacing from the apex. Furthermore, the Tbx18 injected hearts responded appropriately to autonomic perturbation with intravenous isoproterenol and acetylcholine. Perhaps most interesting is data suggesting persistence of the Tbx18 reprogramming after Tbx18 is no longer expressed. Hearts transduced with Tbx18 continued to exhibit the retrograde QRS polarity up to four weeks after transduction. Moreover, single cell qRT-PCR data from spontaneously beating pacemaker-like ventricular cells in Tbx18 transduced animals indicate small to negligible amounts of detectable Tbx18 at four weeks compared to the robust amounts seen three to four days after transduction. This is expected as adenoviral expression typically only lasts one to two weeks (*55*). These so-called induced SA node cells (“iSAN” cells) offer a promising departure from the previous channel expression/repression gene delivery studies. However, as with all adenoviral approaches, in vivo persistence remains an issue; transduced cells are thought to be cleared by the immune system. Kapoor et al. reported an approximately 70% reduction in iSAN-like cells between three days and six weeks post Tbx18 transduction.

Inducing Automaticity Using Modified Non-cardiac Cells

While most approaches to create a biological pacemaker have used adenoviral gene therapy to modify existing host myocardium (see section: Modification of Non-pacemaker Cardiomyocytes by Gene Delivery), three studies from the Rosen group have used genetically modified non-cardiac cells as exogenous current sources meant to induce pacemaking activity in quiescent cells (*49*–*51*). In the first study, Potapova et al. transiently expressed murine HCN2+GFP or GFP alone in human mesenchymal stem cells (hMSCs) (*49*). Patch clamp studies of HCN2 expressing hMSCs revealed appropriate I_f electrophysiological behavior, including β-adrenergic and muscarinic sensitivity. Automaticity was not observed because hMSCs are not excitable and lack the ion channels necessary to drive an action potential. Next, HCN2-expressing hMSCs were cocultured in vitro with rat ventricular myocytes. Although spontaneous beating was observed in both HCN2 and GFP control cocultures, the beating rate was significantly faster in the HCN2 group. Ultimately, HCN2 expressing hMSCs were injected into the anterior left ventricular wall of a canine model. Ventricular escape rhythms were measured under vagal stimulation-induced sinus arrest one week after injection. Five of six HCN2 treated animals displayed an escape rhythm that was both localized to the anterior left ventricle and significantly faster than the animals that were injected with hMSCs only expressing GFP (where the escape rhythms originated from both the left and right ventricles). Histology revealed connexin 43 staining at the interface of many ventricular myocyte/hMSC pairs, suggesting formation of functional gap junctions between the host and engrafted cells. Taken together, the data suggest engrafted non-excitable hMSCs that express a hyperpolarization activated inward current can electrically couple with ventricular myocardium and drive a pacemaking current.

This first study of the pacemaking potential of I_f-expressing non-cardiac cells only followed animals for one week after cell injection. Plotnikov et al. extended the model to six

weeks and included coincident placement of an electronic backup pacemaker after radiofrequency ablation of the AV node (*50*). To investigate the potential for graft rejection they injected human cells into a canine model and did not immunosuppress the animals. No evidence of cellular or humoral rejection was observed six weeks after the xenotransplantation. Although no asystole was seen when backup pacemakers were turned off, heart rates were as low as 30 beats per minute (bpm). Furthermore, upon sympathetic stimulation the maximal heart rates only went as high as 90 bpm, lower than an ideal maximal rate of ~125-150 bpm. Similar to the results of Qu et al. and Plotnikov et al. discussed above, these results suggest that HCN2 alone does not provide ideal pacemaking conditions. Finally, although not reported by the Rosen group until a review paper was published in 2010, it appears that while the engrafted hMSCs functioned well six weeks after injection, most cells had disappeared by 10 weeks, presumably because of migration or attrition (*56*).

Valiunas et al. continued the hMSC coupling work of Potapova et al. and Plotnikov et al. by taking a detailed look at the in vitro coupling behavior of two-cell combinations of one HCN2-expressing non-myocyte and one quiescent canine ventricular cardiomyocyte (*51*). They reported data from HCN2-expressing hMSCs and HEK293 cells (which both endogenously express connexin 43) as well as HeLa cells cotransfected with HCN2 and connexin 43. While the work of Potapova et al. and Plotnikov et al. demonstrated robust HCN2 activity in non-myocytes and the ability of these cells to form gap junctions and influence pacemaking activity of ventricular myocardium, the time course of coupling and the ability of a single myocyte/non-myocyte pair to elicit automaticity was unknown. Spontaneous pacemaking was observed in otherwise quiescent ventricular cardiomyocytes when paired with all three non-myocyte cell types (hMSCs, HEK293 cells and HeLa cells). This automaticity was reversibly blocked by administration and washout of either the gap junction blocker carbenoxolone or the HCN2 channel blocker tetrahydroacridine, suggesting the automaticity depended on both functional

HCN2 currents and cell-cell coupling via gap junctions. Time course data revealed functional coupling in the two-cell system was established within 24 to 36 hours of coculture.

While these three studies present convincing data for the use of non-myocytes as a means to deliver pacemaking currents to existing myocardium, there are still unanswered questions with regard to long-term stability, the choice of pacemaking currents to deliver, and the potential for an immune response against delivered cells.

Cell Therapy With Early Human Embryonic Stem Cell-derived Cardiomyocytes

Embryonic stem cells (ESCs) provide a promising cell source for regenerative therapies because they are infinitely self-renewing and can be differentiated into all tissue types (see section: Human Embryonic Stem Cells: Identification, Derivation and Modification). Cardiomyocyte-like cells derived from human embryonic stem cells (hESCs) were first described by Kehat et al. in 2001 (*57*) and have since been recognized as definitive cardiomyocytes (*58*–*60*).

Cardiomyocytes derived from hESCs (hESC-CMs) are an attractive cell population to consider when creating a biological pacemaker because they exhibit almost universal automaticity upon differentiation. Two studies have demonstrated effective ectopic pacemaking with transplantation of beating hESC-CMs. In the first study, Kehat and colleagues isolated spontaneously beating regions from embryoid body type hESC differentiations (*52*). These cells synchronously beat with neonatal rat ventricular myocytes in coculture and lost synchronicity in the presence of heptanol, a gap junction uncoupling agent. In vivo pacemaking potential was assayed in a porcine model of complete AV block (via AV node radiofrequency ablation) in the presence of a backup electronic pacemaker. Electrophysiological mapping detected an ectopic rhythm originating from the site of hESC-CM implantation in 11 of 13 animals a few days after injection. In contrast, animals with control injections of media or non-cardiomyocytes displayed

typical junctional escape rhythms and ECG morphology that did not originate at the site of injection.

In a similar study, Xue et al. implanted beating GFP-expressing hESC-CMs in the anterior epicardium of guinea pig hearts (*61*). Hearts were isolated and perfused two to three days after implantation and AV block was induced via ex vivo AV node cryoablation. A slow ventricular heart rate was observed after cryoablation only in hearts that had received hESC-CMs. Isopotential mapping of the perfused hearts indicated that the ventricular depolarization originated at the site of hESC-CM implantation.

While both of these cell therapy studies present strong evidence of hESC-CM-driven ectopic pacemaking activity, early differentiated cells, where all cardiomyocytes are expected to demonstrate automaticity, were used. Furthermore, admixed early hESC-CMs contain distinct subpopulations (nodal-like, ventricular-like etc.) that display unique electrophysiological signatures similar to the subpopulations seen in adult cells (*59*). No effort was made to distinguish nodal from non-nodal cells in these hESC-CM pacemaker studies. An important concern is if a more mature mixed hESC-CM population, where most non-nodal cells likely lack automaticity, can act as a stable, long-term biological pacemaker.

Summary of Previous Studies

In the preceding sections I have discussed the wide variety of previous approaches to engineering a biological pacemaker. While these methods have demonstrated pacemaking potential *in vitro* and *in vivo*, most continue to have significant drawbacks. Gene delivery to existing tissue is often difficult to precisely target, lacks persistent expression, and, particularly with retroviruses, presents potential health concerns (*62*). Endogenous pacemaking cells express a unique combination of ion channels that facilitate automaticity. While forced transgenic overexpression of some of these channels or dominant-negative competing channels

can induce pacemaking activity in non-nodal cells, these methods represent a crude approximation of the finely-tuned electrophysiological environment of endogenous nodal tissue; indeed, even within the sinoatrial node there is variable expression of ion channels and gap junctions that facilitate appropriate function and redundancy (*63*). Furthermore, even if cells are engineered to exhibit automaticity, responses to autonomic neurohormonal cues do not always fall within the physiologic range of similar responses in endogenous pacemaking tissue. Finally, in the hESC-CM studies, the observed automaticity is confounded by the early age of cells used. It remains uncertain if these cells will demonstrate stable, long-term pacemaking behavior.

One method that stands apart from others is the Tbx18-induced reprogramming of non-pacemaking myocardium into pacemaker-like cells. This approach appears to address many of the above concerns, producing cells that are very similar to existing nodal cells. While the adenoviral method of expressing Tbx18 suffers from the same drawbacks mentioned above, the idea that short-term expression of a single transcription factor might produce permanently altered cells is therapeutically appealing. One could imagine in vitro methods of transient Tbx18 expression in cardiomyocytes before subsequent transplantation. Regardless, reprogramming remains a new area of study, particularly in the cardiac arena, and long-term phenotypic stability remains to be reported.

Human Embryonic Stem Cells: Identification, Derivation and Modification

Stem cells are clonal cells that self-renew as well as differentiate into adult tissues. The term “stem cell” includes both multipotent populations of cells in the adult, such as bone marrow stem cells, and pluripotent embryonic stem cells (ESCs), which are the naturally occurring inner cell mass of a blastocyst in an early stage vertebrate embryo. ESCs are defined by two properties. First, ESCs are pluripotent; all three primary germ layers, ectoderm, mesoderm and endoderm, can be derived from ESCs. Second, ESCs are capable of infinite self-renewal. In

conditions that support maintenance of the undifferentiated state, ESCs are capable of propagating themselves indefinitely.

Two groups independently reported the first derivations and ex vivo maintenance of ESCs from the mouse in 1981 (*64*, *65*). It was not until 1998 that Thomson et al. first isolated and cultured human ESCs (hESCs) from fertilized human embryos destined to be destroyed after in vitro fertilization (*66*). Similar to ESCs derived in other species, hESCs exhibit a high nucleus to cytoplasm ratio, prominent nucleoli, and tightly packed colony morphology in vitro. Early derivations required coculture with mouse embryonic feeder cells to maintain the undifferentiated state (*67*). More recently, feeder-free culture conditions have maintained hESCs without differentiation (*68*).

ESCs have contributed enormously to the biological literature, especially in the areas of developmental biology, disease modeling, tissue engineering and drug discovery. However, working with hESCs presents several challenges. First, pluripotency can be difficult to quantify when deriving new lines or verifying the undifferentiated state of existing lines. Second, there are unavoidable ethical hurdles to ending the development of a fertilized human embryo. Third, genetic modification is a common tool in ESC biology. hESCs have proven difficult to genetically manipulate using methods that are successful in other ESC species, such as the mouse.

Identifying pluripotency

Pluripotency is defined as the ability to give rise to ectoderm, mesoderm and endoderm, the three embryonic germ layers. In the order of least stringent to most stringent, tests of functional pluripotency include: teratoma formation (in vivo tumor growth that demonstrates differentiated progeny of the three germ layers), chimera formation (developmental contribution when combined with other cells in a blastocyst), germline contribution (the ability to generate

functional germ cells), and tetraploid complementation (where cells are injected into a 4n stage blastocyst and the entire resulting embryo is derived from the donor cells). While state and federal laws banning human cloning are inconsistent, a 2005 United Nations Declaration on Human Cloning called for an international ban on all forms of human cloning (*69*). Of the previously mentioned pluripotency assays, only teratoma formation is compatible with the UN declaration, making it the most rigorous functional assay of pluripotency available for hESCs.

Molecular and phenotypic measurements offer an indirect method of assessing pluripotency. From qualitative colony morphology to immunocytochemistry, PCR and microarray measurement of genes that are correlated with pluripotency, indirect measurement of pluripotency has rarely been accepted as definitive proof of "stemness" (*70*). Recent efforts have tried to bolster molecular characterization as an accepted assay of pluripotency. One such example is PluriTest, a machine learning algorithm that analyzes microarray data and computes both a "pluripotency score" and a "novelty score" for a given sample based on an extensive database of existing stem cell lines (*71*). PluriTest is quicker, less expensive, does not involve the use of animals, and is more quantitative than the in vivo teratoma assay. However, PluriTest scores fall along a range that can yield results that are not always as easy to interpret as the bimodal result of a teratoma assay. It is important to mention, however, that data increasingly suggests a range of cellular states might be considered undifferentiated; individual lines of stem cells have distinct genetic and epigenetic characteristics (*72*). Accordingly, the continuum of scores offered by an assay like PluriTest, where undifferentiated cell lines can often be distinguished, might be a more accurate representation of the underlying biology.

Induced Pluripotent Stem Cells

Classical models of cellular differentiation describe the process as mostly irreversible. However, dedifferentiation, where a cell reverts to a less-differentiated stage of its own lineage, is being described more frequently as a mechanism for tissue repair, such as limb regeneration in amphibians (*73*). More recently, dedifferentiation was reported as the mechanism of cardiac repair in zebrafish, which can fully regenerate myocardium after amputation of up to 20% of the ventricle (*74*). In 2006, Takahashi and Yamanaka virally overexpressed genes in mouse fibroblasts that are normally highly expressed by pluripotent cells. This resulted in a dramatic phenotypic change where cells became similar to undifferentiated mouse ESCs (*75*). These cells were called induced pluripotent cells (iPSCs) and were later shown to be pluripotent through the generation of viable mouse chimera. In 2007, human iPSCs (hiPSCs) were created independently by two groups (*76*, *77*).

Human iPS cells are an exciting discovery because they bypass the ethical issues of hESC derivation. Furthermore, the potential for taking a small sample of a patient's somatic cells, reprogramming them to the undifferentiated state and differentiating them into an autologous cellular therapeutic, is an exciting prospect for regenerative medicine. While an early report suggested syngeneic mouse iPSCs were immunogenic upon transplantation (*78*), recent evidence demonstrates widespread tolerance and a lack of an immune response to differentiated cells generated from autologous iPSCs (*79*).

hiPSCs have been successfully derived using many approaches (for review see (*80*)). Initial retroviral methods were questioned for the presence of constitutively active oncogenes in the resulting pluripotent cells and their progeny, while more recent non-integrating methods struggle with low efficiency and success in a limited number of somatic cell types. However, hiPSC derivation methods and potential cell sources are rapidly changing. Overall, hiPSCs

represent a promising alternative to hESCs and many studies are being completed in both populations.

Genetic Modification of Human Embryonic Stem Cells

Genetic modification is an important strategy in biological research. The addition, subtraction, and/or modification of endogenous or exogenous genes allows scientists to better understand how cells differentiate and function. Exogenous genes can be expressed transiently or integrated into the host genome for long-term expression. Integration of new DNA into a host cell genome has traditionally been accomplished using integrating viral vectors or endogenous homologous recombination (HR). While viral methods can be highly efficient, they have significant drawbacks including random copy number and insertion site(s), insertional mutagenesis, transgene or endogenous gene silencing, and limited transgene capacity. Stable integration of large (>4.5kb), multi-component transgenes, at a known locus and with a known copy number, is virtually impossible using traditional viral strategies.

Gene targeting is a genetic technique that uses homologous recombination to mutate, delete or add genes. For over twenty years, genes in mouse embryonic stem cells (mESCs) have been successfully targeted by HR with efficiencies better than one cell in a thousand (*81*). However, since the first derivation of hESCs in 1998, only a handful of genes have been successfully targeted in these cells using traditional HR; for unknown reasons, hESCs are about one thousand times less efficient than mESCs when targeting or inserting genes by HR (*82*).

An alternative to traditional HR gene targeting is nuclease-assisted HR. In nuclease-assisted HR a targeted double stranded break is made by a nuclease. This break is repaired using either the endogenous non-homologous end joining (NHEJ) or HR machinery. If an exogenous template with regions of homology to either side of the double stranded break is provided, this template is occasionally used during HR-directed repair. Manipulation of the

exogenous template permits gene mutation, addition or deletion. Zinc-finger nuclease (ZFN)-facilitated gene targeting is one example of a nuclease-assisted technique (see Figure 1.2). Another example of facilitated gene targeting is the use of transcription activator-like effector nucleases (TALENs) (*83*). A ZFN is created through fusion of the FokI nuclease domain and an engineered DNA recognition domain composed of zinc-finger motifs. These DNA recognition domains can be engineered to be highly specific to a unique site in the genome. ZFN-mediated gene targeting was first used in human cells in 2005 (*84*). Hockemeyer et al. brought ZFN-mediated targeting to hESCs in 2009 (*85*). ZFN-mediated targeting has yielded many useful hESC lines including the mTmG-2a-Puro hESC line described in Chapter 2 (*86*).

ZFN-mediated gene targeting is not without potential disadvantages. Off-target double stranded breaks have been well documented (*87*). Without a repair template, these breaks are most likely repaired through non-homologous end joining, a process prone to addition or deletion errors. While off-target double strand breaks are a potential drawback of ZFN targeting, successfully targeted cells (which are relatively rare themselves) can be genetically selected, reducing the background of off-target insertion or deletion errors. Furthermore, with the ability to integrate transgenes greater than 12 kb, ZFN-mediated targeting offers an important alternative to the limitations of viral gene targeting.

Cardiac-Directed Differentiation of Human Embryonic Stem Cells

The ultimate goal of a biological pacemaker should be to mimic the healthy endogenous pacemaking system, both in form and in function. However, new authentic pacemaking tissue remains to be created in the laboratory. One particularly promising area is the differentiation of pluripotent stem cells (see section: Human Embryonic Stem Cells: Identification, Derivation and Modification). Cardiomyocytes derived from hESCs (hESC-CMs) were first described by Kehat et al. in 2001 (*57*) and have since been recognized as definitive cardiomyocytes (*58–60*).

Initial methods of hESC differentiation transferred the adherent undifferentiated cultures into suspension culture where they readily formed small aggregates of cells termed embryoid bodies (EBs). EBs differentiate when serum is added to the culture media. Occasionally, a differentiating EB contains an area of spontaneously beating cells. Microdissection of these beating regions yields hESC-CMs. Obtaining hESC-CMs through EB differentiation is inefficient, with cardiac yields <1%.

Our group and others have refined initial serum-based protocols to model differentiation after the developmental cues cardiomyocytes typically see in development (*88*, *89*). In cooperation with a team of scientists lead by Dr. Joseph Gold of Geron Corporation, we developed a cardiac-directed differentiation protocol where hESCs are grown to form a high-density monolayer. Growth media is then switched from mouse embryonic fibroblast-conditioned media to RPMI + B27 supplement when cells reach sufficient density. The mesoderm-inducing signaling molecule activin A is added to the RPMI/B27 media for 24 hours followed by addition of BMP4, a secreted factor in the anterior endoderm, for four days. Cultures exhibit spontaneous beating activity approximately twelve days after activin A exposure. This protocol typically yields cardiac purities of >60% as measured by cardiac troponin T expression. A recent modification to our protocol by Zhang et al. modulates the insulin levels in the media prior to spontaneous beating activity and deposits an extra layer of Matrigel (the substrate on which the high density monolayer is formed) on top of the cells (*90*). This "Matrigel sandwich" protocol has increased cardiac yields to average purities >70%. Our group has had success scaling up this protocol, routinely producing batches of cells that contain more than $1x10^9$ cardiomyocytes.

Our high-density monolayer protocol is not the only efficient cardiac-directed differentiation protocol. Wnt/β-catenin signaling promotes mesodermal specification during the early stages of cardiac differentiation while inhibiting cardiogenesis in later stages (*91*). With

this in mind, the Keller group developed a differentiation protocol where the cells are differentiated as EBs and Wnt signaling is inhibited four days after induction (*89*). More recently, Lian and colleagues have reported a completely defined protocol that yields up to 98% cardiac purity while modulating Wnt/β-catenin signaling without exogenous growth factors (*92*).

Although directed differentiation protocols continue to increase resulting cardiac purity, no existing protocol produces a pure cardiac population without using genetically modified cells. Pioneering work by Dr. Loren Field and colleagues successfully demonstrated small and large-scale isolation of mouse ESC-CMs using a transgene in which the alpha-myosin heavy chain promoter drives antibiotic resistance (*93*, *94*). Early work purifying hESC-CMs using a Percoll gradient resulted in highly enriched preparations compared to prior tedious microdissection techniques, but cardiomyocytes still were only 35-66% of resulting populations (*95*). A few years later, Dr. Mark Mercola's group demonstrated lentiviral constructs incorporating both fluorescence and antibiotic selection of hESC-CMs that yielded cardiac troponin-I-expressing cell purities as high as 96% (*96*). An alternate technology that doesn't rely on genetic markers is Raman micro-spectroscopy, which scans cells with a laser and looks for a unique cardiomyocyte "signature." Although recent iterations of this technique are specific and sensitive for cardiomyocytes, the throughput is still extremely slow (approximately 5 seconds per cell) (*97*). However, it is unclear if cardiomyocyte subtypes can be distinguished using Raman micro-spectroscopy. In other fields, heterogeneous cell populations are typically separated using genetic selection techniques involving the Cre-lox system or cell surface markers. However, an efficient floxed hESC reporter line had not been reported until we described the mTmG-2a-Puro hESC line detailed in Chapter 2. Furthermore, no cardiac-specific cell surface markers had been reported until 2011 when Dubois et al. identified signal-regulatory protein alpha (SIRPA) (*98*) and Uosaki et al. identified vascular cell adhesion molecule 1 (VCAM1) (*99*).

As efforts to create populations of pure hESC-CMs progress, all reported cardiac-directed differentiation protocols and subsequent purification steps continue produce a heterogeneous population of cardiomyocytes with electrophysiological phenotypes that resemble early-stage nodal, atrial and ventricular cardiomyocytes. Isolating these cardiac subpopulations will be an important step toward understanding the developmental cues that control subtype development. Furthermore, we expect the subtype purity of future cardiac cell therapy preparations to influence the safety and efficacy of these therapies. Cardiomyocyte subtype cell surface markers remain to be reported. We believe the method detailed in Chapter 3, where cardiac subpopulations are genetically selected in a promoter-specific manner, is the first such report, and a crucial stepping stone toward finding ways of isolating subpopulations without genetic manipulation.

The Road to a Biological Pacemaker

In a normal heart, the sinoatrial node is the origin of the action potential because it displays the fastest rate of automaticity. However, automaticity is demonstrated throughout the cardiac conduction system, albeit at slightly slower basal rates than in the SAN. This is an important consideration when engineering a biological pacemaker. Should we only consider a biological pacemaker composed of SAN cells? True SAN cells should be a model and perhaps the gold standard against which cells of a biological pacemaker are measured. However, the significant number of studies that demonstrate successful ectopic pacing using cells that are often quite different from SAN cells suggests a range of phenotypes might be acceptable (see section: Potential Cell Sources for a Biological Pacemaker). Similar to the development of electronic pacemakers, where early devices were unsophisticated and lacked most of the features seen in modern devices, the sophistication of biological pacemakers should be given time to mature. A biological pacemaker that exhibits stable pacing at physiologically appropriate

rates may be a viable treatment alternative if it can overcome at least some of the drawbacks that remain with electronic pacing. While electronic pacemakers are reliable and effective devices that do significantly more good than harm, certain patient populations, such as pediatric patients or patients that have had an electronic pacemaker removed due to infection, are particularly vulnerable to the drawbacks of electronic pacing. Careful selection of the appropriate initial recipients of biological pacemakers will be critical to the success of the field.

Thesis Overview

In vitro embryonic stem cell differentiation is an excellent opportunity to better understand the signals that control lineage specification. The Cre-lox system has proven to be a very effective genetic manipulation method to follow differentiating cells in many animal models. Unfortunately, a suitable floxed reporter had not been reported in human embryonic stem cells.

In response to this deficit, we created a floxed dual fluorescence reporter line of hESCs to generate candidate subpopulations of human-embryonic stem cell-derived cardiomyocytes based on the activation of a user-specified genetic reporter. Chapter 2 discusses the creation of this genetically engineered hESC line. We show that the engineered cells can be permanently marked and highly purified in a promoter-specific manner in both the undifferentiated and cardiac differentiated states. While we created this system for the purposes of selecting subpopulations of hESC-derived cardiomyocytes, we believe these cells are broadly applicable to the study of hESC differentiation.

Chapter 3 describes the isolation and characterization of two cardiomyocyte subpopulations, cGATA6 and MLC2v-activating cardiomyocytes, using of the selectable hESCs described in Chapter 2. The automaticity, beating rate, action potentials, net ionic currents and immunophenotype of these two populations suggest they are distinct from each other and

represent putative early stage AV nodal (cGATA6) and ventricular (MLC2v) populations. Characterization of the bulk automaticity and beating rates of purified cGATA6 and MLC2v cardiomyocyte aggregates revealed significant differences that highlight the influence of subtype purity on bulk electrical behavior. Aggregates of cGATA6 cells beat significantly faster and maintained automaticity better than aggregates of MLC2v or admixed hESC-CMs. These data question the safety and long-term efficacy of using an admixed population of hESC-CMs as a biological pacemaker. Furthermore, these data suggest that an admixed population and a population where nodal cells have been removed have similar bulk behavior. This questions the need to remove nodal cells in non-pacemaking therapeutic situations such as ventricular infarct repair.

The differences between cGATA6 and MLC2v-activating hESC-CMs outlined in Chapter 3 warrant additional study to further characterize the electrical phenotype, expression profiles, cell surface markers, changes that happen with long-term culture, and therapeutic potential of these populations. Chapter 4 summarizes the significance of the work presented in this dissertation and the future studies we are planning or have in progress with these populations.

A

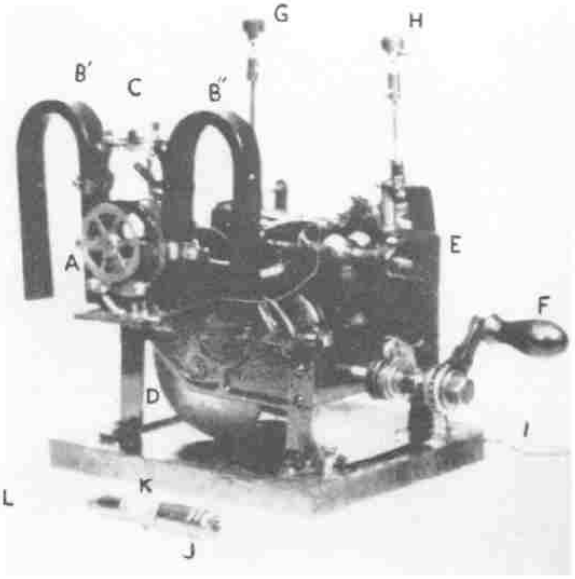

B

C

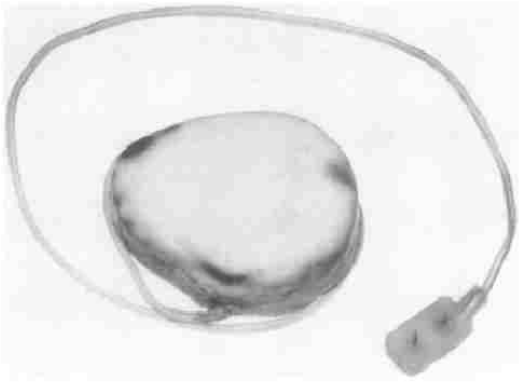

D

Figure 1.1: Electronic Pacemakers Over the Last 80 Years Electronic pacemakers have made significant technological advances in the past 80 years. The earliest pacemakers, such as Hyman's example from 1932 seen in **A** (*100*), provided only short term pacing, used painful external electrodes, and required turning a handle to generate rhythmic pulses of electricity. (**B**) In 1958, Dr. Seymour Furman implanted the first patient with a long-term transvenous pacemaker (*101*). The pacing was effective for 96 days but the device still required wall power; the patient was allowed to ambulate on a 50-foot extension cord. (**C**) Transistor technology and component shrinkage allowed the pacemaker to become a battery-powered implantable device by 1960 (*32*). (**D**) Modern pacemakers often have multiple leads, long lasting batteries and are remotely programmable (image from Medtronic Advisa product literature).

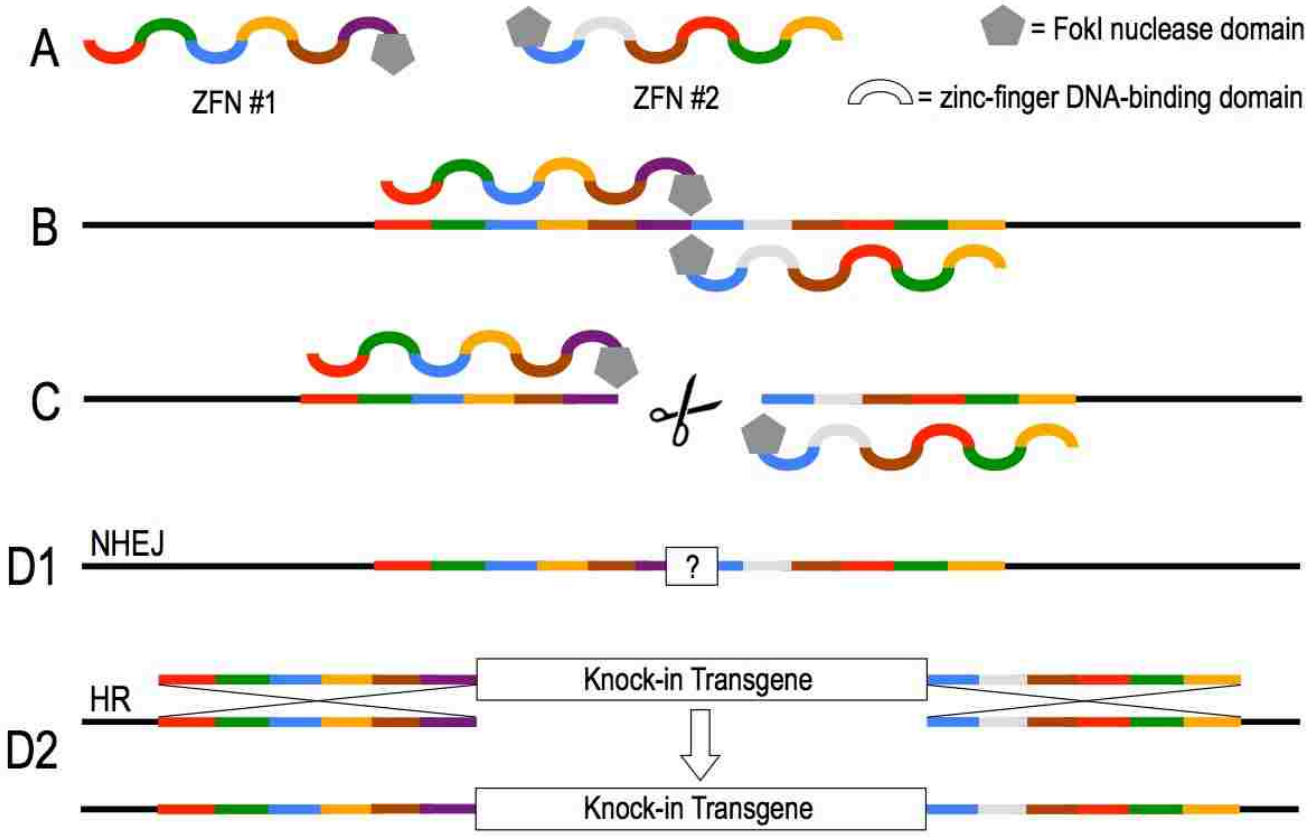
A
ZFN #1
ZFN #2
= FokI nuclease domain
= zinc-finger DNA-binding domain
B
C
D1
NHEJ
?
D2
HR
Knock-in Transgene
Knock-in Transgene

Figure 1.2: Diagram of ZFN-Mediated Gene Targeting (**A**) Zinc-finger nucleases (ZFN) are created by fusing the FokI nuclease domain with a sequence-specific, engineered zinc-finger DNA-binding domain. Alignment of paired ZFNs at the target locus (**B**) creates the obligate FokI dimer that causes a locus-specific double-strand break (**C**). The double strand break can be repaired by either non-homologous end-joining (NHEJ) (**D1**), a process prone to addition and deletion errors, or homologous recombination (HR) using a transfected transgene template (**D2**).

Chapter 2: Targeted Genomic Integration of a Selectable Floxed Dual Fluorescence Reporter in Human Embryonic Stem Cells

Summary

Human pluripotent stem cells have the potential to be an excellent cell source for regenerative cellular therapies if they can be sufficiently well differentiated to become target cell types. Pluripotent stem cells differentiate into functional tissues through a highly coordinated series of intra- and intercellular signals. To understand the timing and identity of these signals the field needs improved genetic tools for the labeling, lineage tracing and selection of specific cell types from heterogeneous differentiating populations, particularly in human embryonic stem cells (hESCs). Traditional gene targeting methods have proven inefficient in human pluripotent cells and viral targeting methods have significant drawbacks. We used zinc finger nuclease technology to stably insert a unique, selectable, floxed dual-fluorescence reporter transgene into the AAVS1 locus of RUES2 hESCs. This ‘‘stoplight’’ transgene, mTmG-2a-Puro, strongly expresses membrane-localized tdTomato red fluorescent protein until Cre-dependent recombination causes a switch to expression of membrane-localized enhanced green fluorescent protein (eGFP) and puromycin resistance. First, to validate this system in undifferentiated cells, we transduced transgenic hESCs with a lentiviral vector driving constitutive expression of Cre and observed the expected phenotypic switch. Next, to demonstrate utility in lineage-specific selection, we transduced cardiac-differentiated cultures with a lentiviral vector in which the striated muscle-specific CK7 promoter drives Cre expression. This yielded near-homogenous populations of $eGFP^{+}$ hESC-derived cardiomyocytes. The mTmG-2a-Puro hESC line described here represents a useful new tool for both in vitro fate mapping studies and the selection of useful differentiated cell types.

Introduction

The successful development of safe and efficacious stem cell-based therapies will require an improved understanding of the lineage relationships between stem cells and their differentiating progeny, as well as the detailed molecular properties of cells in the initial, transitional and final differentiated states. In model organisms (e.g. Xenopus, Drosophila, mouse etc.), these issues have often been addressed by fate mapping studies using elegant genetic labeling approaches, in particular, the Cre-lox system. Currently, there are over 500 genetically modified mouse lines expressing Cre recombinase under the control of various promoter elements, as well as a large cohort of transgenic lines with Cre-responsive reporter elements (*102*).

While human embryonic stem cells (hESCs) have become a valuable in vitro model of human development and a potential source for cell-based therapies, Cre-lox mediated fate mapping has not been widely applied to hESCs. In this study, zinc finger nuclease (ZFN)-mediated genetic engineering was used to generate a stable human ESC line that expresses a selectable floxed dual fluorescence reporter element. The random integration of transgenes is susceptible to silencing, positional effects and off-target effects on cellular function, so we instead targeted our reporter to the so-called “safe harbor” AAVS1 locus, which affords stable transgene expression in a wide variety of cell types including hESCs (*85*). The reporter element couples a fluorescence color switch with puromycin resistance to allow isolation of nearly homogeneous cellular subtypes from heterogeneous populations after Cre-mediated recombination. Here, we demonstrate the efficacy of this system in the purification of cardiomyocytes differentiated from hESCs, but it should be widely applicable to the selection of diverse cell lineages when combined with appropriate cell type-specific regulatory cassettes driving Cre.

Results

Transgene Design

Mazmudar et al. reported the creation of a non-selectable floxed, dual fluorescence "stoplight" reporter element (mTmG), in which the ubiquitously active CMV early enhancer/chicken β-actin (CAG) promoter drives expression of either membrane-restricted tdTomato or eGFP (after Cre-mediated recombination) (*103*). To facilitate the selection of cell populations not amenable to fluorescence-activated cell sorting, we modified the mTmG transgene to express puromycin N-acetyl transferase (i.e. puromycin resistance) in addition to eGFP in cells that have undergone recombination. The resultant transgene is hereafter referred to as mTmG-2a-Puro. Next, to allow the selection of cells successfully modified with the mTmG-2a-Puro transgene, we also added a PGK-Neo cassette, cloned in the opposite orientation to the CAG-mTmG-2a-Puro cassette (see Figure 2.1A).

Transgene Integration Using Zinc Finger Nucleases

Standard methods for plasmid transfection are inefficient in hESCs (*104*), and successfully integrated transgenes are prone to silencing (*105*). This makes the generation of stable transfectant hESC lines very challenging. Lentiviral vectors are commonly used as an alternative in the hESC system (*106*), but they have limited packaging capacity, result in the random integration of an unknown number of gene copies, and are also prone to silencing. To avoid these limitations and because the mTmG-2a-Puro coding region exceeds the packaging capacity of most viral vectors, we instead used zinc finger nuclease (ZFN) mediated recombination to insert the mTmG-2a-Puro construct into the human AAVS1 locus in RUES2 hESCs (see Figure 2.1). The AAVS1 "safe harbor" locus at 19q13.3 was chosen as the insertion target site because this locus is reported to have a relatively open chromatin configuration that facilitates strong, stable transgene expression in both undifferentiated and

differentiated cell states (*85*, *107*). To create the transgenic line, we co-electroporated RUES2 hESCs with two plasmids: one in which the floxed CAG-mTmG-2a-Puro reporter was flanked by AAVS1 homology arms, and a second encoding containing a ZFN pair specific to the AAVS1 site (*85*). The successfully targeted cells were purified with G418 selection, resulting in hESC cultures that were greater than 95% tdTomato$^+$ by epifluorescent microscopy and flow cytometry (see Figure 2.2A&B). We used Southern blot to confirm that selected transgenic hESC populations with strong, stable tdTomato expression had been properly targeted at the AAVS1 locus was confirmed by Southern blot (see Figure 2.2C), and these cultures were shown to have a normal female karyotype (see Figure 2.2D). Of note, following this protocol, we infrequently obtained tdTomato$^+$ hESC populations that were later found by Southern blot to have resulted from random integration events. Interestingly, such cultures also showed highly variable tdTomato fluorescence (both from cell-to-cell and over time), and so they were discarded (see Figure 2.3).

Next, we validated the functionality of the floxed stoplight reporter in the correctly targeted cultures, hereafter referred to as mTmG-2a-Puro hESCs. We began with studies in the pluripotent state, transducing undifferentiated transgenic hESCs with a lentiviral vector in which the ubiquitously expressed elongation factor 1α promoter drives Cre recombinase (hereafter, EF1α-Cre). After transduction, cells were analyzed for eGFP and tdTomato expression by flow cytometry at regular intervals (see Figure 2.4A&B). eGFP expression was detected within 24 hours of EF1α-Cre transduction. By 48 hours post-transduction, distinct eGFP$^+$/tdTomato$^+$ and eGFP$^-$/tdTomato$^+$ cell populations had emerged. Between days 3 to 6 post-transduction, the eGFP$^+$ population became increasingly distinct as the tdTomato fluorescence in these cells decreased. By day 6, ~50% of the cells were either tdTomato$^+$ or eGFP$^+$ (see Figure 2.4B). This is in line with our previously reported transduction efficiency of ~50% (*15*).

To demonstrate the capacity of our system to purify Cre-marked hESCs and their progeny, we next subjected the EF1α-Cre transduced cells to puromycin selection. After three days of selection, the resultant cell population was nearly 100% $eGFP^+$ (see Figure 2.4C**)**. Although some $eGFP^+$ cells remained $tdTomato^+$ at this time-point, rare $tdTomato^+/GFP^-$ cells were retained. Qualitatively similar results were obtained during fluorescence imaging of live cells treated with EF1α-Cre lentivirus (see Figure 2.4D). When we immunostained the latter cultures with an antibody against Cre-recombinase, Cre expression was only detected in the nuclei of hESCs that also expressed eGFP (see Figure 2.4E). Importantly, these data show that puromycin resistance is constrained in a cell autonomous manner to $eGFP^+$ hESCs, greatly facilitating the purification of $eGFP^+$ cells from an initially heterogeneous cell population.

Next, we validated the use of mTmG-2a-Puro reporter hESCs in the isolation of a specific cell type (in this case, cardiomyocytes) from a heterogeneous population of differentiated cells. We differentiated mTmG-2a-Puro hESCs using a monolayer-based cardiac induction protocol previously reported by our group (*88*, *108*). This protocol typically yields differentiated cultures in which a majority of the hESC progeny are cardiomyocytes. When we applied it to mTmG-2a-Puro hESCs, we obtained populations of 68 ± 2.5% cardiac troponin T positive (cTnT+) cardiomyocytes (see Figure 2.5A&B). To test the hypothesis that genetic selection could yield an even higher degree of cardiac purity, we transduced these cultures with a lentiviral vector that expresses Cre under the striated muscle-specific regulatory gene cassette MCK-CK7. MCK-CK7 is derived from modified portions of the mouse muscle creatine kinase gene enhancer and proximal promoter (*109*, *110*). We then dual-labeled the transduced cultures using antibodies against eGFP and the cardiomyocyte marker α-actinin. As expected, the cultures contained a mixture of recombined and non-recombined cardiomyocytes prior to puromycin selection ($eGFP^+$ α-$actinin^+$: 45.8 ± 7.7%, eGFP- α-$actinin^+$: 34.5 ± 2.9%, $eGFP^+$ α-$actinin^-$: 1.0 ± 1.2%, $eGFP^-$ α-$actinin^-$: 19.5 ± 8.7%) (see Figure 2.5C&D). However, after

puromycin selection, we obtained highly enriched populations of $eGFP^+$ α-$actinin^+$ cardiomyocytes ($eGFP^+$ α-$actinin^+$: 98.6 ± 0.2%, $eGFP^-$ α-$actinin^+$: 0.8 ± 0.2%, $eGFP^+$ α-$actinin^-$: 0.6 ± 0.3%, $eGFP^-$ α-$actinin^-$: 0.0 ± 0.0%) (see Figure 2.5C&D). Taken collectively, these data show that, when combined with suitable vectors for cell-type specific expression of Cre recombinase, the mTmG-2a-Puro floxed reporter hESC line described here can be used to isolate specific cell populations that approach homogeneity.

Discussion

Genetic approaches to fate mapping and the selective enrichment of specific cell types have provided useful insights into the developmental potential of stem and progenitor cells in vivo and in vitro (*111*). However, our ability to apply these approaches and isolate specific subpopulations has been severely limited in the hESC system. In this report, we describe the generation and validation of mTmG-2a-Puro RUES2 hESCs, which contain a unique floxed reporter transgene that includes both fluorescent reporters and an antibiotic resistance cassette. We also show that this stably integrated transgene allows the labeling and selection of Cre-recombined cells in both undifferentiated and differentiated cultures in a promoter-specific manner. In this study, we validated the mTmG-2a-Puro concept using the RUES2 hESC line, but the same approach and genetic constructs should be applicable in any human cells, including other hESC lines and human induced pluripotent stem cell (iPSCs). For example, insertion of the mTmG-2a-Puro transgene into patient-derived iPSC lines might be particularly useful for future disease modeling or drug screening efforts that require the isolation of a particular differentiated cell type (e.g. cardiomyocytes).

In a previous study, Nolden et al. described a floxed two-color reporter hESC line as part of a study designed to test the activity of cell-permeant Cre-recombinase (*112*). Here, we have further refined the floxed "stoplight" reporter concept, while also developing genetic tools that

could be used to conveniently insert such a reporter into multiple human pluripotent stem cell lines. Indeed, our ZFN-based strategy offers two advantages over conventional plasmid transfection or viral vectors: all of the successfully targeted cells should have a single copy of the reporter transgene in a defined genetic locus, and ZFNs can accommodate larger, more complicated constructs such as mTmG-2a-Puro. The mTmG-2a-Puro transgene incorporates a number of features that we expect will be useful for investigators in the field. First, it encodes for two bright fluorescent proteins, both of which also happen to be membrane-restricted. (This subcellular localization aids in distinguishing true fluorescent signal from autofluorescent background, and it is particularly helpful in recognizing structures such as axonal projections (*103*).) Second, we have added a Cre-dependent puromycin selection component, which can be used to purify a single cell type from a heterogeneous starting population. We predict that this feature will prove particularly useful in the isolation of differentiating cell types that may be otherwise distinguished only by a weak or transiently activated promoter. We have been encouraged by multiple requests for these cells from other labs for this exact reason.

Finally, it should be noted that the mTmG-2a-Puro RUES2 hESCs described in this study do not represent a clonal hESC line, so we cannot exclude a minority population of randomly integrated cells (albeit below the level of detection by Southern blot). If a particular application required a 100% homogenous transgenic hESC population, this limitation could be overcome by dilution cloning and expansion from a single cell. While time-consuming and technically challenging, such methodologies have been successfully applied to hESCs (*113*). In practice, we have found that the polyclonal mTmG-2a-Puro RUES2 hESC populations that result from G418 selection exhibit very little phenotypic variation making them suitable for most fate-mapping and cell purification applications.

Materials and Methods

Zinc Finger Nuclease Co-Expression Plasmid

To target the donor cassette to the AAVS1 human genomic locus, we generated a single plasmid system in which expression of the left and right AAVS1 ZFNs are both driven by independent, constitutively active human PGK promoters (pAAVS1ZFN; see Figure 2.1A). The human PGK promoter was kindly provided by Dr. Mark Mercola (Sanford Burnham Institute for Medical Research). Sequences for the AAVS1 right and left ZFNs were generated by human codon optimization of the amino acid sequences reported by Hockemeyer et al (*85*). The nucleotide sequences for the right and left ZFNs driven by the PGK promoter were then synthesized de novo as separate plasmids by Genscript. These PGK-ZFN cassettes were then cloned together in CIS orientation into a single expression plasmid, which was then sequence-verified. Of note, we initially compared outcomes using two different versions of this expression plasmid in which the PGK-ZFN cassettes were oriented in either CIS or TRANS orientation. We only observed successful targeting and the emergence of fluorescent hESCs when using the plasmid with the two cassettes in the CIS orientation.

AAVS1 Targeting Vector

The AAVS1 donor vector, pZDonor mTmG-2a-Puro was generated as follows. A plasmid containing the floxed non-selectable dual fluorescence reporter (mTmG) by Muzumdar et al. (*103*) was acquired commercially (Addgene, 17787). A targeting vector for the human AAVS1 locus (19q13.3-qter), pZDonor, was provided with the AAVS1 CompoZr Targeted Integration kit (Sigma, Z3027-100UG). The mTmG plasmid was restriction digested with EcoRV, EcoRI, and SacI to isolate the 5.6 kb fragment containing the CAG promoter and mTmG expression cassette. The pZDonor vector was restriction digested with EcoRV and PmeI into which the 5.6 kb mTmG expression cassette was ligated. The E2a element containing a unique

XhoI site at the 3` end was inserted using PCR-cloning distal to the mTmG expression cassette. The puromycin resistance cassette was inserted using Infusion-HD (Clontech) into the XhoI site. A cassette encoding for PGK-driven expression of neomycin/kanamycin resistance was cloned in the reverse orientation into a SalI site 5` of the CAG mTmG-2a-Puro cassette. The resultant pZDonor mTmG-2a-Puro plasmid (see Figure 2.1B) was then sequence verified.

Genomic Integration and Cell Culture

RUES2 hESCs were kindly provided by Dr. Ali H. Brivanlou of The Rockefeller University (*114*, *115*). RUES2 hESCs are listed on the NIH Human Embryonic Stem Cell Registry (Approval Number: NIHhESC-09-0013), and all experiments were approved by the University of Washington Embryonic Stem Cell Research Oversight (ESCRO) Committee. $5x10^5$ undifferentiated RUES2 hESCs were dispersed to single cells using Versene (Gibco) and electroporated with 5 µg of pAAVS1ZFN and 15 µg of pZDonor mTmG-2a-Puro (Lonza, Kit 1 (Cat#: VAPH-5012), program A-23). After electroporation, hESCs were plated onto Matrigel (BD Biosciences) coated plates in mouse embryonic fibroblast (MEF) conditioned media containing 5 ng/mL hbFGF (Peprotech) and 10 uM Y-27632 (Sigma). The cultures were maintained for 7 days and then selected with 75 µg/mL G418 (Invitrogen) in MEF conditioned media for 3 days. A polyclonal $tdTomato^+$, G418-resistant RUES2 hESC population was expanded and analyzed for purity by flow cytometry. Karyotype analysis was performed by Cell Line Genetics (Madison, Wisconsin). Thereafter, RUES2 mTmG-2a-Puro hESCs showing proper targeting to the AAVS1 locus and a normal karyotype were maintained under feeder-free conditions, using MEF-conditioned media supplemented with 5 ng/mL hbFGF (*67*). These cells and plasmids are available for non-commercial distribution via a standard Uniform Biological Materials Transfer Agreement with our institution.

Kinetics Studies

To determine the kinetics of the transition from tdTomato to eGFP expression, undifferentiated RUES2 mTmG-2a-Puro cultures were dispersed with Versene and transduced with a lentiviral vector in which expression of Cre recombinase is driven by the constitutive EF1α promoter. Cells were harvested and analyzed by flow cytometry at 24-hour intervals for up to 6 days following transduction. To test the capacity of our system to purify an $eGFP^+$ subpopulation after Cre-mediated recombination, transduced cultures were also subjected to selection with 1 μg/mL puromycin for 4 days and analyzed by flow cytometry. Flow cytometry was performed using a FACSCANTO 2 instrument (Beckton Dickinson, San Jose, CA) controlled by FACSDiva software (BD Biosciences). Cells were analyzed using a 488-nm argon laser plotting PE (585/42 filter) against FITC (530/30 filter). Instrument settings were adjusted to avoid spectral overlap. Data analysis was performed using FlowJo software (Tree Star, Ashland, Oregon).

Southern Blot

15 μg of WT RUES2 and mTmG-2a-Puro RUES2 genomic DNA were digested with KpnI, NdeI, and NheI and electrophoresed on a 1% polyacrylamide gel. DNA was transferred onto a BioRad Zeta Probe membrane (Cat#: 162-0196), which was washed with 2x SSC, dried at 80°C in a hybridization oven for 2 hours, and then exposed for 1 hour to a pre-hybridization buffer (50% formamide, 0.12 M NaH2PO4, 0.25 M NaCl, 7% SDS, 1 mM EDTA and 0.2 mg/mL Salmon Sperm DNA). The hybridization probe for the 3` genomic region of the AAVS1 locus was generated using the following primers: sense: TGGGCGGAGGAATATGTCCCA; antisense: CACACCCCCATTTCCTGGAGC. The probe for the neomycin cassette was generated using the following primers: sense: AGTCGATGAATCCAGAAAAGC; antisense: GCCGTGTTCCGGCTGTCAG. The probes were labeled with ^{32}P dCTP (Amersham

Megaprime DNA labeling system, RPN1607 with non-incorporated radiolabeled nucleotides removed by column purification (Illustra Microspin G-50 columns, GE Healthcare, Cat# 27-5330-01). Probe hybridization was performed overnight in hybridization buffer at 43°C. After 24 hours, the membrane was washed for 20 minutes with 2x SSC/0.1% SDS followed by 20 minutes in 0.1x SSC/0.1% SDS. The membrane was then exposed to autoradiographic film for 3 days. The WT AAVS1 band is expected at 1.6 kb whereas the targeted locus is expected to shift to 3.2 kb. Note that the neomycin probe is not locus-specific and indicates the number of genomic integration sites.

Human ESC Cardiac Differentiation

The cardiac differentiation of RUES2 mTmG-2a-Puro hESCs was performed as previously described for other hESC lines (*88*, *108*). In brief, undifferentiated hESCs were dispersed to single cells with Versene and then plated in a high-density monolayer in the presence of MEF-conditioned media supplemented with 5 ng/mL hbFGF. After confluence was reached, the cultures were induced to differentiate by switching to RPMI media (Gibco) containing 100 ng/mL recombinant activin A (R&D Systems), 1:60 diluted Matrigel (BD), and insulin-free B27 supplement (Invitrogen). After 24 hours, the latter media was exchanged with insulin-free RPMI-B27 supplemented with 10 ng/mL recombinant BMP4 (R&D Systems). On days 5 and 7 post-induction with activin A, the cultures were re-fed with insulin-free RPMI-B27 without any exogenous growth factors and then this step was repeated using insulin-containing RPMI-B27 on day 9 and every other day thereafter.

Transduction and Phenotyping of hESC-Derived Cardiomyocytes

Differentiated cultures containing hESC-derived cardiomyocytes were dispersed with Versene and trypsin. A fraction of the cells were plated onto 0.1% PEI / 0.5% gelatin coated

chamber slides in RPMI-B27 medium supplemented with 10% FBS, 10 uM Y-27632 (Sigma), Polybrene (Millipore) and 5000 particles per cell of a lentivirus expressing Cre under the striated muscle-specific CK7 regulatory cassette, based on the muscle creatine kinase promoter (MCK) (*109*, *110*, *116*). This medium was exchanged with RPMI-B27 at 24 hours after replating and transduction. Where indicated, cultures were subjected to selection with puromycin (1 µg/mL) at 48 hours following transduction with the MCK-CK7 lentiviral vector.

With each plating step, a separate fraction of dispersed cells was set aside for parallel analysis by flow cytometry. Cells were fixed in 4% paraformaldehyde and then labeled with either a mouse anti-cardiac troponin T (cTnT) antibody (1:100 dilution, ThermoScientific, Cat# MS-295) or isotype control (1:100, eBioscience, Cat# 14-4714). Detection was performed using an Alexafluor 660-conjugated anti-mouse secondary antibody (Molecular Probes). Flow cytometry and analysis was then performed as described above. Cells were gated against the isotype control as detected using a 633-nm argon laser plotting APC (660/20 filter).

Immunofluorescence: Undifferentiated RUES2 mTmG-2a-Puro Cells

Cells were fixed for six minutes with 2% paraformaldehyde, permeabilized in PBS containing 0.025% Triton-X, and blocked in PBS containing 1.5% normal goat serum. Cells were stained with anti-Cre recombinase monoclonal antibody (1:100, Covance, Cat#: MMS-106P) followed by secondary staining with Alexa Fluor 660 (1:100, Molecular Probes). Nuclei were counterstained in PBS containing a 1:2000 dilution of Hoechst 33342 (Thermo Scientific).

Immunofluorescence: RUES2 mTmG-2a-Puro Cardiomyocytes

Cells were fixed with 2% paraformaldehyde and blocked with 1.5% normal goat serum. Cells were then stained with anti-α-actinin monoclonal (1:100, Sigma, Cat#: A7811) and anti-GFP (1:400, Molecular Probes, Cat#: A11122). Secondary staining was performed by

incubation with species-specific Alexa Fluor conjugates (1:500, Molecular Probes). Nuclei were counterstained in PBS containing a 1:2000 dilution of Hoechst 33342 (Thermo Scientific).

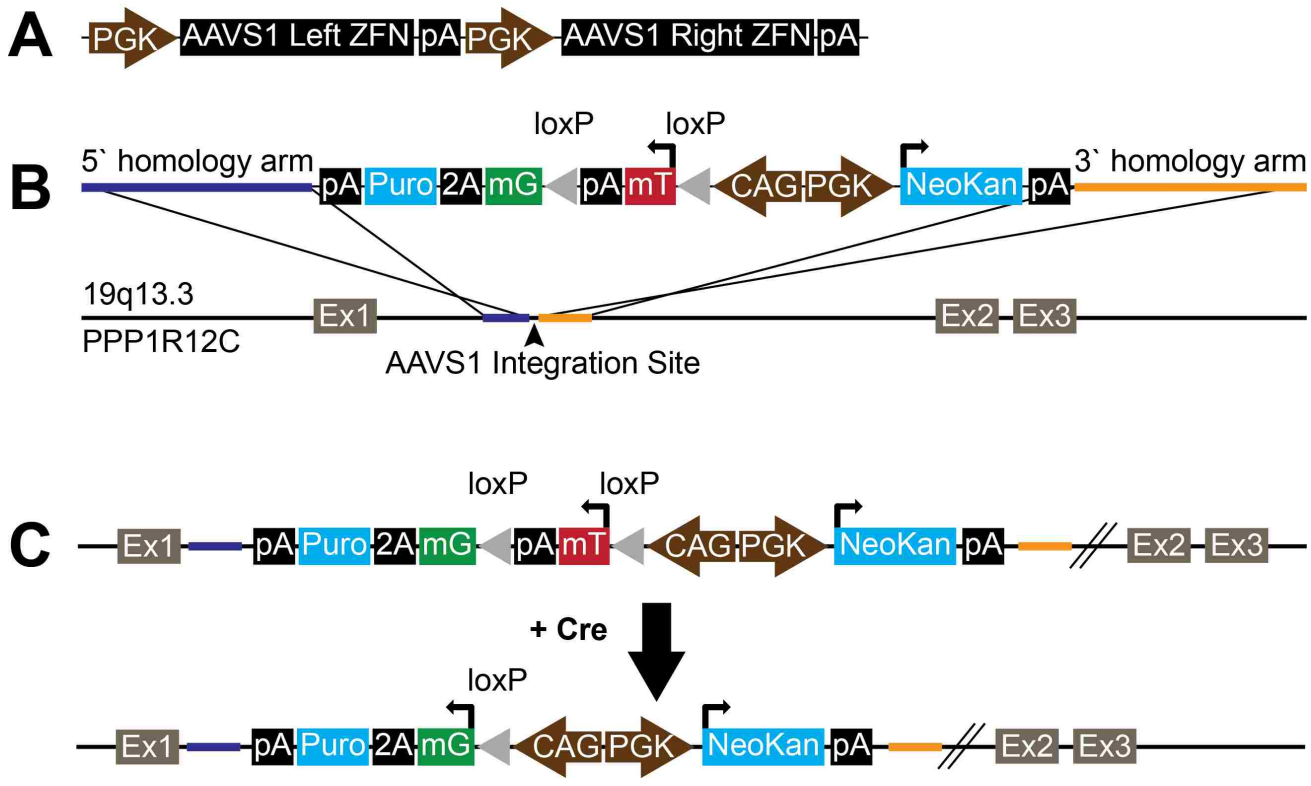
A
PGK
AAVS1 Left ZFN
pA
PGK
AAVS1 Right ZFN
pA
B
loxP
loxP
5` homology arm
pA
Puro
2A
mG
pA
mT
CAG
PGK
NeoKan
pA
3` homology arm
19q13.3
PPP1R12C
Ex1
Ex2
Ex3
AAVS1 Integration Site
C
loxP
loxP
Ex1
pA
Puro
2A
mG
pA
mT
CAG
PGK
NeoKan
pA
Ex2
Ex3
+ Cre
loxP
Ex1
pA
Puro
2A
mG
CAG
PGK
NeoKan
pA
Ex2
Ex3

Figure 2.1: Transgene Plasmid Construction (**A**) pAAVS1ZFN vector diagram showing two CIS oriented human PGK promoters driving the left and right AAVS1 zinc finger nucleases (ZFNs). (**B**) pZDonor-mTmG-2a-Puro vector diagram and the AAVS1 genomic integration site on chromosome 19 in the first intron of the PPP1R12C gene. The PGKNeoKan cassette enables selection of cells with stable transgene integration and the CAG-mTmG-2a-Puro selectable "stoplight" cassette allows for visual and antibiotic selection of cells that have been recombined by Cre recombinase. Yellow and blue colored bars represent ~800 bp stretches of sequence homologous to either side of the AAVS1 target locus. (**C**) In coordination with the AAVS1 ZFNs, the mTmG-2a-Puro transgene was integrated into the AAVS1 site by homologous recombination. Cre mediated recombination of LoxP sites removes the tdTomato expression cassette and results in eGFP-2a-Puro expression. Abbreviations: pA = bovine growth hormone polyadenylation signal, mT = myristoylated tdTomato, mG = myristoylated eGFP, NeoKan = neomycin/kanamicin resistance, Puro = puromycin resistance, loxP = Cre recombinase locus of chromosomal crossover, Ex = exon.

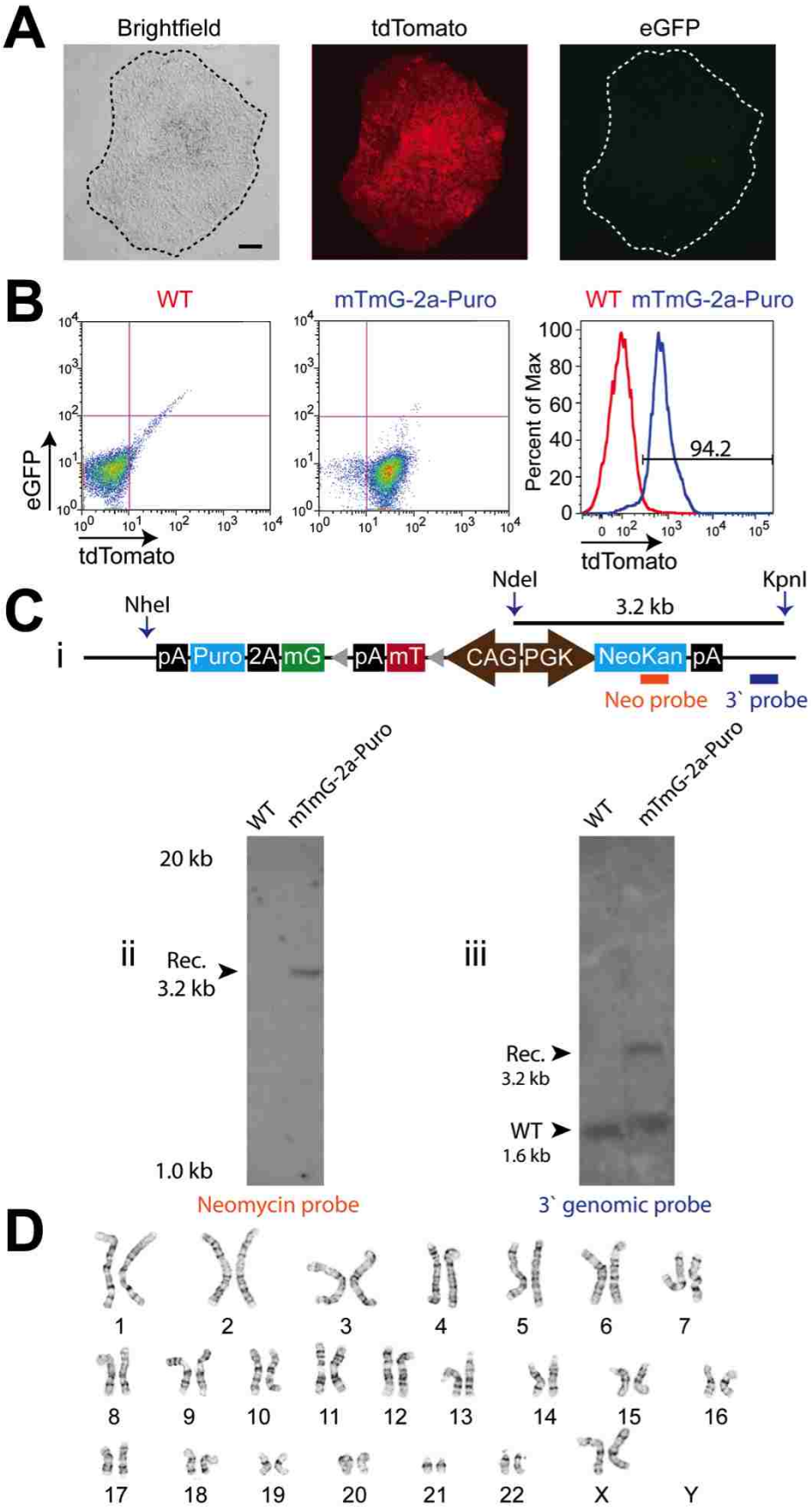
A
Brightfield
tdTomato
eGFP
B
WT
mTmG-2a-Puro
WT mTmG-2a-Puro
eGFP
tdTomato
Percent of Max
94.2
C
i
NheI
NdeI
KpnI
3.2 kb
pA
Puro
2A
mG
pA
mT
CAG
PGK
NeoKan
pA
Neo probe
3` probe
ii
WT
mTmG-2a-Puro
20 kb
Rec.
3.2 kb
1.0 kb
Neomycin probe
iii
WT
mTmG-2a-Puro
Rec.
3.2 kb
WT
1.6 kb
3` genomic probe
D
1
2
3
4
5
6
7
8
9
10
11
12
13
14
15
16
17
18
19
20
21
22
X
Y

Figure 2.2: Generation of Stable Transgenic RUES2 mTmG-2a-Puro Undifferentiated hESCs Photomicrographs of an undifferentiated mTmG-2a-Puro RUES2 colony (**A**) under brightfield, tdTomato (red) and eGFP (green) fluorescent illumination. Note that the transgenic hESCs are tdTomato^{+} and eGFP^{-}. Scale bar is 75 μm. (**B**) eGFP and tdTomato flow cytometry of wild type RUES2 hESCs (WT) and RUES2 mTmG-2a-Puro undifferentiated hESCs after G418 selection (mTmG-2a-Puro). G418 selection produces >94% purity of mTmG-2a-Puro cells as measured by flow cytometry for tdTomato fluorescent expression (see the panel on the right). (**C**) (i) Schematic showing the NheI, NdeI and KpnI cut sites within the transgene. The orange bar represents the binding site for the neomycin probe. The blue bar represents the binding site for the 3' genomic probe. Non-locus-specific Southern blot detection of the neomycin transgene detects only a single copy of the mTmG-2a-Puro construct (ii), while Southern blot analysis of the AAVS1 locus shows heterozygous targeting of the mTmG-2a-Puro transgene to the AAVS1 locus (iii). (**D**) G-banded karyotyping of mTmG-2a-Puro RUES2 undifferentiated cells demonstrating a normal (46, XX) karyotype.

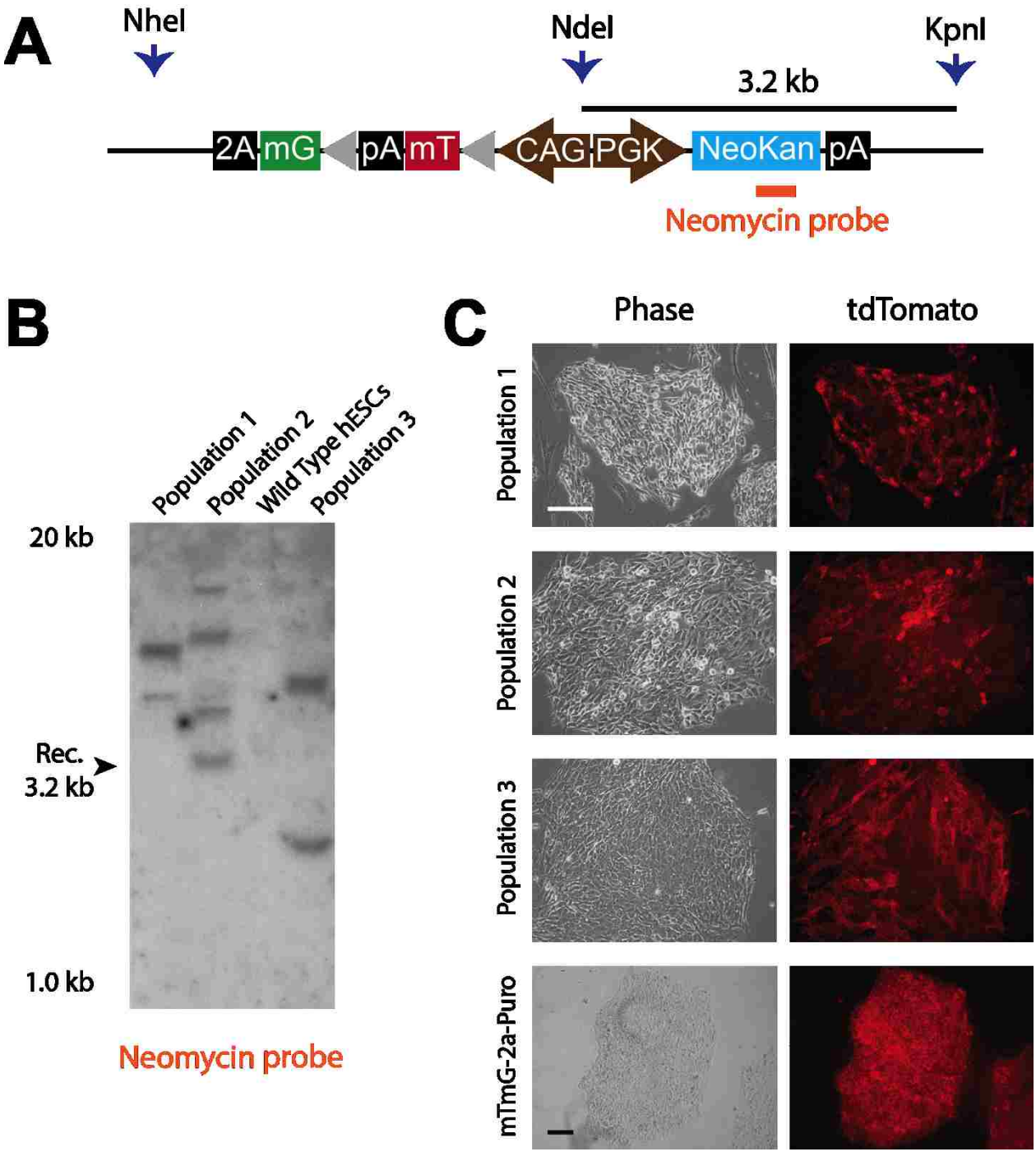
A
NheI
NdeI
KpnI
3.2 kb
2A
mG
pA
mT
CAG
PGK
NeoKan
pA
Neomycin probe
B
Population 1
Population 2
Wild Type hESCs
Population 3
20 kb
Rec.
3.2 kb
1.0 kb
Neomycin probe
C
Phase
tdTomato
Population 1
Population 2
Population 3
mTmG-2a-Puro

Figure 2.3: Multiple Transgene Integrations Result in Variable Phenotypes ZFN transgene integration occasionally yields cells with multiple, random transgene integrations. (**A**) Diagram of basic mTmG-2a transgene where any gene can be inserted after the 2a sequence. Diagram indicates NheI, NdeI and KpnI restriction sites for Southern blot assay. The orange bar represents the binding site for the non-locus-specific Southern blot Neomycin probe. AAVS1 targeted transgenes will have a band at 3.2kb by Southern blot. (**B**) Southern blot from three different mTmG-2a populations and wild type hESCs. Only population 2 shows a correctly targeted transgene at the AAVS1 locus, while populations 1, 2 and 3 all show multiple random integrations. (**C**) Phase contrast and tdTomato fluorescence photomicrographs of populations 1, 2, 3 and mTmG-2a-Puro cells showing heterogeneous tdTomato fluorescence intensity in the populations with multiple transgene insertions and homogeneous tdTomato expression in the properly targeted, mTmG-2a-Puro cells.

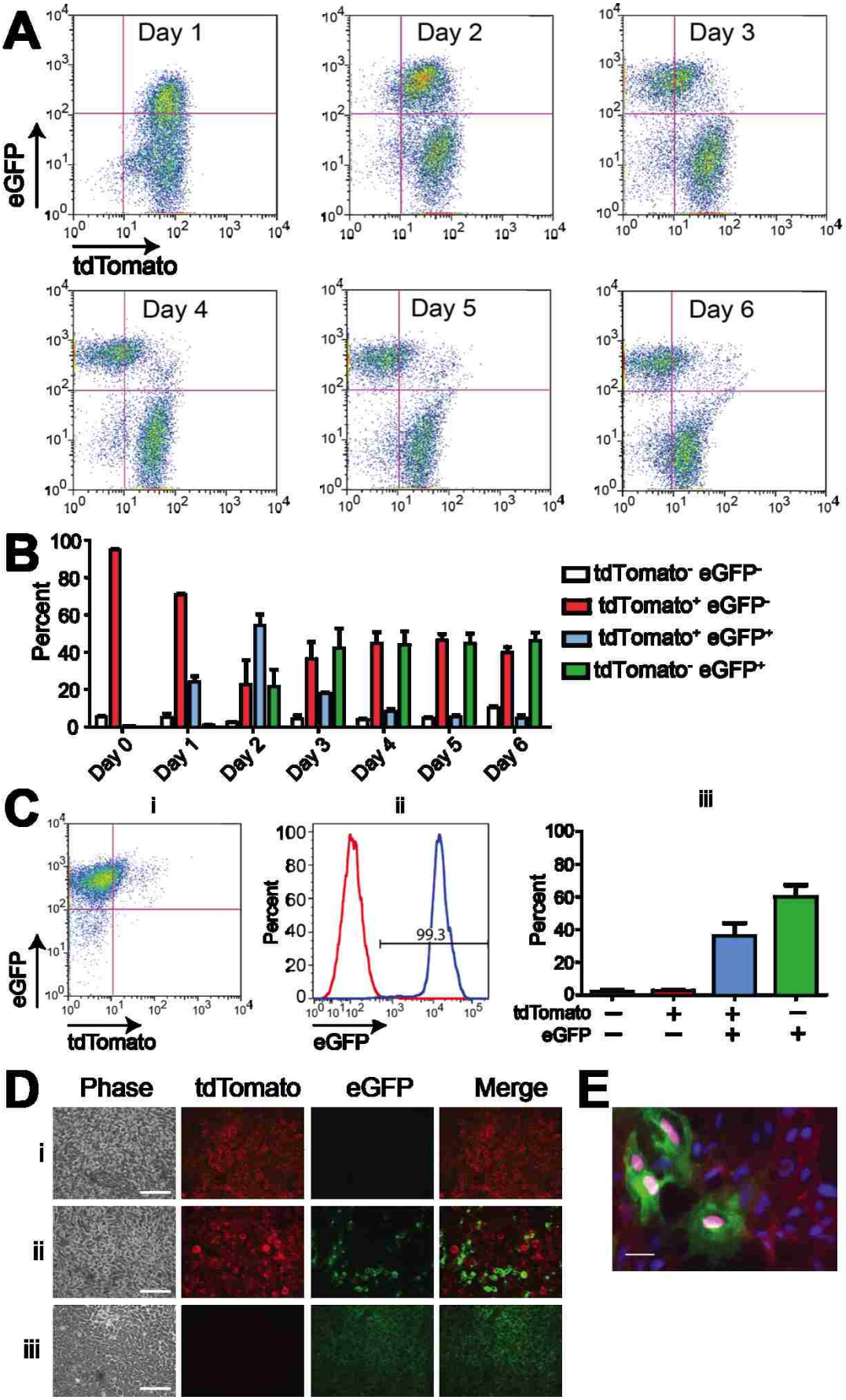
A
Day 1
Day 2
Day 3
Day 4
Day 5
Day 6
eGFP
tdTomato
B
Percent
tdTomato- eGFP-
tdTomato+ eGFP-
tdTomato+ eGFP+
tdTomato- eGFP+
Day 0
Day 1
Day 2
Day 3
Day 4
Day 5
Day 6
C
i
ii
iii
99.3
Percent
tdTomato
eGFP
D
Phase
tdTomato
eGFP
Merge
E

Figure 2.4: Cre Expression Mediates a Fluorescence Switch in Undifferentiated mTmG-2a-Puro Floxed Reporter hESCs (**A**) Flow cytometry showing changing numbers of tdTomato$^+$ and eGFP$^+$ RUES2 mTmG-2a-Puro cells at various timepoints after transduction with an EF1α-Cre lentivirus. (**B**) Quantitation of the fluorescence switch shown in panel A (n=3 biological replicates). (**C**) Scatter plot of undifferentiated mTmG-2a-Puro cells treated with EF1α-Cre lentivirus and then selected with puromycin for 48 hours. Note that the resultant cultures were >99% eGFP$^+$ by flow cytometry (i). Comparison of untreated (red) and EF1α-Cre treated, puromycin selected (blue) undifferentiated mTmG-2a-Puro cells (ii). Quantitation of flow cytometry data from three independent experiments in which cells were transduced with EF1α-Cre and puromycin selected (iii). (**D**) Phase contrast and fluorescent photomicrographs of undifferentiated mTmG-2a-Puro cells (i), mTmG-2a-Puro cells treated with EF1α-Cre lentivirus (ii), and mTmG-2a-Puro cells treated with EF1α-Cre and selected with puromycin (iii). Scale bars are 50 μm. Error bars represent +/- one standard error of the mean. (**E**) mTmG-2a-Puro cells transduced with EF1α-Cre lentivirus were immunostained with an anti-Cre recombinase antibody. Note that Cre (magenta) co-localizes only with eGFP$^+$ cell nuclei. Scale bar is 10 μm.

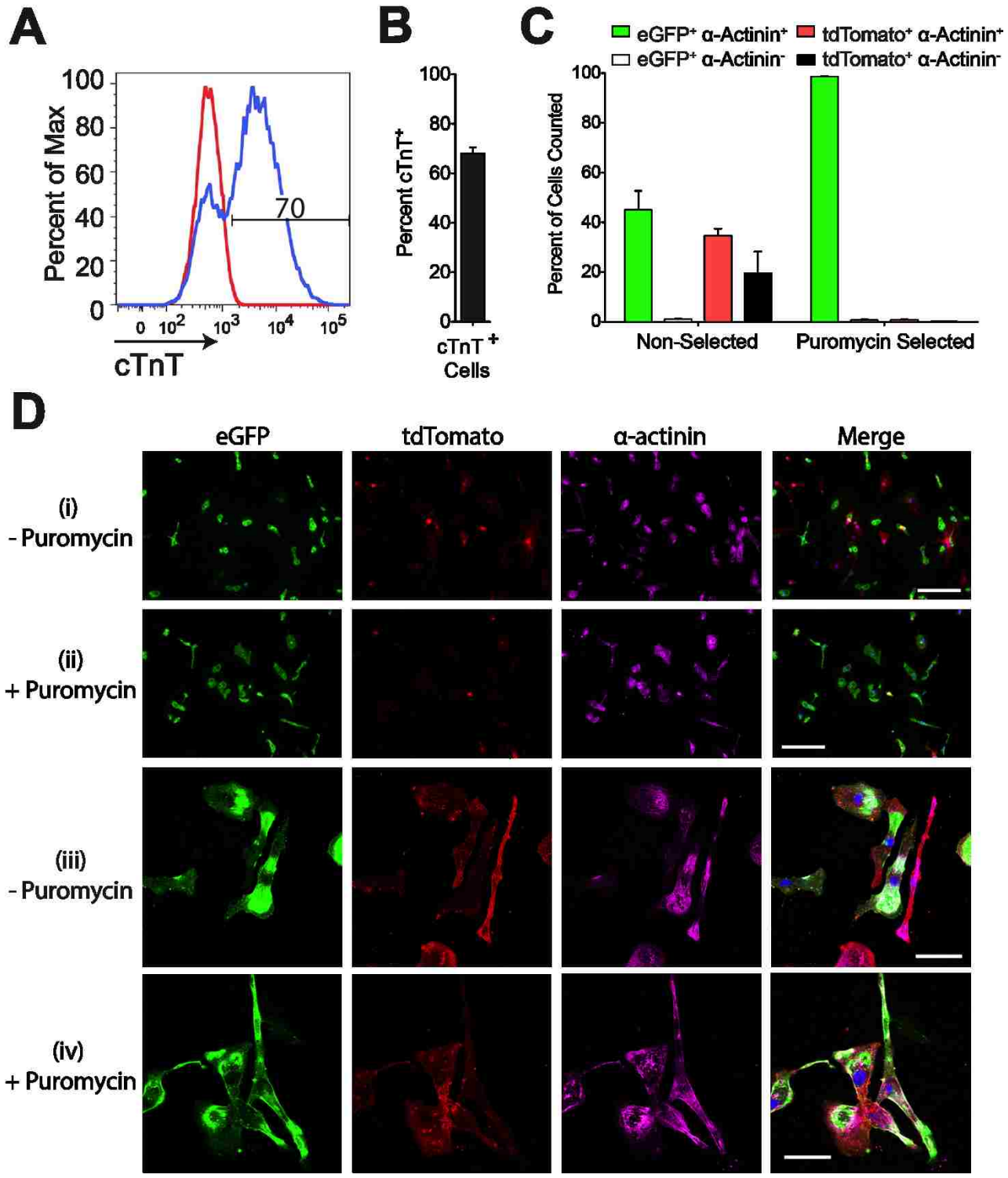
A
Percent of Max
100
80
60
40
20
0
70
0 10^2 10^3 10^4 10^5
cTnT
B
Percent cTnT+
100
80
60
40
20
0
cTnT + Cells
C
eGFP+ α-Actinin+
tdTomato+ α-Actinin+
eGFP+ α-Actinin-
tdTomato+ α-Actinin-
Percent of Cells Counted
100
80
60
40
20
0
Non-Selected
Puromycin Selected
D
eGFP
tdTomato
α-actinin
Merge
(i) - Puromycin
(ii) + Puromycin
(iii) - Puromycin
(iv) + Puromycin

Figure 2.5: Using CK7-Cre in Combination With mTmG-2a-Puro Cells Enables Cardiomyocyte Purification (**A**) Flow cytometry for cardiac troponin T (cTnT) indicating the percentage of cardiomyocytes present after mTmG-2a-Puro hESCs were subjected to a directed cardiac differentiation protocol. (**B**) Mean percentage of $cTnT^+$ cells resulting from three independent differentiation runs. (**C**) The percentage of cells that immunostained for eGFP, tdTomato, and/or the cardiomyocyte marker α-actinin was determined before and after puromycin selection (n=230-600 cells per condition for three independent differentiation runs). (**D**) Magnification at 10x (i and ii) and 60x (iii and iv) showing fluorescent photomicrographs of cardiac differentiated mTmG-2a-Puro cells before (i and iii) and after (ii and iv) puromycin selection. Scale bars are 200 μm in (i and ii) and 50 μm in (iii and iv). Error bars represent one standard error of the mean.

Chapter 3: Genetic Selection of Cardiac Subtypes: cGATA6- and MLC2v-Marked Populations of hESC-Derived Cardiomyocytes

Summary

Current protocols to produce cardiomyocytes from human pluripotent stem cells yield populations that are neither purely cardiac nor specific in the electrophysiological phenotype of resulting cells. While stem cell-derived cardiomyocytes have shown promise as a regenerative cell therapy, the ability to study how specific cardiac subpopulations develop is a critical step toward developing safe and effective therapies. Here we use the mTmG-2a-Puro selectable hESC reporter line to isolate and characterize subpopulations of cardiomyocytes that are marked by activation of either the cGATA6 or MLC2v promoter. We compared the automaticity, beating rate and electrophysiological phenotype of isolated cells from these two populations and immunostained for subtype-specific markers. The $Nkx2.5^{+}/Tbx3^{+}/HCN4^{+}/KCNJ5^{+}/MYL2^{-}$ cGATA6 population beat faster and displayed significantly more automaticity than the $Nkx2.5^{+}/Tbx3^{-}/HCN4^{-}/KCNJ5^{-}/MYL2^{+}$ MLC2v population. We then formed aggregates of purified cGATA6 and MLC2v cells to test the hypothesis that an aggregate of cGATA6 cells would beat faster and maintain this rate over time better than an aggregate of MLC2v or admixed cells. cGATA6 aggregates initially beat 16% faster than aggregates of either MLC2v or pan-cardiac cells. This gap increased to >40% by differentiation day 48 while the beating rates of MLC2v and pan-cardiac populations did not significantly change. hESC-CM subtypes have previously only been able to be studied as single cells; our data suggest the mTmG-2a-Puro hESC line is an ideal platform to study hESC-derived cardiomyocyte subtypes and highlight the importance of subtype purity in bulk automaticity.

Introduction

Cardiomyocytes derived from human pluripotent stem cells have a tremendous potential to become a beneficial clinical therapy. However, reported methods of deriving cardiomyocytes from human pluripotent stem cells have two significant drawbacks. First, the resulting populations are not pure. While the most recent protocols have substantially increased cardiac purity (*92*), the presence of uncharacterized non-cardiac cells could result in unintended and potentially harmful consequences, such as arrhythmia or teratomas, when introduced in vivo. Second, the resulting populations are electrophysiologically heterogeneous containing cardiomyocytes that have action potential characteristics of nodal, atrial and ventricular cells (*117*). Stem cell-derived cardiac cell therapies are more likely to become a reality if the electrophysiological phenotype of implanted cell populations is well defined; pure populations of specific cardiomyocyte subtypes will be important candidate populations for cardiac cell therapy.

In this study we use the mTmG-2a-Puro transgenic hESC line we previously reported (see Chapter 2) to genetically select subpopulations of cardiomyocytes. We looked to the developmental literature to identify candidate promoters to drive the selection. A combination of the core chicken GATA6 (cGATA6) promoter and upstream regulatory elements was first identified as a marker of the developing atrioventricular canal by He et al. in 1997 (*118*). See section in Chapter 1: Cardiac Conduction System Development and Pacemaker Identification for further discussion of the cGATA6 promoter. Our group examined the specificity of cGATA6 in hESC-CMs and reported highly specific expression in cells that display a nodal phenotype (*15*). To identify a putative non-nodal population we chose the myosin light chain 2v (MLC2v) promoter. While MLC2v expression is abundant in ventricular cells (*119*), expression on developing human nodal structures remains unclear (*120*, *121*). However, mouse ESC-CMs that activate MLC2v have exclusively demonstrated working type action potential phenotypes (*122*).

We isolated three populations: a putative nodal population using the cGATA6 promoter-enhancer, a distinctly non-nodal population using the MLC2v promoter, and a pan-cardiac population using the CK7 muscle creatine kinase promoter. We demonstrate significant differences in automaticity and beating rate, action potential phenotype, ion currents, aggregate automaticity and beating rate, and immunostaining for subtype-specific markers between the cGATA6 and MLC2v populations. These findings underscore the importance of subtype purity in bulk electrophysiological behavior and question the appropriate use of admixed cardiomyocyte populations in the setting of a biological pacemaker.

Results

The Proportion of MLC2v-Activating hESC-CMs is Different in H7 and RUES2 hESCs

We hypothesized that the MLC2v and cGATA6 promoters would be activated in different subpopulations of hESC-CMs. Before we examined the phenotype of these populations we quantified the proportion of cells that activate either promoter. We quantified the proportion of cells that activate the MLC2v and cGATA6 promoters in both RUES2 and H7 hESC lines to compare the mTmG-based cell marking strategy with cGATA6-eGFP data we reported previously in the H7 line (*15*).

Our transduction strategy included two lentiviral controls, EF1α-CRE and CK7-CRE. All cells used in this study followed the same differentiation protocol, including lentiviral transduction on differentiation day 15 (see Figure 3.1). 50.5 ± 3.8% (n = 3) of H7 hESCs became GFP-positive when transduced with EF1α-CRE. RUES2 cells tended to exhibit slightly higher proportions of GFP-positive cells when transduced with EF1α-CRE (64.5 ± 4.8%, n = 6), but the difference between cell lines was not statistically significant (see Figure 3.2A).

Cardiac-directed hESC differentiations frequently yield variable proportions of cardiomyocytes. To control for this variability we included a parallel CK7-CRE control lentivirus.

Qualitatively, both the RUES2 and H7 populations exhibited variable cardiac purity (data not shown). We quantified this variability by counting the number of GFP-positive cells in the CK7-CRE transduced samples. Counts were normalized to EF1α activation to account for variable transduction efficiency. RUES2 cells demonstrated more variability and lower average cardiac purity than did H7 cells (58.0 ± 13.9% GFP^+ n = 6 vs 76.9 ± 2.4% n = 3 GFP^+) but the difference between cell lines was not statistically significant (see Figure 3.2B). The CK7-CRE control also allowed us to purify a pan-cardiac population against which to compare potential subpopulations.

We compared cGATA6 and MLC2v activation after adjusting for cardiac purity by normalizing to CK7 activation. cGATA6-CRE transduced RUES2 cells expressed GFP in 8.0 ± 0.6% (n = 6) of the bulk population (see Figure 3.2A). When normalized for cardiac purity 28.0 ± 6.0% (n = 6) of RUES2 cardiomyocytes activated the cGATA6 promoter (see Figure 3.2C). In H7 cells 15.5 ± 3.1% (n = 3) of the bulk population expressed GFP when transduced with cGATA6-CRE (see Figure 3.2A). This proportion becomes 20.0 ± 3.6% (n = 3) when normalized to CK7-CRE expression (see Figure 3.2C), which is both similar to the cGATA6 expression we previously reported in the H7 line and not significantly different than the RUES2 line. MLC2v-CRE transduced RUES2 cells expressed GFP in 12.2 ± 1.6% (n = 6) of the bulk population (see Figure 3.2A). When normalized for cardiac purity, 38.1 ± 3.3% (n = 6) of RUES2 cardiomyocytes activated the MLC2v promoter (see Figure 3.2C). In H7 cells 21.6 ± 1.2% (n = 3) of the bulk population expressed GFP when transduced with MLC2v-CRE (see Figure 3.2A). This proportion becomes 55.8 ± 1.5% (n = 3) when normalized to CK7-CRE expression (see Figure 3.2C) and is a significantly higher proportion than we observed in the RUES2 line ($P<0.0001$).

cGATA6 hESC-CMs Beat Faster than MLC2v or CK7 hESC-CMs

We measured the beating rate of isolated CK7-, MLC2v-, and cGATA6-activating early stage (day 20) hESC-CMs to test the hypothesis that the cGATA6 cells would have a faster beating rate and display more automaticity than MLC2v cells. cGATA6-activating cells displayed a significantly higher mean beating rate (29.4 ± 3.4 beats per minute, n = 47) than either the MLC2v (10.2 ± 3.0 beats per minute, n = 47) or CK7 populations (17.0 ± 3.2 beats per minute, n = 47) ($P<0.0001$ and $P = 0.0104$ respectively) (see Figure 3.3). The beating rates of MLC2v and CK7 were not significantly different. These beating rate means include significant numbers of quiescent cells; 76.6% (36 of 47) of MLC2v-activating cells were quiescent while only 29.7% (14 of 47) of cGATA6-activating cells were quiescent. In the CK7 pan-cardiac population 53.2% (25/47) of cells were quiescent.

The Action Potentials of cGATA6 and MLC2v Cells Differ

We measured the action potential phenotype of cGATA6 and MLC2v-activating cells at both early (differentiation day 25-35) and late (differentiation day 100-130) stages using single cell patch clamping in current and voltage clamp modes. The beat rate of cGATA6 cells was significantly faster than the beat rate of MLC2v cells at both the early and late timepoints (early: 10.6 ± 2.1 bpm vs. 46.4 ± 7.3 bpm; late: 4.3 ± 1.9 bpm vs. 60.7 ± 16.2 bpm) (see Figure 3.4C). While there was no significant difference between the early and late timepoints within either the cGATA6 or MLC2v populations, the cGATA6 cells tended to beat faster over time while the MLC2v cells tended to slow down. Importantly, there were significant differences in the number of quiescent cells within each population. 27 of 46 (58.6%) early stage MLC2v cells were quiescent while only 1 of 25 (4%) early stage cGATA6 cells was quiescent. In the late stage 6 of 12 (50%) of MLC2v cells were quiescent while only 1 of 12 (8.3%) cGATA6 cells was quiescent.

The maximum diastolic potential of cGATA6 cells was significantly more depolarized than that of MLC2v cells at both early and late timepoints (early: -66.5 ± 1.2 mV vs. -59.6 ± 1.7 mV; late: -63.0 ± 1.6 mV vs. -57.6 ± 1.6 mV) but there was no significant difference between the early and late timepoints within either the cGATA6 or MLC2v populations (see Figure 3.4B).

The maximum upstroke velocity was not significantly different between cGATA6 and MLC2v cells at either the early or late stage (early: 158.7 ± 27.8 V/s vs. 203.1 ± 26.9 V/s, late: 82.6 ± 20.0 V/s vs. 60.7 ± 20.8 V/s) (see Figure 3.4D). However, the maximum upstroke velocity in both populations tended to decrease over time and the difference was significant in the cGATA6 population.

The action potential amplitudes (APA) of early stage MLC2v and cGATA6 cells were not significantly different (108.5 ± 2.3 mV, 107.8 ± 2.8 mV) while the late stage MLC2v cells had a significantly smaller APAs than the late stage cGATA6 population (75.4 ± 2.7 mV, 89.4 ± 3.4 mV) (see Figure 3.4A). Furthermore, the APA of both the MLC2v and cGATA6 populations decreased significantly between early and late timepoints.

The action potential duration at 50% repolarization (APD_{50}, see Figure 3.4E) and 90% repolarization (APD_{90}, see Figure 3.4F) was neither significantly different between the cGATA6 and MLC2v populations nor significantly different within a population between the early and late timepoints (APD_{50} early: 162.2 ± 42.7 ms vs. 157.1 ± 20.4 ms, late: 49.4 ± 7.68 ms vs. 149.5 ± 33.7 ms; APD_{90} early: 214.5 ± 49.7 ms vs. 229.2 ± 24.9 ms, late: 101.0 ± 13.4 ms vs. 202.0 ± 40.6 ms). While the action potential duration was not significantly different within either population between the early and late timepoints, the MLC2v cells tended to decrease both their APD_{50} and APD_{90} over time.

During patch clamp studies we also measured capacitance, an indirect measure of cell size. At both early and late timepoints, cGATA6 cells were significantly bigger than MLC2v cells

(early: 14.2 ± 1.1 pF vs. 24.5 ± 2.7 pF, late: 14.7 ± 2.4 pF vs. 30.3 ± 5.8 pF) although neither the cGATA6 cells nor the MLC2v cells significantly changed their size between the early and late timepoints.

cGATA6 Cells Display More Hyperpolarization-Activated Inward Current than MLC2v Cells

After recording action potentials in current-clamp mode, we switched to voltage clamp mode to measure the net ionic current across the cell membrane. We used physiological ionic constituents in the bath and pipette solutions to measure whole-cell net currents thinking that this experiment would suggest which currents we should isolate in future experiments. Our voltage clamp protocol was modeled after the published methods of Cho et al. (*123*). Each of our cells was stepped from -40 mV to a range of one-second test potentials from -120 mV to +60 mV. cGATA6 cells displayed more inward current (or less outward current) at all but the most positive test potential at both early and late timepoints (see

Figure 3.5). This inward current was significantly greater than MLC2v cells at hyperpolarized potentials (-90 to -120 mV) and at 20 mV (see

Figure 3.5A) in early cells. While the statistical difference between MLC2v and cGATA6 was no longer significant at hyperpolarized potentials at the late timepoint, the trends were similar (see

Figure 3.5B). Of note is a small inward current around -30 to -40 mV that we only observed in late stage cells.

Aggregates of cGATA6 Cells Beat Faster than Aggregates of Either MLC2v or CK7 Cells

Hanging drop culture was used to form aggregates of $5x10^3$, $1x10^4$, or $1.5x10^4$ puromycin-selected CK7, MLC2v and cGATA6 cells (see Figure 3.6). The spontaneous beating rate of individual aggregates at 37°C was measured at day 32, day 48 and day 62. On day 32 cGATA6 aggregates beat 16% faster ($P<0.0001$) than either MLC2v or CK7 aggregates (which were not significantly different from each other) (22.4 ± 1.5 bpm vs. 19.1 ± 1.7 bpm and 19.3 ± 2.8 bpm) (see Figure 3.7). By day 48, cGATA6 aggregates had significantly increased this gap to be >40% faster than MLC2v or CK7 aggregates (28.9 ± 1.5 bpm) while MLC2v and CK7 aggregate beating rates did not significantly change (20.7 ± 4.4 bpm and 18.2 ± 4.2 bpm). Finally, on day 62, cGATA6 aggregates were beating more than twice as fast (106%, 24.0 ± 0.75 bpm) as either MLC2v or CK7 aggregates (11.7 ± 0.72 bpm vs. 9.5 ± 0.67 bpm). There was no significant correlation between aggregate size and beating rate (data not shown).

cGATA6 Cells Express Markers of the Atrioventricular Conduction System

We immunostained cGATA6 and MLC2v cells for a pan-cardiac marker (alpha actinin) in addition to markers expected to be differentially expressed in nodal and working-type cardiomyocytes (Nkx2.5, Tbx3, HCN4, KCNJ5 and MYL2). See Table 1 for a detailed list of antibodies. Importantly, the tdTomato and eGFP membrane-bound proteins that are expressed in the mTmG system survived fixation and permeabilization and did not require immunostaining. Alpha actinin (ACTN2) staining was robust in all cGATA6 and MLC2v cells indicating these promoters were only activated in cardiomyocytes (see Figure 3.8A). The transcription factor Nkx2.5 has been shown to be active in all cardiomyocytes except those in the sinoatrial node (*8*,

124). Both cGATA6 and MLC2v cells demonstrated robust nuclear Nkx2.5 staining (see Figure 3.8B). The transcription factor Tbx3 is only highly expressed in the cardiac pacemaker and conduction system (*11*). cGATA6 cells exhibited significantly stronger Tbx3 staining than did MLC2v cells (see Figure 3.8C). The hyperpolarization-activated cyclic nucleotide-gated HCN4 channel plays a significant role in the hyperpolarization-activated inward currents that contribute to pacemaking activity. While all cardiomyocytes express HCN4 mRNA at some level (*125*), strong HCN4 expression is seen in the cardiac conduction system. We observed robust membranous HCN4 staining in cGATA6 cells that was not seen in the MLC2v population (see Figure 3.8D). The acetylcholine-activated inward-rectifying potassium channel (I_{KACh}) is a heteromultimeric ion channel composed of KCNJ3 and KCNJ5 subunits (*126*). I_{KACh} is more prominent in sinoatrial and atrioventricular nodal tissue where it plays a critical role in heart rate regulation by activity of the vagus nerve (*127*). cGATA6 cells displayed significantly stronger KCNJ5 staining than did MLC2v cells (see Figure 3.8E). Finally, to test the specificity of the MLC2v promoter, we immunostained for MYL2 (MLC2v). MYL2-positive cells were only observed in the MLC2v population (see Figure 3.8F).

Discussion

We anticipate future cardiac cell therapies will require specific cardiac subpopulations. Electrophysiological mismatch between implanted cells and host tissue will, in the best case, reduce therapeutic efficacy, and, in the worst case, threaten patient health and safety. In this report we describe the genetic selection and characterization of two cardiac subpopulations based on the activation of either the cGATA6 promoter-enhancer or the MLC2v promoter. cGATA6 hESC-CMs exhibit many similarities to AV node cardiomyocytes including: prominent automaticity that is maintained over time; a faster beating rate than a pan-cardiac population both as single cells and as aggregates; a more depolarized maximum diastolic potential;

prominent hyperpolarization-activated inward membrane current; and immunostaining positive for Nkx2.5, Tbx3, HCN4 and KCNJ5, and negative for MYL2. Conversely, MLC2v hESC-CMs have many characteristics of immature ventricular working myocardium including: sparse automaticity; slow beating rate; an increase in quiescence over time; less hyperpolarization-activated inward current; expression of Nkx2.5 and MYL2 and reduced or absent expression of Tbx3, KCNJ5, and HCN4.

We isolated cGATA6 and MLC2v populations using the selectable floxed dual fluorescence reporter we have previously described (*86*). Importantly, we show that the proportion of cells that activate the cGATA6 promoter using the indirect mTmG-2a-Puro system is comparable to the directly driven fluorescent reporter system we used in previous work with the cGATA6 promoter (*15*). We were also able to assess the difference in cGATA6 and MLC2v activation between the H7 and RUES2 cell lines. While cGATA6 was activated in a similar proportion of H7 and RUES2 cells, we found a significantly higher proportion of H7 cells activate MLC2v than do RUES2 cells. This is not altogether unexpected; the cardiomyogenic potential of different hESCs lines is variable (*128*). Furthermore, both a) the proportion of nodal and working type hESC-CMs, and b) the proportion of atrial to ventricular cells within working type hESC-CM populations, have been reported to differ between stem cell lines (*129*). The difference in MLC2v activation we see between H7 and RUES2 cells might indicate these lines yield different proportions of atrial and ventricular-like hESC-CMs, although further experiments are needed to confirm this difference.

We used two important lentiviral controls in our experiments, EF1α-CRE and CK7-CRE. EF1α is a constitutively active promoter in all human cells. Any mTmG cell that is transduced with EF1α-CRE will express Cre recombinase and switch from constitutive tdTomato expression to constitutive eGFP expression. This control allowed us to quickly and quantitatively compare the transduction efficiency between biological replicates and between cell lines. The CK7-

variant of the muscle creatine kinase promoter is constitutively active in all striated muscle and served as our second control (*116*). We have previously shown that all cells in our cardiac-directed differentiations that activate CK7 are cardiomyocytes (*86*) so we consider a CK7-activating population to be pan-cardiac.

While our GFP-expression data indicate that cGATA6 and MLC2v are activated in different proportions of hESC-CMs, this data cannot interrogate the potential overlap of these two populations or determine if one population is a subset of the other. However, our immunostaining results, specifically the differences in Tbx3, HCN4, KCNJ5 and MYL2 staining, suggest these populations are distinct from each other.

The MLC2v and cGATA6 populations were further distinct from each other when we measured their automaticity. We measured the beating rate of isolated early stage cells in culture and isolated early and late stage cells under patch clamp. cGATA6 cells beat faster and displayed significantly more automaticity than MLC2v cells in both conditions. Furthermore, MLC2v cells became increasingly quiescent over time while cGATA6 cells maintained their automaticity and even had an upward trend in beating rate over time.

The action potentials of nodal and working type cells have several distinct differences. Nodal cells have a smaller action potential amplitude, a more depolarized maximum diastolic potential, a slower maximum upstroke velocity and a shorter action potential duration than working type cells. We saw many, but not all, of these differences in cGATA6 and MLC2v cells. The action potential amplitudes (APA) of cGATA6 and MLC2v cells were similar in early stage cells and both cell types had smaller APAs in late stage cells. While the APA of cGATA6 late stage cells is similar to values we have reported previously for nodal hESC-CMs (*15*), the APA of MLC2v cells is only similar to working type cells at the early timepoint. The significant decrease in MLC2v APA in late stage cells is unexpected and not typical of ventricular cells. cGATA6 cells had a significantly more depolarized maximum diastolic potential than MLC2v

cells in both early and late stage cells. There was no significant difference in maximum upstroke velocity between early stage cGATA6 and MLC2v cells and only cGATA6 cells had a significant decrease in maximum upstroke velocity in late stage cells.

Hyperpolarization-activated inward currents are thought to be one of the major mechanisms that control cardiomyocyte automaticity. Nodal cells display significantly more hyperpolarization-activated inward current, mainly through the HCN4 ion channel, than working type cells. Our voltage clamp data in cGATA6 cells is suggestive of a nodal phenotype, although it is important to note that we used physiological pipette and bath conditions where individual currents cannot be isolated. Interestingly, the loss of inward current around 0mV in late stage MLC2v cells suggests the loss of the L-type calcium current over time. This could explain the decrease in the MLC2v action potential duration at the late timepoint, as the L-type calcium current is responsible for maintaining the phase 2 plateau of the action potential. Finally, the increase in inward current around -30 mV in both MLC2v and cGATA6 late stage cells is suggestive of the appearance of a strong sodium current or T-type calcium current, but additional experiments will confirm the identity of the current(s) involved.

While measuring the electrophysiological phenotype of individual cells is important, many cardiac electrical characteristics are a result of bulk source/sink current dynamics. For example, nodal stability and resistance to atrial electrical influence is ensured by the multicellular architecture of the pacemaker itself (53; 54). This electrical stability is maintained by the predominant expression of low conductance gap junctions in nodal cells and the sparse electrical connections the pacemaker establishes with the surrounding atrial muscle. Similarly, coordinated ventricular contraction is a result of ventricular cells that are tightly coupled with high conductance gap junctions. We hypothesized that cGATA6 and MLC2v cells would have different bulk characteristics, specifically that an aggregate of cGATA6 cells would beat faster and maintain this rate over time better than an aggregate of MLC2v cells. The data support our

hypothesis and add an important new insight: not only did cGATA6 aggregates beat faster than MLC2v aggregates, they also beat significantly faster and maintained automaticity better than aggregates of pan-cardiac cells. This is perhaps the strongest data we have collected supporting the notion that a biological pacemaker should be composed exclusively of pacemaker-like cells, not an admixed population of pacemaker and working type cells. These data also question the long-term pacemaking stability of previously reported hESC-CM biological pacemakers that were composed of early stage admixed cells (*52*, *61*).

It is still unclear if hESC-CMs can mature in vitro to match the phenotype of adult cardiomyocytes. We recently reported that hESC-CMs slowly transition to more closely resemble adult myocardium with prolonged in vitro culture (*130*). However, even after four months of culture, hESC-CMs were still distinctly immature. In this study, the majority of early stage MLC2v cells were quiescent. While the mean beating rate trended down over time, the number of quiescent cells did not significantly change. This could indicate that only a subpopulation of MLC2v cells will ever be quiescent, or taken differently, it could mean that only some MLC2v cells are destined to become ventricular cardiomyocytes. This could also be a result of aberrant promoter activation. While the use of lentiviruses to deliver the promoter-specific CRE cassettes is efficient, overtransduction increases the chance of transgene integration into a constitutively translated region. Similarly, aberrant promoter activation could also explain the small proportion of cGATA6 cells that are quiescent.

We believe that this is the first report of purified hESC-CM subtypes. While further experiments are needed to determine the suitability of these populations for cell therapy applications such as a biological pacemaker or ventricular infarct repair, the mTmG-2a-Puro system has proven to be an efficient way to isolate candidate subpopulations. Furthermore, while it is unlikely that genetically modified cells will be used in the clinic, the ability to isolate

large numbers of specific cardiomyocytes opens the door for high throughput cell surface marker screens that could identify subpopulations without the need for genetic modification.

Materials and Methods

Human ESC Cardiac Differentiation

All studies were either performed with the mTmG-2a-Puro RUES2 transgenic hESCs that we have previously reported (*86*) or with H7 hESCs that were stably transfected with the non-selectable mTmG transgene reported by Muzumdar et al. (*103*). The cardiac differentiation of both cell lines was performed as previously described for other hESC lines (*88*, *108*). In brief, undifferentiated hESCs were dispersed to single cells with Versene (Invitrogen) and then plated in a high density monolayer in the presence of MEF-conditioned media supplemented with 5 ng/mL hbFGF. After confluence was reached, the cultures were induced to differentiate by switching to RPMI media (Gibco) containing 100 ng/mL recombinant activin A (R&D Systems), 1:60 diluted Matrigel (BD), and insulin-free B27 supplement (Invitrogen). After 24 hours, the latter media was exchanged with insulin-free RPMI-B27 supplemented with 10 ng/mL recombinant BMP4 (R&D Systems). On days 5 and 7 post-induction with activin A, the cultures were re-fed with insulin-free RPMI-B27 without any exogenous growth factors and then this step was repeated using insulin-containing RPMI-B27 on day 9 and every other day thereafter.

Lentiviral Generation and Transduction

The pPD46.21 plasmid containing the proximal (-1.5/+0.0) promoter-enhancer region of the chicken GATA6 (cGATA6) gene was generously provided by Dr. John Burch (Fox Chase Cancer Center) (*17*). The modified murine muscle creatine kinase promoter CK7 variant was generously provided by Dr. Stephen Hauschka (University of Washington) (*116*). The lentiviral transfer plasmid pJGL2-EGFP and a plasmid containing Cre recombinase were generously

provided by Drs. Jonathan Golob and Charles Murry (University of Washington). The EF1α-CRE lentiviral vector was created by first removing the EGFP sequence from pJGL2-EGFP by restriction enzyme digestion. The CRE recombinase sequence was PCR amplified with appropriate adaptor sequences and ligated into the cut plasmid using the In-Fusion Cloning kit (Clontech). To create the cGATA6-CRE lentiviral vector, the 1.5 kb cGATA6 promoter-enhancer sequence was PCR amplified from pPD46.21 and ligated into the EF1α-CRE vector that had been digested with SalI and AgeI to remove the EF1α promoter. The CK7-CRE plasmid was created in a similar manner with PCR amplification of the CK7 promoter from the plasmid provided by Dr. Hauschka. Finally, the –513 – +47 upstream sequence of the human MLC2v promoter sequence was PCR amplified as previously described (*119*) from human cDNA with the following primers: sense – GGAAGATCTGCCACAGTGCCAGCCTTCATGG, antisense – CCCAAGCTTGTGGAAAGGACCCAGCACTGCC. The PCR amplified MLC2v promoter was then ligated into the EF1α-CRE vector that had been digested with SalI and AgeI to remove the EF1α promoter.

VSV-G-pseudotyped lentiviral particles were generated and concentrated as previously described (*131*, *132*). In brief, $6x10^6$ HEK293 cells seeded on a 15 cm^2 plate 24 hours prior to co-transfection with the following plasmids: 8 μg of envelope plasmid pMK-VSVG, 15 μg of pMDL-G/P-RPE plasmid expressing the HIV-1 *gap*/*pol* and *tat* genes, 11.5 μg of pRSV-REV plasmid expressing the HIV-1 rev protein, and 29 μg of the cGATA6-CRE, EF1α-CRE, CK7-CRE or MLC2v-CRE lentiviral transfer vector construct. Supernatant containing the resultant viral particles was collected at 72 hours following transfection, concentrated 100x using Peg-It (System Biosciences), and stored at -80°C. Lentiviral stocks were titered by viral $p24^{gag}$ ELISA (QuickTiter Lentiviral Quantitation kit, Cell Biolabs).

All lentiviral transduction was performed on differentiation day 15. Briefly, hESC-CMs were harvested into a single cell suspension using trypsin (see section: Replating hESC-CMs).

hESC-CMs were incubated in suspension with 5000 lentiviral particles per cell at a concentration of $4x10^6$ cells/mL in RPMI-B27 media for 30 minutes at 37°C with occasional agitation. Next, fresh RPMI-B27 was added and cells were disbursed onto either a Matrigel (BD) coated plastic or 0.1% PEI/0.6% gelatin-treated glass plating substrate. Media containing lentiviral particles was removed and replaced with lentiviral-free media after 18 hours.

Replating hESC-CMs

The following protocol was used whenever hESC-CMs were replated. Cells were washed with calcium and magnesium free PBS (Gibco) and then incubated with 0.05% trypsin-EDTA supplemented with 200 U/mL DNAse for five to ten minutes at 37°C or until cells were observed to be rounded up and loosely attached to the plate. Next, the cells were gently triturated to a single cell suspension and pipetted directly into a 10x volume of RPMI-B27 supplemented with 20% fetal bovine serum and 200 U/mL DNAse and centrifuged at 300*g* for five minutes. Following centrifugation the cell pellet was resuspended in 10 mL of RPMI-B27 supplemented with 200 U/mL DNAse and centrifuged a second time at 300*g* for five minutes. Cells were subsequently resuspended in the final plating volume of RPMI-B27 supplemented with 10 μM ROCK inhibitor Y-27632 (Sigma) and plated onto either Matrigel (BD) coated tissue culture plastic or 0.1% PEI/0.6% gelatin-treated glass substrates.

Puromycin Selection of GFP^+ mTmG-2a-Puro Cells

GFP-2a-Puro-expressing populations of mTmG-2a-Puro cells were antibiotically selected with puromycin a minimum of one week after lentiviral transduction. Briefly, admixed populations of GFP and tdTomato-expressing hESC-CMs were replated in RPMI-B27 media supplemented with 2 μg/mL puromycin (Invitrogen) onto Matrigel (BD) coated tissue culture plastic at a density of $4x10^4$ cells/cm^2. Twenty-four hours later the media was replaced with

identical media. Forty-eight hours after replating, cells were fed with standard RPMI-B27 media. In total, cells were exposed to 2 μg/mL puromycin for forty-eight hours. Cell death of GFP-2a-Puro-negative populations was not observed until the second twenty-four hour period of puromycin exposure.

Proportion of GFP$^+$ Cells

To measure the proportion of GFP-positive cells in the four lentiviral treatment groups (EF1α-CRE, CK7-CRE, MLC2v-CRE and cGATA6-CRE), transduced populations were replated at low density onto Matrigel (BD) coated tissue culture plastic. GFP-positive and GFP-negative cell populations were counted on a Zeiss Axiovert 200 inverted epifluorescent microscope. A minimum of ten high-powered fields containing a total minimum of 350 cells was counted. High-powered fields were sequentially selected by uniform XY rastering of the microscope stage to minimize bias.

Patch Clamp Studies

hESC-CMs were replated at low density onto 0.1% PEI/0.6% gelatin treated glass coverslips a minimum of five days before patch clamp experiments. Spontaneously generated action potentials (APs) of the hESC-CMs were recorded using a HEKA EPC-10 amplifier (HEKA, Lambrecht, Germany), operated in current-clamp mode. After obtaining a gigaohm seal, electrical access to the cells was obtained via gentle membrane rupture. Patch pipettes with a resistance of 2-4 MΩ were used; cells with a series resistance of >10 MΩ were discarded. The capacitance of all examined cells was 19.3 ± 1.3 pF (range 5.3-91.2 pF), in comparison to the ~150 pF typically reported for adult human ventricular myocytes (*133*). All recordings were performed at 36 ± 1 °C, using the following bath medium: (in mM) 140 NaCl, 5.4 KCl, 1.8 $CaCl_2$, 1.0 $MgCl_2$, 0.33 NaH_2PO_4, 5 dextrose, and 10 HEPES, adjusted to pH 7.40 with NaOH. The

pipette solution was (in mM) 135 KCl, 5 Na_2 creatine phosphate, 5 MgATP and 10 HEPES, adjusted to pH 7.20 with KOH. Data were digitized at 10 Hz and filtered at 2.9 Hz. Action potential parameters were analyzed by an individual blinded to culture conditions, using Patchmaster (HEKA) and IgorPro software.

The voltage clamp studies comparing cGATA6 and MLC2v cells were modeled after a study by Cho et al., which analyzed membrane currents in primary murine sinoatrial myocytes (*123*). After obtaining spontaneous action potential recordings as previously described, each hESC-CM was switched to voltage clamp mode and held at -40 mV with no change in ionic conditions. The cell was then cycled at 0.5 Hz through a series of test potentials ranging from -120 mV to +60 mV at 10 mV intervals; each test potential was 1 second in duration. The magnitude of the resultant initial membrane current was then measured either at the peak of the inward current (in the case of depolarizing test potentials) or 5 milliseconds after the step (hyperpolarizing test potentials). The magnitude of the late membrane current was measured by averaging the current amplitude over the final 15 milliseconds of the test pulse.

Immunostaining

Cells were fixed for ten minutes with 4% paraformaldehyde, permeabilized for seven minutes in PBS containing 0.25% Triton-X, and blocked for one hour in PBS containing either 1.5% normal goat serum or 1.5% normal donkey serum. The endogenous fluorescence of membrane-bound eGFP and tdTomato proteins survived fixation and permeabilization. Primary antibodies were as follows: goat anti-Nkx2.5 polyclonal antibody (1:500, R&D Systems, Cat#: AF2444), rabbit anti-KCNJ5 polyclonal antibody (1:500, Abcam, Cat#: ab75238), rabbit anti-MYL2 polyclonal antibody (1:100, ProtenTech, Cat#: 10906-1-AP), mouse anti-HCN4 monoclonal antibody (1:100, NeuroMab, Cat#: 75-150), mouse anti-TBX3 monoclonal antibody (1:500, Novus Biosciences, Cat#: H00006926-M06), mouse anti-ACTN2 monoclonal antibody

(1:500, Abcam, Cat#: ab9465). Cells were incubated with species appropriate AlexaFluor 680 secondary antibodies (1:100, Molecular Probes). Nuclei were counterstained in PBS containing a 1:1000 dilution of Hoechst 33342 (Thermo Scientific). Cells were visualized on a Nikon A1R confocal microscope.

Aggregate Formation

Aggregates of puromycin-selected cells were formed in hanging drop culture. Briefly, cells were trypsinized into a single cell suspension and washed as described above. Cells were counted and resuspended in an appropriate volume of RPMI-B27 media supplemented with 20% fetal bovine serum to concentrations of $5x10^3$, $1x10^4$ or $1.5x10^4$ cells per 25 µL. 25 µL droplets of suspended cells were pipetted onto the sterile inner surface of a 15cm tissue culture dish and carefully inverted onto the lower half of the dish that contained 20 mL of PBS for humidity maintenance. Cells formed tightly packed, spontaneously beating spheroid aggregates after 48-72 hours of hanging drop culture. Single beating aggregates were carefully removed from the hanging drops via pipette and placed into individual wells of a 96-well round bottom ultra low attachment plate containing 250 µL of RPMI-B27 media. 200 µL of media was removed and replaced with fresh media every five days.

Beat Rate Measurement

Single cells: Culture media was replaced 24 hours before beat rate measurement. Beating rates were measured a minimum of five days after replating. Tissue culture dishes containing cells at low density were placed on a 37°C heated stage of an inverted epifluorescent microscope. Beating rates were assessed by counting the number of beats of all GFP^+ cells in a given high powered field during a fifteen second period. A minimum of ten high-powered fields containing a total minimum of 47 cells in each condition was counted. High-powered

fields were sequentially selected by uniform XY rastering of the microscope stage to minimize bias.

Aggregates: Aggregate culture media was replaced 24 hours before beat rate measurement. Beating rates were measured a minimum of five days after aggregate formation. 96-well round bottom ultra low attachment plates containing one aggregate per well were placed on a 37°C heated microscope stage. Beating rates were assessed by counting the number of beats in a given aggregate during a twenty second period. The beating rates of a minimum of eighteen aggregates in each condition were counted.

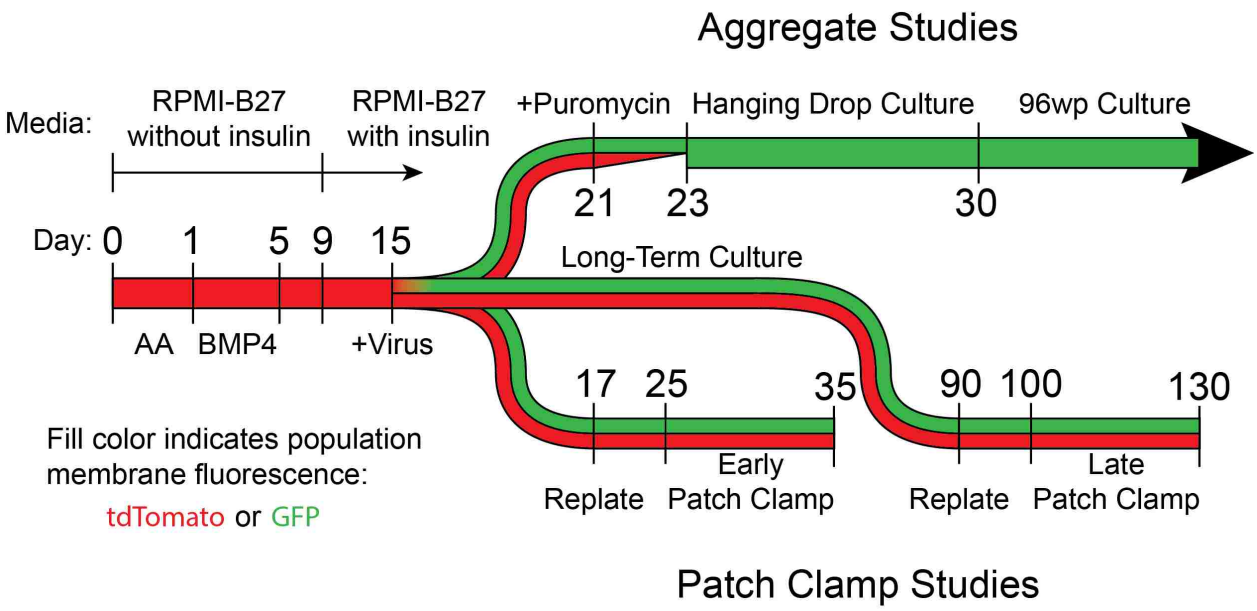
Aggregate Studies
Media:
RPMI-B27 without insulin
RPMI-B27 with insulin
+Puromycin
Hanging Drop Culture
96wp Culture
Day: 0 1 5 9 15
21 23 30
Long-Term Culture
AA BMP4 +Virus
17 25 35 90 100 130
Fill color indicates population membrane fluorescence:
tdTomato or GFP
Early
Replate Patch Clamp
Late
Replate Patch Clamp
Patch Clamp Studies

Figure 3.1: Derivation of Cardiomyocyte Subpopulations for Aggregate and Patch Clamp Studies RUES2 mTmG-2a-Puro and H7 mTmG undifferentiated hESCs were directed toward cardiac differentiation by exposure to activin a for 24 hours (differentiation day 0) followed by 96 hours of exposure to BMP4. Spontaneous beating activity began in cultures between day 9 and day 11. Cells were replated in the presence of lentivirus on day 15 and designated for either aggregate studies or patch clamp studies. H7 mTmG cells served as a control to compare promoter activation between cell lines and were not used in the aggregate or patch clamp studies. Cells for aggregate studies were selected by 48 hours of puromycin treatment starting on day 21. GFP^+ cells were transferred to hanging drop culture after puromycin treatment where they formed tight aggregates (see Figure 3.6). At day 30 aggregates were transferred to 96-well non-adherent round bottom plates for long-term culture. Cells for patch clamp studies were replated at low density on day 17 for early patch clamp studies or day 90 for late patch clamp studies. The fill color of the timeline indicates the expression of membrane-bound fluorescent molecules; GFP fluorescence is only observed after lentiviral-mediated CRE expression. Only GFP^+cells are puromycin-resistant.

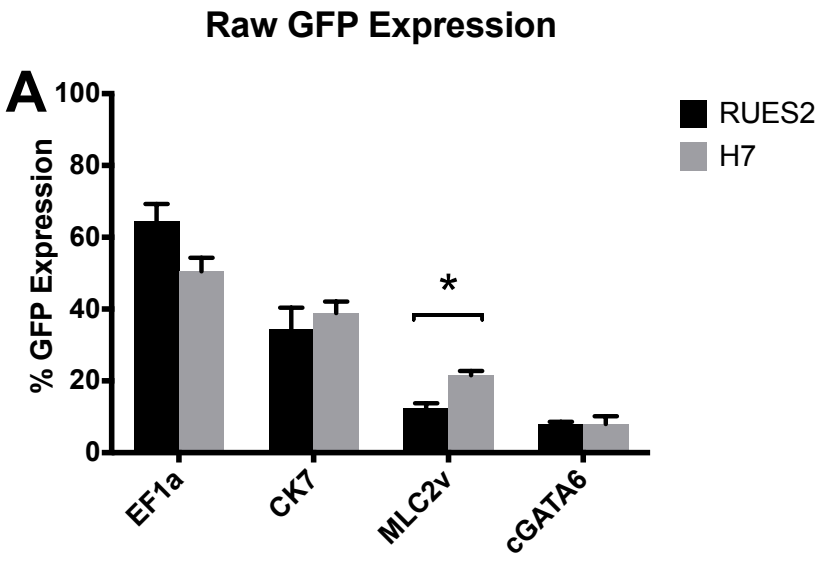
Raw GFP Expression
A
% GFP Expression
100
80
60
40
20
0
*
RUES2
H7
EF1a
CK7
MLC2v
cGATA6

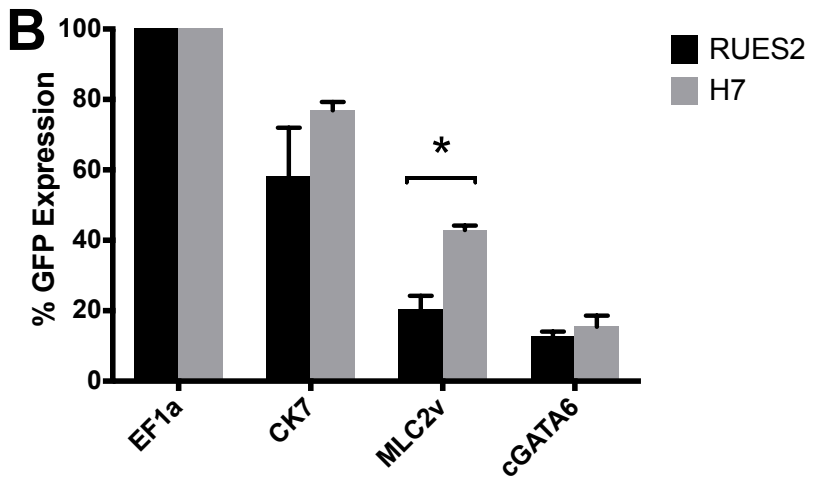
GFP Expression Normalized to EF1α Activation
B
% GFP Expression
100
80
60
40
20
0
*
RUES2
H7
EF1a
CK7
MLC2v
cGATA6

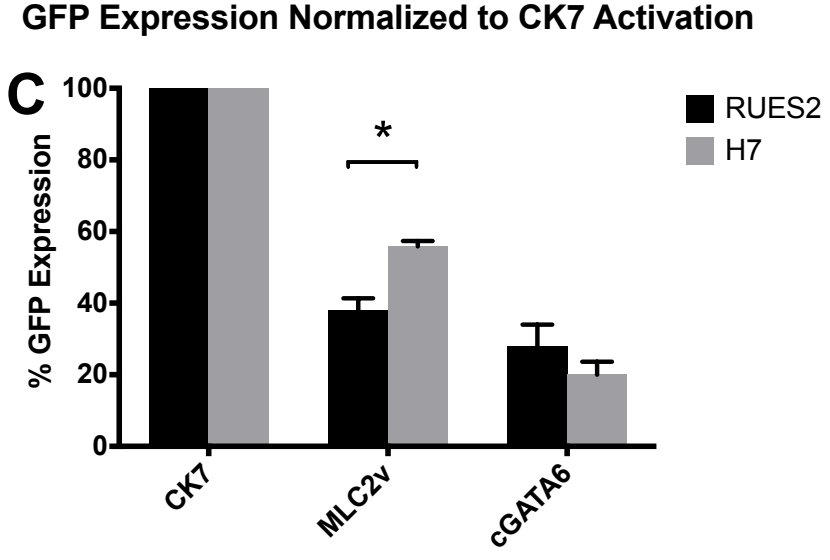
GFP Expression Normalized to CK7 Activation
C
% GFP Expression
100
80
60
40
20
0
*
RUES2
H7
CK7
MLC2v
cGATA6

Figure 3.2: Cardiomyocyte Subtype Proportions Vary With Stem Cell Line (**A**) Absolute percentage of GFP^+ cells in EF1α, CK7, MLC2v, and cGATA6 treated populations of differentiation day 20 RUES2 mTmG-2a-Puro and H7 mTmG hESC-CMs. (**B**) The data from panel (**A**) normalized to EF1α transduction control. (**C**) The data from panel (**A**) normalized to CK7 pan-cardiac control. n = 47 for each condition. Error bars = mean + SEM. * = $P < 0.0001$.

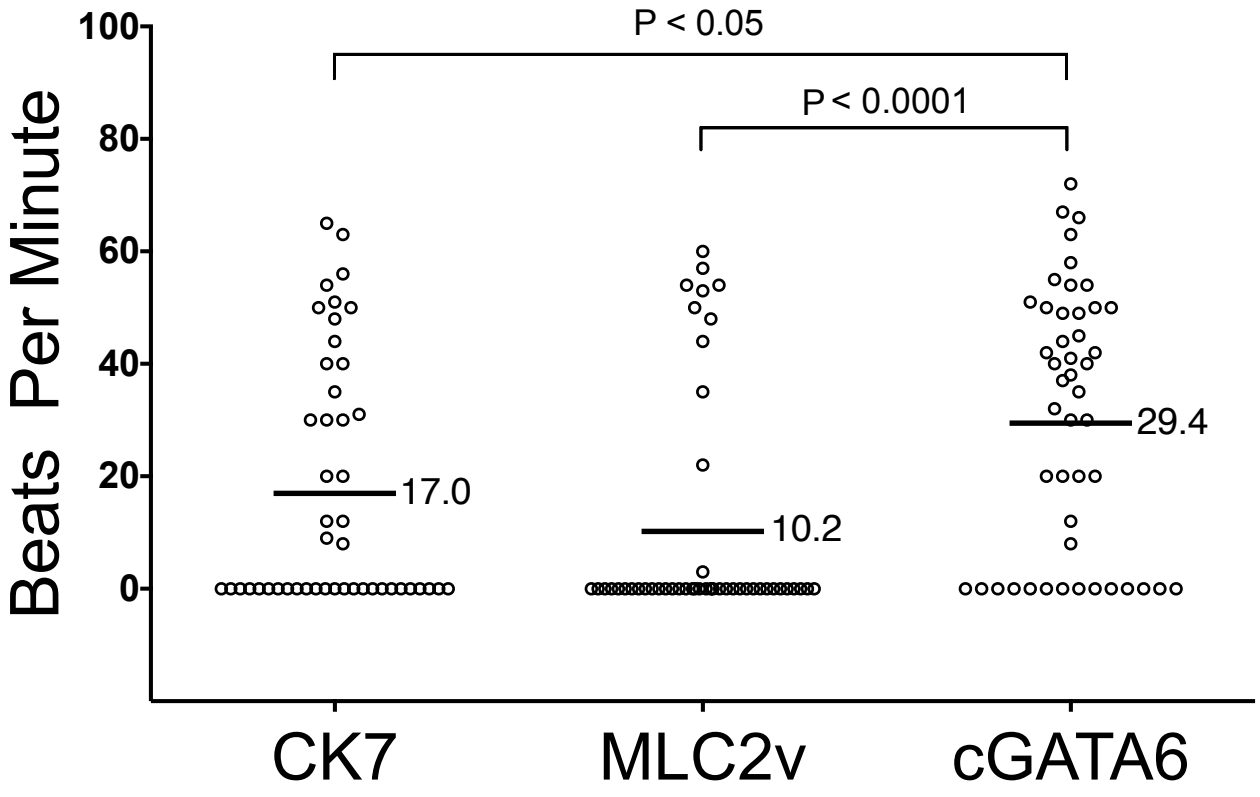
P < 0.05
P < 0.0001
Beats Per Minute
100
80
60
40
20
0
17.0
10.2
29.4
CK7
MLC2v
cGATA6

Figure 3.3: cGATA6 hESC-CMs Beat Faster Than CK7 or MLC2v Cells at Day 20 In vitro spontaneous beating rates (including quiescent cells) of isolated CK7, MLC2v and cGATA6-activating mTmG-2a-Puro hESC-CMs at differentiation day 20. Each point corresponds to one measured cell. n = 47 per group. Error bars = mean ± SEM.

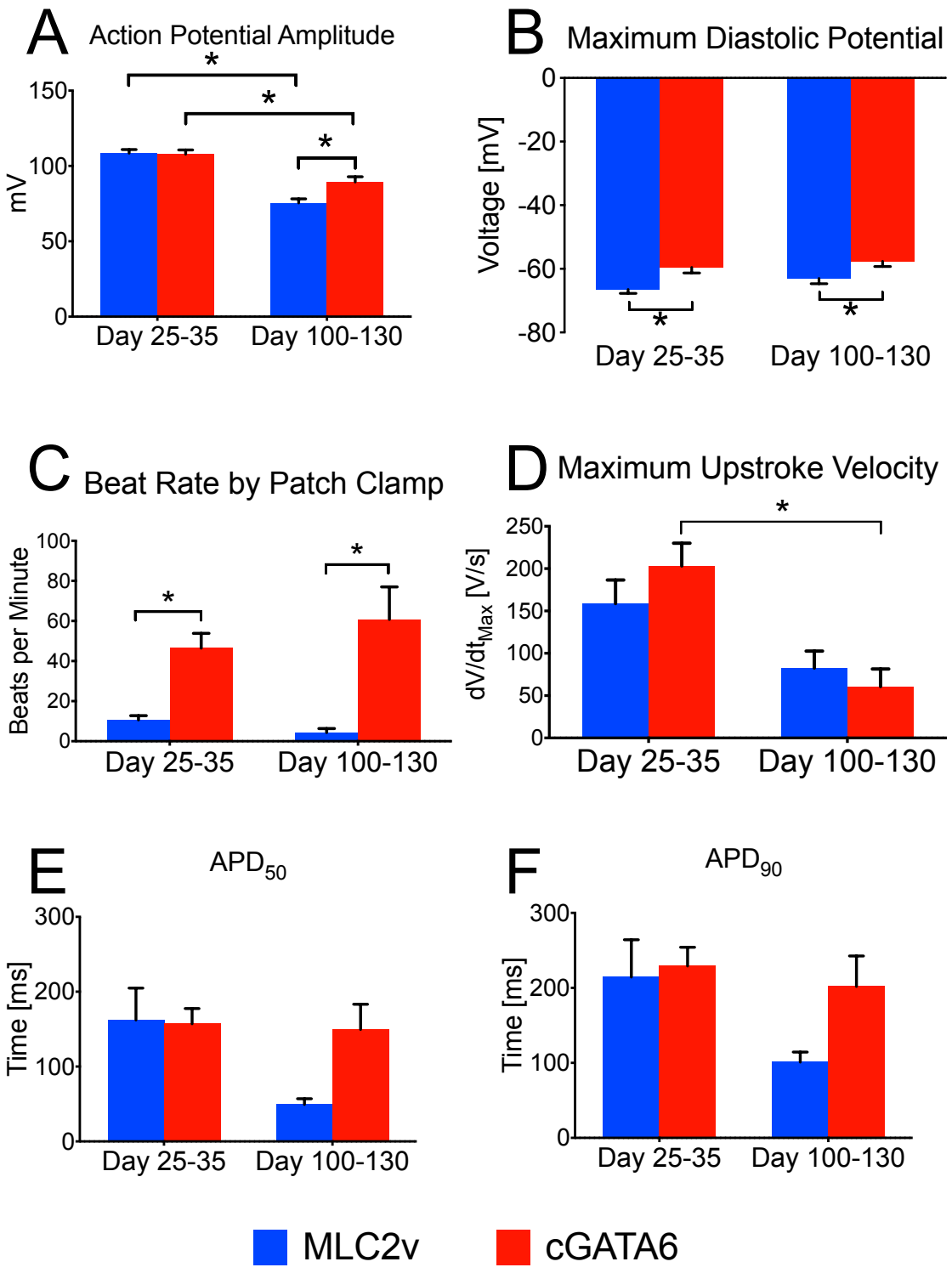
A
Action Potential Amplitude
mV
150
100
50
0
Day 25-35
Day 100-130
B
Maximum Diastolic Potential
Voltage [mV]
0
-20
-40
-60
-80
Day 25-35
Day 100-130
C
Beat Rate by Patch Clamp
Beats per Minute
100
80
60
40
20
0
Day 25-35
Day 100-130
D
Maximum Upstroke Velocity
dV/dtMax [V/s]
250
200
150
100
50
0
Day 25-35
Day 100-130
E
APD50
Time [ms]
300
200
100
0
Day 25-35
Day 100-130
F
APD90
Time [ms]
300
200
100
0
Day 25-35
Day 100-130
MLC2v
cGATA6

Figure 3.4: Action Potential Characteristics of Early and Late-Stage cGATA6 and MLC2v hESC-CMs Early (day 25-35) and late (day 100-130) stage MLC2v (blue bars) and cGATA6 (red bars) hESC-CM action potential characteristics. (**A**) Action potential amplitude. (**B**) Maximum diastolic potential. (**C**) Beating rate (including both spontaneous and quiescent cells). (**D**) Maximum upstroke velocity. Action potential duration at 50% (**E**) and 90% (**F**) repolarization. Cell numbers: cGATA6 early stage n = 24, late stage n = 13. MLC2v early stage n = 27, late stage n = 6. * = $P < 0.001$. Error bars = SEM.

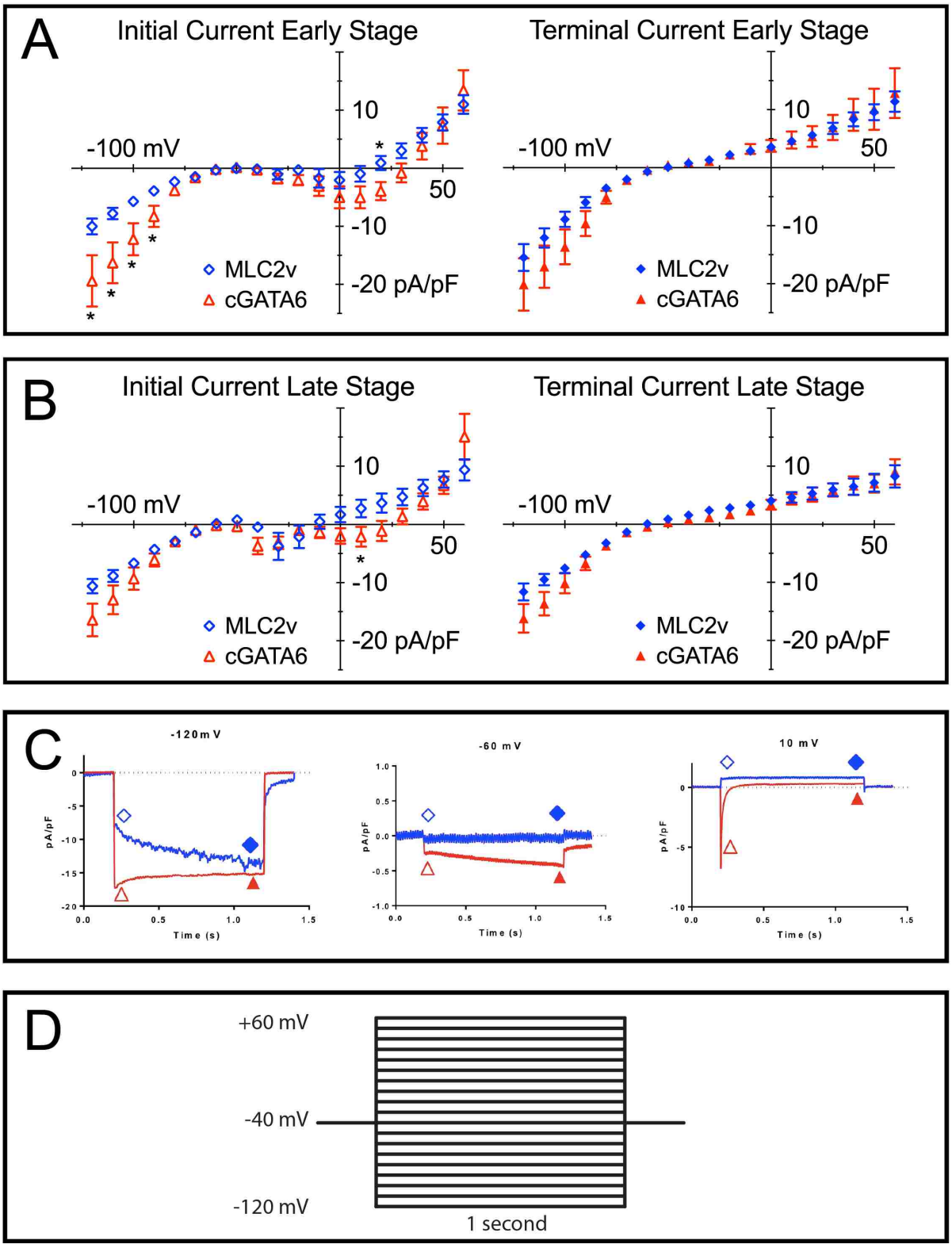
A
Initial Current Early Stage
Terminal Current Early Stage
-100 mV
10
50
-10
-20 pA/pF
MLC2v
cGATA6
B
Initial Current Late Stage
Terminal Current Late Stage
C
-120 mV
-60 mV
10 mV
pA/pF
Time (s)
D
+60 mV
-40 mV
-120 mV
1 second

Figure 3.5: Voltage Clamp Recordings of Early and Late-Stage cGATA6 and MLC2v hESC-CMs After completing current clamp action potential recordings, each cell was switched to voltage clamp mode and stepped at 0.5 Hz from a holding potential of -40 mV to a range of test potentials from -120 mV to +60 mV at 10 mV increments; each test potential lasted 1 second. The resultant membrane currents for each cell (MLC2v: blue, cGATA6: red) were then measured at the beginning (initial) and end (terminal) of each voltage step for both early stage (day 25-35, **A**) and late stage (day 100-130, **B**) cells. (**C**) Representative current traces for MLC2v (blue) and cGATA6 (red) at -120 mV, -60 mV and +10 mV. (**D**) Cells were held at -40 mV before net current was recorded during 1 second test potentials ranging from -120 mV to +60 mV. n = 17 MLC2v early cells, n = 10 cGATA6 early cells, n = 9 MLC2v late cells, n = 8 cGATA6 late cells. * = $p < 0.05$

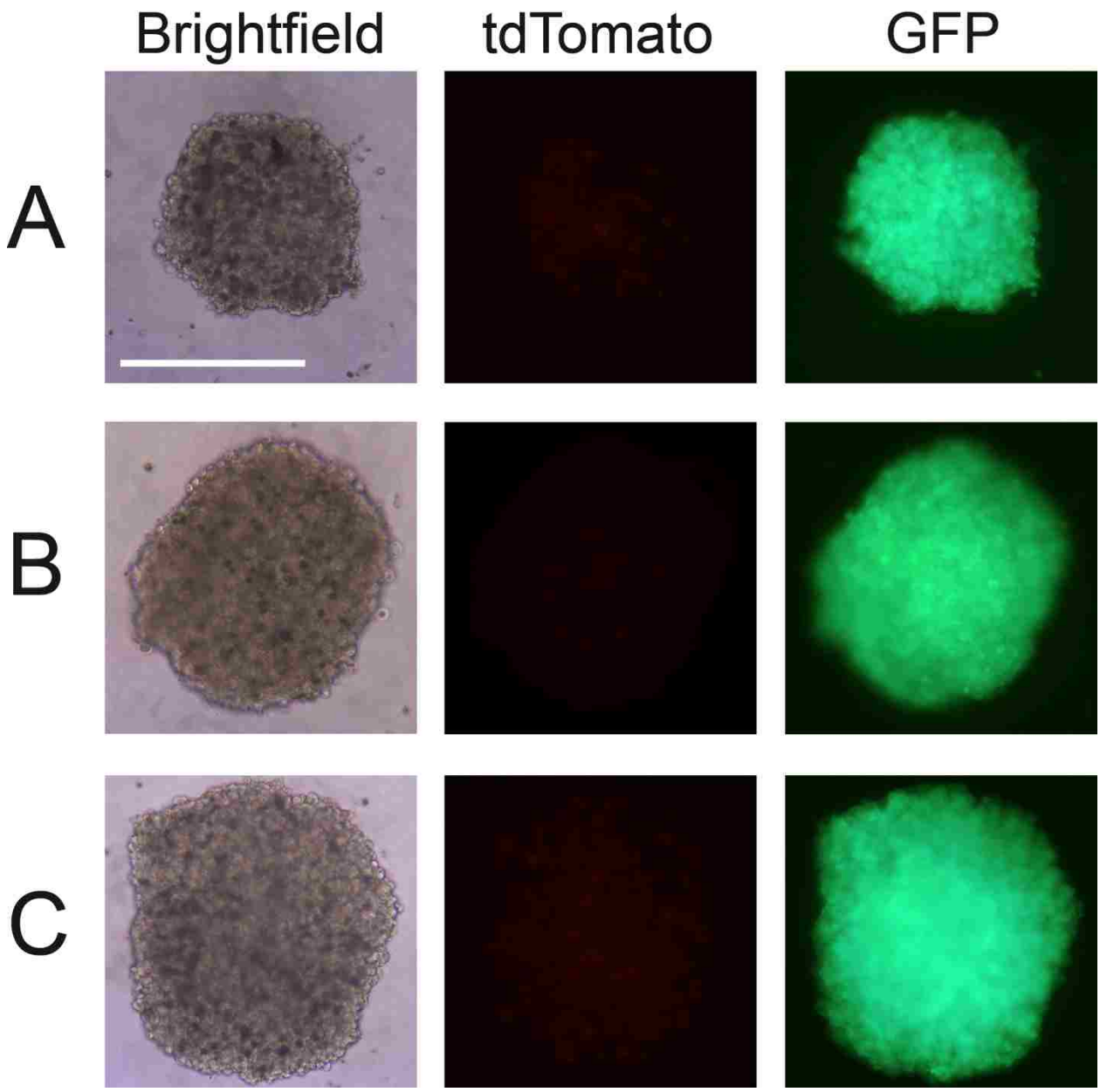
Brightfield
tdTomato
GFP
A
B
C

Figure 3.6: Cellular Aggregates Form Spontaneously in Hanging Drop Culture Brightfield, tdTomato fluorescence and GFP fluorescence photomicrographs of aggregates of (**A**) $5x10^3$, (**B**) $1x10^4$, or (**C**) $1.5x10^4$ puromycin-selected mTmG-2a-Puro hESC-CMs. The beating aggregates spontaneously form in hanging drop culture. Scale bar = 500 μm. All images were collected at the same magnification.

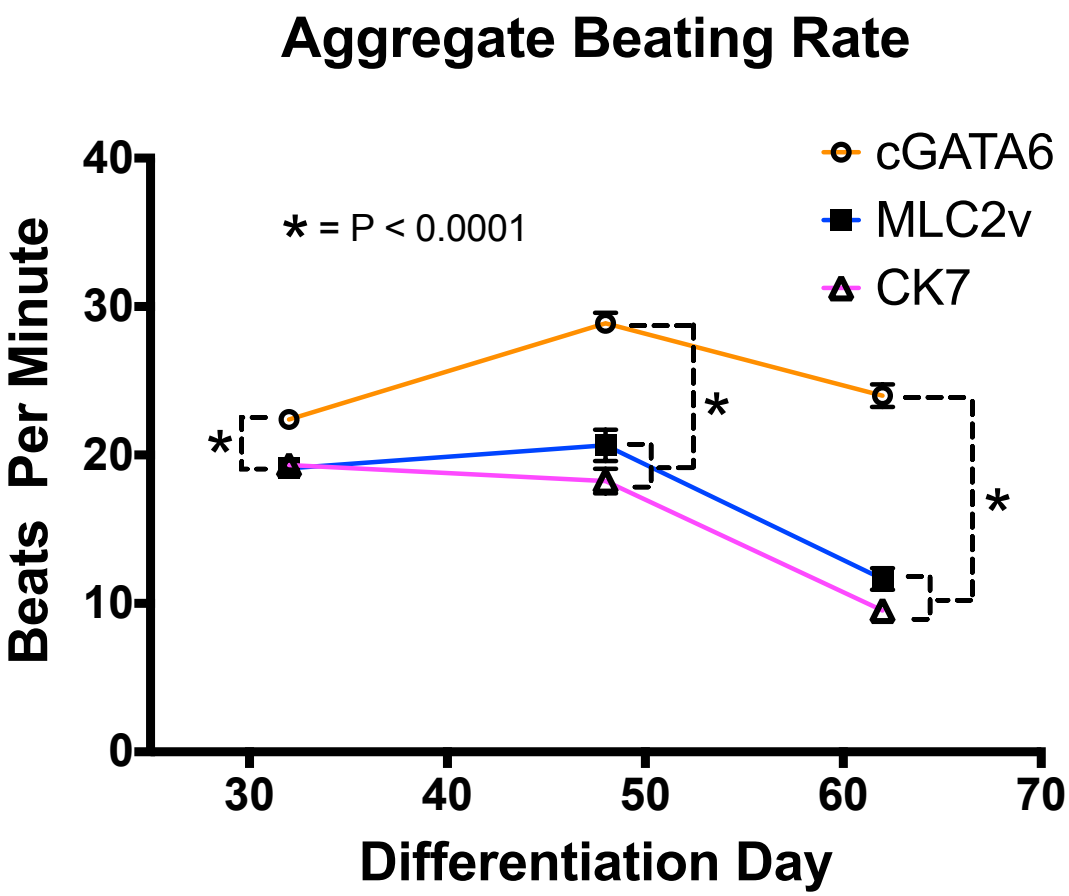
Aggregate Beating Rate
cGATA6
MLC2v
CK7
* = P < 0.0001
Beats Per Minute
40
30
20
10
0
30
40
50
60
70
Differentiation Day
*
*
*

Figure 3.7: Aggregates of cGATA6 hESC-CMs Beat Faster Than Aggregates of MLC2v or CK7 hESC-CMs A graph of the average spontaneous beating rate of Day 32, Day 48 and Day 62 aggregates of purified cGATA6, MLC2v or CK7-marked mTmG-2a-Puro hESC-CMs. n=20-28. Error bars = mean ± SEM.

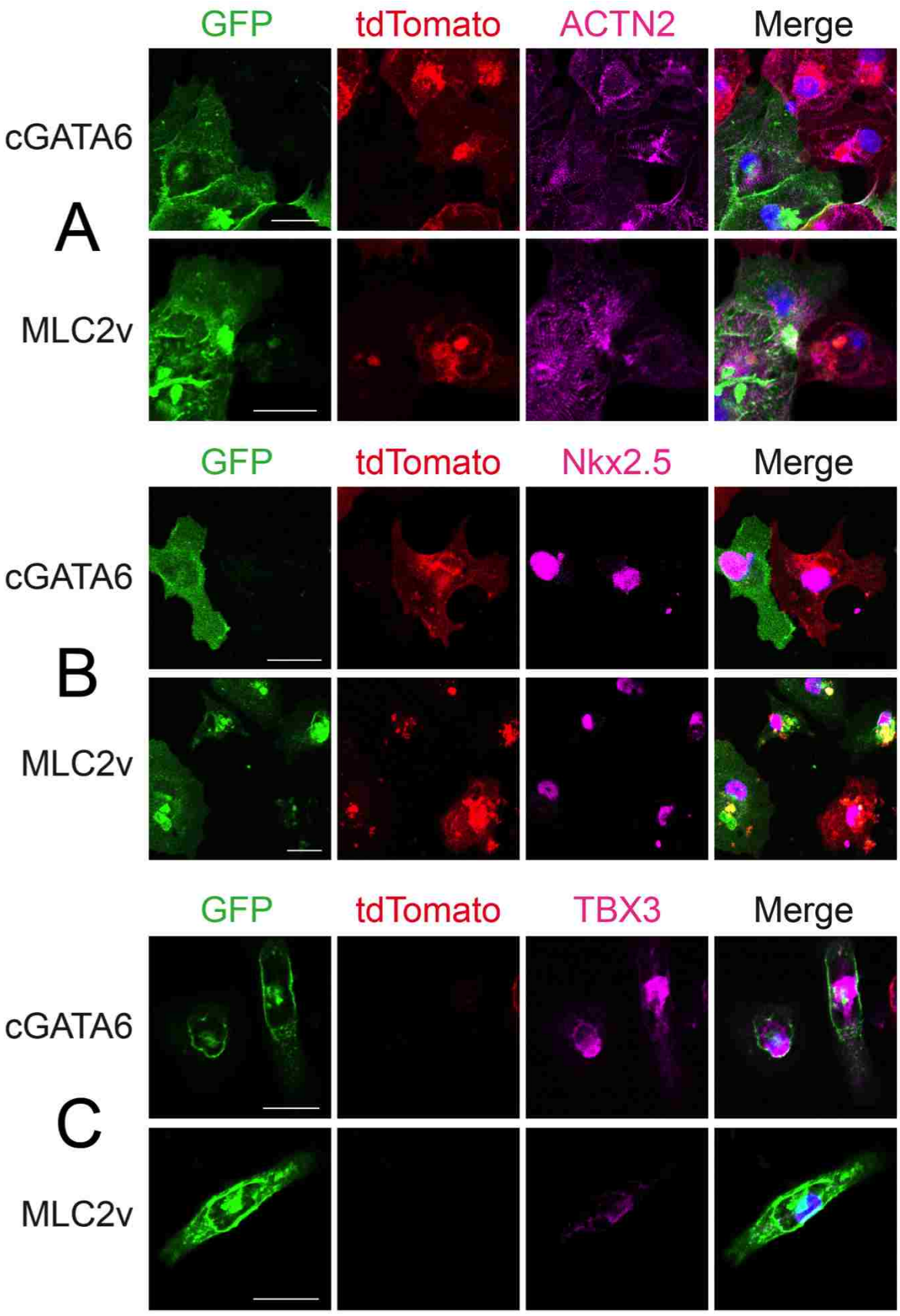
GFP
tdTomato
ACTN2
Merge
cGATA6
A
MLC2v
GFP
tdTomato
Nkx2.5
Merge
cGATA6
B
MLC2v
GFP
tdTomato
TBX3
Merge
cGATA6
C
MLC2v

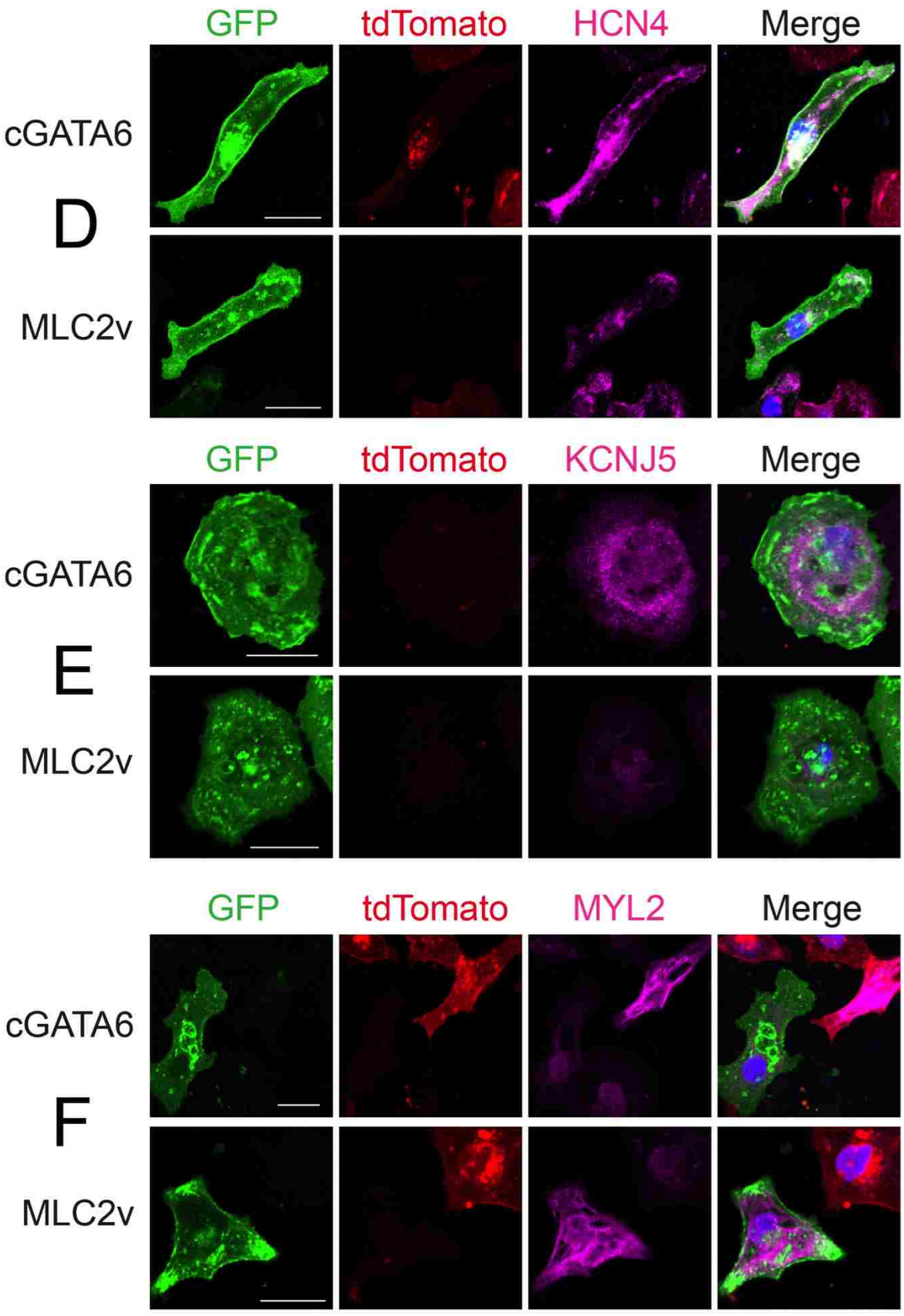
GFP
tdTomato
HCN4
Merge
cGATA6
D
MLC2v
GFP
tdTomato
KCNJ5
Merge
cGATA6
E
MLC2v
GFP
tdTomato
MYL2
Merge
cGATA6
F
MLC2v

Figure 3.8: Immunostaining of cGATA6 and MLC2v hESC-CMs GFP expression indicates activation of either the cGATA6 (top row) or MLC2v (bottom row) promoter in mTmG-2a-Puro hESC-CMs. Cells were immunostained for (**A**) sarcomeric alpha actinin, (**B**) transcription factor Nkx2.5, (**C**) transcription factor Tbx3, (**D**) ion channel HCN4, (**E**) ion channel subunit KCNJ5, (**F**) cardiac myosin MLC2v. Membrane-bound GFP and tdTomato fluorescent proteins were genetically encoded and survived fixation and permeabilization. Scale bars = 25 μm.

Table 1: Primary Antibodies Employed

Antigen	Antibody Type (Clone or Catalog #)	Vendor	Fixative	Titer	Positive Control(s)
ACTN2	Mouse monoclonal (AB9465)	Abcam	PF	1:500	Human myocardium
Nkx2.5	Goat polyclonal (AF2444)	R&D Systems	PF	1:500	Rat and human myocardium
TBX3	Mouse monoclonal (Clone 3A7)	Novus Biosciences	PF	1:500	HEK293 cells
HCN4	Mouse monoclonal (Clone N114/10)	UC Davis / NeuroMab	PF	1:100	Porcine sinoatrial node
KCNJ5	Rabbit polyclonal (AB75238)	Abcam	PF	1:500	A549 cells
MYL2	Rabbit polyclonal (10906)	ProteinTech	PF	1:100	Human myocardium

Abbreviations are as follows: PF = paraformaldehyde

Chapter 4: Conclusions and Implications for Future Studies

In the last decade, cardiac-directed differentiation of human pluripotent stem cells has transformed from crude and inefficient serum-based protocols to highly optimized procedures that introduce signaling agonists and antagonists during specified stages of differentiation. The most recent approaches routinely yield nearly pure populations of cardiomyocytes. While our understanding of the signals that direct cardiac differentiation continues to be refined, the resulting populations remain a heterogeneous mix of multiple cardiomyocyte phenotypes and still contain non-cardiac cells. In this dissertation, I have outlined a novel method of isolating particular subpopulations of differentiating human pluripotent stem cells and used this system to study two subtypes of differentiating cardiomyocytes. The most important result of this work, that the subtype purity of bulk cardiomyocyte populations significantly affects the automaticity and beating rate of the population, has important implications in the design of a biological pacemaker and the selection of candidate populations for cardiac cell therapy. Many, including our group, expect cardiac tissue therapies will require well-characterized cell populations that are electrophysiologically-matched to a given application. For example, if cardiomyocytes used in ventricular infarct repair contain pacemaker cells that demonstrate robust automaticity, the therapy might prove arrhythmogenic. Similarly, as demonstrated in this dissertation, the bulk pacemaking behavior of genetically selected subtypes can be significantly different from an admixed sample.

The mTmG-2a-Puro hESC population described in Chapter 2 can be used to isolate and study any cell lineage derived from hESCs, not just cardiomyocytes. This approach has previously been unavailable in hESCs. Furthermore, when combined with CK7-CRE, mTmG-2a-Puro cells offer an alternative to the technically challenging and often inefficient method of using cell surface antibodies to derive a purified pan-cardiac population. We hope that there will

be interest in the mTmG-2a-Puro cells outside the cardiac arena. We have been encouraged by requests for the cells from labs studying blood disorders, blood cancers and neural regeneration in the short time since we reported the line.

The isolation of cGATA6 and MLC2v hESC-CMs described in Chapter 3 has prompted many questions for further study. What are the significant differences in the gene expression profiles of these populations? How do these profiles change over time? Which ion currents define the cGATA6 and MLC2v action potentials? Do further changes occur after 130 days? Are there cell surface markers that are specific for these populations? Will the cGATA6 cells make a better in vivo biological pacemaker than MLC2v or admixed cells? Will MLC2v cells have a lower incidence of arrhythmia compared to a cGATA6 or pan-cardiac population when used for infarct repair? The ability to purify large numbers of select cells using the mTmG-2a-Puro system opens the door to answering many of these questions.

Previously, we could not determine the electrophysiological phenotype of a cell without using patch clamping, a destructive measurement. By combining genetic selection with the tight correlation between promoter-activation and action potential phenotype we can collect subtype-specific samples of hESC-CM RNA for the first time. We are interested in using an RNASeq approach to compare the gene expression of cGATA6, MLC2v and CK7-selected populations with a particular interest in ion channel expression (*134*). Furthermore, while immunostaining is a useful tool to measure large differences in protein expression, RNASeq is capable of measuring small differences in transcript levels. Serial RNASeq data could outline subtype-specific developmental programs.

In ongoing studies we are examining the hyperpolarization-activated inward current(s) that are prominent in cGATA6 cells. Candidates include I_f, I_{K1}, I_{KACh} and the recently described I_{KCa} currents (*135*), but RNASeq data could inform additional currents to investigate. We are

also isolating what we believe to be calcium currents in both the cGATA6 and MLC2v populations.

Genetically modified cells are unlikely to be approved for use in humans. While genetic modification and selection is a useful tool in the lab, non-invasive techniques such as cell sorting will likely be required to bring cardiac subpopulations to the clinic. Wild type cell sorting depends on the differential expression of cell surface proteins. Immunolabeling or immunocapture of these proteins is then the basis for sorting. While two pan-cardiac cell surface markers have recently been reported and used to purify hESC-CMs, there are no known subtype-specific surface markers. An assay of cell surface markers requires purified populations to compare. With the large-scale purification of candidate subtypes afforded by the mTmG-2a-Puro system, we are in an excellent position to look for subtype-specific cell surface markers. We have established a collaboration with one of the groups that reported a pan-cardiac surface marker and will use the same system to look for subtype-specific markers.

Our group is also planning in vivo studies with the cGATA6 and MLC2v populations. The two previously reported biological pacemakers made of admixed hESC-CMs (*52*, *61*) are encouraging proof-of-concept studies. However, the aggregate data in Chapter 3 suggest a biological pacemaker made of cGATA6 cells would beat faster and maintain this beating rate better than one made from admixed cells.

We recently reported the arrhythmia suppressive effect of transplanting admixed hESC-CMs into the ventricles of injured guinea pig hearts (*136*). We were encouraged by these results and have transitioned this work to a non-human primate model. Surprisingly, preliminary data in the non-human primates suggest an increase in arrhythmias in hearts implanted with admixed hESC-CMs. While the dramatic decrease in beat rate and automaticity seen in single MLC2v cells might support the consideration of an MLC2v experimental cohort, it is important to note that there is no significant difference in beating rate between the MLC2v and CK7

aggregate populations. In fact, these data might support the lack of a need to remove nodal cells from cell therapy populations. However, it is also important to point out that the latest timepoint in the aggregate study was 48 days, which is much closer to the early stage single cell measurements. If the decreasing trend in beat rate seen in the late stage single MLC2v cells is manifested in the ongoing aggregate study, this would support the use of a purified MLC2v population in vivo.

In the last fifteen years, human embryonic stem cell derived cardiomyocytes have progressed from their initial description to become a candidate population for human cardiac cell therapy trials. While this is an astonishing rate of progress, it is important to continue ongoing work characterizing the regenerative potential, phenotypic stability and maturation of these cells. Furthermore, as suggested by the data in this dissertation, it will be important to consider the effect of subtype purity in potential therapeutic cell populations.

References

1. CDC, *Leading Causes of Death, 1900-1998* (1998), p. 67.

2. D. L. Hoyert, D. Ph, J. Xu, V. Statistics, National Vital Statistics Reports Deaths : Preliminary Data for 2011, *CDC* **61** (2012).

3. T. Thom *et al.*, Heart disease and stroke statistics--2006 update: a report from the American Heart Association Statistics Committee and Stroke Statistics Subcommittee., *Circulation* **113**, e85–151 (2006).

4. M. Sylva, M. J. B. van den Hoff, A. F. M. Moorman, Development of the Human Heart., *American journal of medical genetics. Part A* (2013), doi:10.1002/ajmg.a.35896.

5. R. G. Kelly, N. a Brown, M. E. Buckingham, The arterial pole of the mouse heart forms from Fgf10-expressing cells in pharyngeal mesoderm., *Developmental cell* **1**, 435–40 (2001).

6. C.-L. Cai *et al.*, Isl1 identifies a cardiac progenitor population that proliferates prior to differentiation and contributes a majority of cells to the heart., *Developmental cell* **5**, 877–89 (2003).

7. K. L. Waldo *et al.*, Conotruncal myocardium arises from a secondary heart field., *Development (Cambridge, England)* **128**, 3179–88 (2001).

8. V. M. Christoffels *et al.*, Formation of the venous pole of the heart from an Nkx2-5-negative precursor population requires Tbx18., *Circulation research* **98**, 1555–63 (2006).

9. M. T. M. Mommersteeg *et al.*, The sinus venosus progenitors separate and diversify from the first and second heart fields early in development., *Cardiovascular research* **87**, 92–101 (2010).

10. N. Gaborit *et al.*, Regional and tissue specific transcript signatures of ion channel genes in the non-diseased human heart., *The Journal of physiology* **582**, 675–93 (2007).

11. V. M. Christoffels, G. J. Smits, A. Kispert, A. F. M. Moorman, Development of the pacemaker tissues of the heart., *Circulation research* **106**, 240–54 (2010).

12. S. Virágh, C. E. Challice, The development of the conduction system in the mouse embryo heart., *Developmental biology* **80**, 28–45 (1980).

13. R. G. Gourdie, T. Mima, R. P. Thompson, T. Mikawa, Terminal diversification of the myocyte lineage generates Purkinje fibers of the cardiac conduction system., *Development (Cambridge, England)* **121**, 1423–31 (1995).

14. R. G. Gourdie *et al.*, Development of the cardiac pacemaking and conduction system., *Birth defects research. Part C, Embryo today : reviews* **69**, 46–57 (2003).

15. W.-Z. Zhu *et al.*, Neuregulin/ErbB signaling regulates cardiac subtype specification in differentiating human embryonic stem cells., *Circulation research* **107**, 776–86 (2010).

16. V. M. Christoffels, A. F. M. Moorman, Development of the cardiac conduction system: why are some regions of the heart more arrhythmogenic than others?, *Circulation. Arrhythmia and electrophysiology* **2**, 195–207 (2009).

17. D. L. Davis *et al.*, A GATA-6 gene heart-region-specific enhancer provides a novel means to mark and probe a discrete component of the mouse cardiac conduction system., *Mechanisms of development* **108**, 105–19 (2001).

18. C. Logan, W. K. Khoo, D. Cado, a L. Joyner, Two enhancer regions in the mouse En-2 locus direct expression to the mid/hindbrain region and mandibular myoblasts., *Development (Cambridge, England)* **117**, 905–16 (1993).

19. S. Rentschler *et al.*, Visualization and functional characterization of the developing murine cardiac conduction system., *Development (Cambridge, England)* **128**, 1785–92 (2001).

20. S. Kupershmidt *et al.*, Replacement by Homologous Recombination of the minK Gene With lacZ Reveals Restriction of minK Expression to the Mouse Cardiac Conduction System, *Circulation Research* **84**, 146–152 (1999).

21. F. A. Ismat *et al.*, Homeobox protein Hop functions in the adult cardiac conduction system., *Circulation research* **96**, 898–903 (2005).

22. F. Chen *et al.*, Hop is an unusual homeobox gene that modulates cardiac development., *Cell* **110**, 713–23 (2002).

23. R. Di Lisi *et al.*, An atrioventricular canal domain defined by cardiac troponin I transgene expression in the embryonic myocardium., *Anatomy and embryology* **202**, 95–101 (2000).

24. L. Miquerol *et al.*, Architectural and functional asymmetry of the His-Purkinje system of the murine heart., *Cardiovascular research* **63**, 77–86 (2004).

25. M. L. Bakker *et al.*, A novel fluorescent marker for molecular, structural and functional analysis of the cardiac conduction system, *Abstracts ingediend voor het Amsterdam Kindersymposium* , 19 (2013).

26. D. Scherf, A. Schott, *Extrasystoles and allied arrhythmias* (Heinemann Medical, 1973).

27. G. Schram, Differential Distribution of Cardiac Ion Channel Expression as a Basis for Regional Specialization in Electrical Function, *Circulation Research* **90**, 939–950 (2002).

28. E. G. Lakatta, D. DiFrancesco, What keeps us ticking: a funny current, a calcium clock, or both?, *Journal of molecular and cellular cardiology* **47**, 157–70 (2009).

29. CDC, *2009 Mortality Multiple Cause Micro-data Files* (2009).

30. J. Vogler, G. Breithardt, L. Eckardt, Bradyarrhythmias and Conduction Blocks, *Revista Española de Cardiología (English Edition)* **65**, 656–667 (2012).

31. G. F. Tomaselli, in *Harrison's Principles of Internal Medicine*, F. AS, Ed. (The McGraw Hill Companies, New York, NY, 2008), pp. 132–146.

32. G. D. Nelson, A brief history of cardiac pacing., *Texas Heart Institute journal / from the Texas Heart Institute of St. Luke's Episcopal Hospital, Texas Children's Hospital* **20**, 12–8 (1993).

33. P. M. Zoll, Resuscitation of the Heart in Ventricular Standstill by External Electric Stimulation, *New England Journal of Medicine* **247**, 768–771 (1952).

34. G. V. L. Lillehei C Hodges PC, Jr., Long DM, Bakken EE, TRansistor pacemaker for treatment of complete atrioventricular dissociation, *Journal of the American Medical Association* **172**, 2006–2010 (1960).

35. R. Elmgvist, J. Landegren, S. O. Pettersson, A. Senning, G. William-Olsson, Artificial pacemaker for treatment of Adams-Stokes syndrome and slow heart rate, *American Heart Journal* **65**, 731–748 (1963).

36. W. Greatbatch, C. F. Holmes, History of implantable devices, *Engineering in Medicine and Biology Magazine, IEEE* **10**, 38–41 (1991).

37. M. R. Rosen, P. R. Brink, I. S. Cohen, R. B. Robinson, Cardiac pacing: from biological to electronic ... to biological?, *Circulation. Arrhythmia and electrophysiology* **1**, 54–61 (2008).

38. A. Voigt, A. Shalaby, S. Saba, Cardiac rhythm management device infections in the United States from 1996 through 2003. An epidemic on the rise?, *Heart Rhythm Society 2006 Scientific Sessions* (2006).

39. J. M. Edelberg, W. C. Aird, R. D. Rosenberg, Enhancement of murine cardiac chronotropy by the molecular transfer of the human beta2 adrenergic receptor cDNA., *The Journal of Clinical Investigation* **101**, 337–43 (1998).

40. J. M. Edelberg, D. T. Huang, M. E. Josephson, R. D. Rosenberg, Molecular enhancement of porcine cardiac chronotropy., *Heart (British Cardiac Society)* **86**, 559–62 (2001).

41. J. Miake, E. Marbán, H. B. Nuss, Biological pacemaker created by gene transfer, *Nature* **419**, 132–133 (2002).

42. J. Qu *et al.*, Expression and Function of a Biological Pacemaker in Canine Heart, *Circulation* **107**, 1106–1109 (2003).

43. A. N. Plotnikov *et al.*, Biological pacemaker implanted in canine left bundle branch provides ventricular escape rhythms that have physiologically acceptable rates., *Circulation* **109**, 506–12 (2004).

44. A. Bucchi *et al.*, Wild-type and mutant HCN channels in a tandem biological-electronic cardiac pacemaker., *Circulation* **114**, 992–9 (2006).

45. H.-F. Tse *et al.*, Bioartificial sinus node constructed via in vivo gene transfer of an engineered pacemaker HCN Channel reduces the dependence on electronic pacemaker in a sick-sinus syndrome model., *Circulation* **114**, 1000–11 (2006).

46. E. Cingolani *et al.*, Biological pacemaker created by percutaneous gene delivery via venous catheters in a porcine model of complete heart block., *Heart rhythm : the official journal of the Heart Rhythm Society* **9**, 1310–8 (2012).

47. N. Kapoor, W. Liang, E. Marbán, H. C. Cho, Direct conversion of quiescent cardiomyocytes to pacemaker cells by expression of Tbx18., *Nature biotechnology* **31**, 54–62 (2013).

48. G. J. J. Boink *et al.*, HCN2/SkM1 Gene Transfer Into Canine Left Bundle Branch Induces Stable, Autonomically Responsive Biological Pacing at Physiological Heart Rates., *Journal of the American College of Cardiology* **61**, 1192–1201 (2013).

49. I. Potapova *et al.*, Human mesenchymal stem cells as a gene delivery system to create cardiac pacemakers., *Circulation research* **94**, 952–9 (2004).

50. A. N. Plotnikov *et al.*, Xenografted adult human mesenchymal stem cells provide a platform for sustained biological pacemaker function in canine heart., *Circulation* **116**, 706–13 (2007).

51. V. Valiunas *et al.*, Coupling an HCN2-expressing cell to a myocyte creates a two-cell pacing unit., *The Journal of physiology* **587**, 5211–26 (2009).

52. I. Kehat *et al.*, Electromechanical integration of cardiomyocytes derived from human embryonic stem cells, *Nature biotechnology* **22**, 1282–1289 (2004).

53. T. Xue *et al.*, Functional integration of electrically active cardiac derivatives from genetically engineered human embryonic stem cells with quiescent recipient ventricular cardiomyocytes: insights into the development of cell-based pacemakers., *Circulation* **111**, 11–20 (2005).

54. D. K. Lieu *et al.*, Overexpression of HCN-encoded pacemaker current silences bioartificial pacemakers., *Heart rhythm : the official journal of the Heart Rhythm Society* **5**, 1310–7 (2008).

55. R. de Martin, M. Raidl, E. Hofer, B. R. Binder, Adenovirus-mediated expression of green fluorescent protein., *Gene therapy* **4**, 493–5 (1997).

56. M. R. Rosen, R. B. Robinson, P. R. Brink, I. S. Cohen, The road to biological pacing., *Nature reviews. Cardiology* **8**, 656–66 (2011).

57. I. Kehat *et al.*, Human embryonic stem cells can differentiate into myocytes with structural and functional properties of cardiomyocytes, *J Clin Invest* **108**, 407–414 (2001).

58. L. Sartiani *et al.*, Developmental changes in cardiomyocytes differentiated from human embryonic stem cells: a molecular and electrophysiological approach., *Stem cells (Dayton, Ohio)* **25**, 1136–44 (2007).

59. J.-Q. He, Y. Ma, Y. Lee, J. a Thomson, T. J. Kamp, Human embryonic stem cells develop into multiple types of cardiac myocytes: action potential characterization., *Circulation research* **93**, 32–9 (2003).

60. W.-Z. Zhu, L. F. Santana, M. A. Laflamme, Local control of excitation-contraction coupling in human embryonic stem cell-derived cardiomyocytes., *PloS one* **4**, e5407 (2009).

61. T. Xue *et al.*, Functional integration of electrically active cardiac derivatives from genetically engineered human embryonic stem cells with quiescent recipient ventricular cardiomyocytes: insights into the development of cell-based pacemakers, *Circulation* **111**, 11–20 (2005).

62. M. R. Rosen, P. R. Brink, I. S. Cohen, R. B. Robinson, Genes, stem cells and biological pacemakers., *Cardiovascular research* **64**, 12–23 (2004).

63. M. R. Boyett, H. Honjo, I. Kodama, The sinoatrial node, a heterogeneous pacemaker structure., *Cardiovascular research* **47**, 658–87 (2000).

64. M. J. Evans, M. H. Kaufman, Establishment in culture of pluripotential cells from mouse embryos, *Nature* **292**, 154–156 (1981).

65. G. R. Martin, Isolation of a pluripotent cell line from early mouse embryos cultured in medium conditioned by teratocarcinoma stem cells., *Proceedings of the National Academy of Sciences of the United States of America* **78**, 7634–8 (1981).

66. J. A. Thomson *et al.*, Embryonic Stem Cell Lines Derived from Human Blastocysts, *Science* **282**, 1145–1147 (1998).

67. C. Xu *et al.*, Feeder-free growth of undifferentiated human embryonic stem cells., *Nature biotechnology* **19**, 971–4 (2001).

68. T. Vazin, W. J. Freed, Human embryonic stem cells: derivation, culture, and differentiation: a review., *Restorative neurology and neuroscience* **28**, 589–603 (2010).

69. U. Nations, *International convention against the reproductive cloning of human beings* (United Nations, Fifty-ninth session, 2005), pp. 1–8.

70. G. Q. Daley *et al.*, Broader implications of defining standards for the pluripotency of iPSCs., *Cell stem cell* **4**, 200–1; author reply 202 (2009).

71. F.-J. Müller *et al.*, A bioinformatic assay for pluripotency in human cells., *Nature methods* **8**, 315–7 (2011).

72. C. Allegrucci, L. E. Young, Differences between human embryonic stem cell lines., *Human reproduction update* **13**, 103–20 (2007).

73. D. L. Stocum, Amphibian regeneration and stem cells., *Current topics in microbiology and immunology* **280**, 1–70 (2004).

74. C. Jopling *et al.*, Zebrafish heart regeneration occurs by cardiomyocyte dedifferentiation and proliferation., *Nature* **464**, 606–9 (2010).

75. K. Takahashi, S. Yamanaka, Induction of pluripotent stem cells from mouse embryonic and adult fibroblast cultures by defined factors.*Cell* **126**, 663–76 (2006).

76. K. Takahashi *et al.*, Induction of pluripotent stem cells from adult human fibroblasts by defined factors, *Cell* **131**, 861–872 (2007).

77. J. Yu *et al.*, Induced pluripotent stem cell lines derived from human somatic cells., *Science (New York, N.Y.)* **318**, 1917–20 (2007).

78. T. Zhao, Z.-N. Zhang, Z. Rong, Y. Xu, Immunogenicity of induced pluripotent stem cells., *Nature* **474**, 212–5 (2011).

79. P. Guha, J. W. Morgan, G. Mostoslavsky, N. P. Rodrigues, A. S. Boyd, Lack of immune response to differentiated cells derived from syngeneic induced pluripotent stem cells.*Cell stem cell* **12**, 407–12 (2013).

80. N. Malik, M. S. Rao, *Pluripotent Stem Cells* U. Lakshmipathy, M. C. Vemuri, Eds. (Humana Press, Totowa, NJ, 2013), pp. 23–33.

81. K. R. Thomas, K. R. Folger, M. R. Capecchi, High frequency targeting of genes to specific sites in the mammalian genome., *Cell* **44**, 419–28 (1986).

82. J. Collin, M. Lako, Concise review: putting a finger on stem cell biology: zinc finger nuclease-driven targeted genetic editing in human pluripotent stem cells., *Stem cells (Dayton, Ohio)* **29**, 1021–33 (2011).

83. A. J. Bogdanove, D. F. Voytas, TAL effectors: customizable proteins for DNA targeting., *Science (New York, N.Y.)* **333**, 1843–6 (2011).

84. F. D. Urnov *et al.*, Highly efficient endogenous human gene correction using designed zinc-finger nucleases, *Nature* **435**, 646–651 (2005).

85. D. Hockemeyer *et al.*, Efficient targeting of expressed and silent genes in human ESCs and iPSCs using zinc-finger nucleases, *Nature biotechnology* **27**, 851–857 (2009).

86. J. A. Gantz *et al.*, Targeted genomic integration of a selectable floxed dual fluorescence reporter in human embryonic stem cells., *PloS one* **7**, e46971 (2012).

87. L. Cheng, B. Blazar, K. High, M. Porteus, Zinc fingers hit off target., *Nature medicine* **17**, 1192–3 (2011).

88. M. A. Laflamme *et al.*, Cardiomyocytes derived from human embryonic stem cells in pro-survival factors enhance function of infarcted rat hearts, *Nature biotechnology* **25**, 1015–1024 (2007).

89. L. Yang *et al.*, Human cardiovascular progenitor cells develop from a KDR+ embryonic-stem-cell-derived population, *Nature* **453**, 524–528 (2008).

90. J. Zhang *et al.*, Extracellular matrix promotes highly efficient cardiac differentiation of human pluripotent stem cells: the matrix sandwich method., *Circulation research* **111**, 1125–36 (2012).

91. S. Ueno *et al.*, Biphasic role for Wnt/beta-catenin signaling in cardiac specification in zebrafish and embryonic stem cells., *Proceedings of the National Academy of Sciences of the United States of America* **104**, 9685–90 (2007).

92. X. Lian *et al.*, Directed cardiomyocyte differentiation from human pluripotent stem cells by modulating Wnt/β-catenin signaling under fully defined conditions., *Nature protocols* **8**, 162–75 (2013).

93. K. B. Pasumarthi, L. J. Field, Cardiomyocyte enrichment in differentiating ES cell cultures: strategies and applications., *Methods in molecular biology (Clifton, N.J.)* **185**, 157–68 (2002).

94. P. W. Zandstra *et al.*, Scalable production of embryonic stem cell-derived cardiomyocytes., *Tissue engineering* **9**, 767–78 (2003).

95. C. Xu, S. Police, M. Hassanipour, J. D. Gold, Cardiac bodies: a novel culture method for enrichment of cardiomyocytes derived from human embryonic stem cells., *Stem cells and development* **15**, 631–9 (2006).

96. H. Kita-Matsuo *et al.*, Lentiviral vectors and protocols for creation of stable hESC lines for fluorescent tracking and drug resistance selection of cardiomyocytes., *PloS one* **4**, e5046 (2009).

97. F. C. Pascut, H. T. Goh, V. George, C. Denning, I. Notingher, Toward label-free Raman-activated cell sorting of cardiomyocytes derived from human embryonic stem cells.*Journal of biomedical optics* **16**, 045002 (2011).

98. N. C. Dubois *et al.*, SIRPA is a specific cell-surface marker for isolating cardiomyocytes derived from human pluripotent stem cells., *Nature biotechnology* **29**, 1011–1018 (2011).

99. H. Uosaki *et al.*, F. Prosper, Ed. Efficient and Scalable Purification of Cardiomyocytes from Human Embryonic and Induced Pluripotent Stem Cells by VCAM1 Surface Expression, *PLoS ONE* **6**, e23657 (2011).

100. H. AS, Resuscitation of the stopped heart by intracardiac therapy, *Archives of Internal Medicine* **46**, 553–568 (1930).

101. S. Furman, D. J. W. Escher, Principles and techniques of cardiac pacing, 269 p. (1970).

102. A. Nagy, L. Mar, G. Watts, W. Wurst, R. Kühn, Eds. Gene Knockout Protocols, **530** (2009), doi:10.1007/978-1-59745-471-1.

103. M. D. Muzumdar, B. Tasic, K. Miyamichi, L. Li, L. Luo, A global double-fluorescent Cre reporter mouse., *Genesis (New York, N.Y. : 2000)* **45**, 593–605 (2007).

104. J. C. Moore *et al.*, Human embryonic stem cells: Genetic manipulation on the way to cardiac cell therapies, *Reproductive Toxicology* **20**, 377–391 (2005).

105. C.-G. Liew, J. S. Draper, J. Walsh, H. Moore, P. W. Andrews, Transient and stable transgene expression in human embryonic stem cells., *Stem cells (Dayton, Ohio)* **25**, 1521–8 (2007).

106. M. Gropp, Stable genetic modification of human embryonic stem cells by lentiviral vectors, *Molecular Therapy* **7**, 281–287 (2003).

107. R. van Rensburg *et al.*, Chromatin structure of two genomic sites for targeted transgene integration in induced pluripotent stem cells and hematopoietic stem cells., *Gene therapy* **20**, 201–14 (2013).

108. W. Zhu, B. Van Biber, M. A. Laflamme, P. H. Schwartz, R. L. Wesselschmidt, Eds. Methods for the derivation and use of cardiomyocytes from human pluripotent stem cells, *Methods in Molecular Biology* **767**, 419–431 (2011).

109. S. L. Amacher, J. N. Buskin, S. D. Hauschka, Multiple regulatory elements contribute differentially to muscle creatine kinase enhancer activity in skeletal and cardiac muscle., *Molecular and cellular biology* **13**, 2753–64 (1993).

110. J. E. Johnson, B. J. Wold, S. D. Hauschka, Muscle creatine kinase sequence elements regulating skeletal and cardiac muscle expression in transgenic mice., *Molecular and cellular biology* **9**, 3393–9 (1989).

111. M. a Laflamme, C. E. Murry, Heart regeneration., *Nature* **473**, 326–35 (2011).

112. L. Nolden *et al.*, Site-specific recombination in human embryonic stem cells induced by cell-permeant Cre recombinase, *Nature methods* **3**, 461–467 (2006).

113. Y. Xu *et al.*, Revealing a core signaling regulatory mechanism for pluripotent stem cell survival and self-renewal by small molecules., *Proceedings of the National Academy of Sciences of the United States of America* **107**, 8129–34 (2010).

114. A. Rosa, F. M. Spagnoli, A. H. Brivanlou, The miR-430/427/302 family controls mesendodermal fate specification via species-specific target selection., *Developmental cell* **16**, 517–27 (2009).

115. D. James, S. a Noggle, T. Swigut, A. H. Brivanlou, Contribution of human embryonic stem cells to mouse blastocysts., *Developmental biology* **295**, 90–102 (2006).

116. M. Z. Salva *et al.*, Design of tissue-specific regulatory cassettes for high-level rAAV-mediated expression in skeletal and cardiac muscle., *Molecular therapy : the journal of the American Society of Gene Therapy* **15**, 320–9 (2007).

117. E. Poon, C.-W. Kong, R. a Li, Human pluripotent stem cell-based approaches for myocardial repair: from the electrophysiological perspective., *Molecular pharmaceutics* **8**, 1495–504 (2011).

118. C. Z. He, J. B. Burch, The chicken GATA-6 locus contains multiple control regions that confer distinct patterns of heart region-specific expression in transgenic mouse embryos., *The Journal of biological chemistry* **272**, 28550–6 (1997).

119. I. Huber *et al.*, Identification and selection of cardiomyocytes during human embryonic stem cell differentiation., *FASEB journal : official publication of the Federation of American Societies for Experimental Biology* **21**, 2551–63 (2007).

120. S. M. Chuva de Sousa Lopes *et al.*, Patterning the heart, a template for human cardiomyocyte development., *Developmental dynamics : an official publication of the American Association of Anatomists* **235**, 1994–2002 (2006).

121. M. Pashmforoush *et al.*, Nkx2-5 pathways and congenital heart disease; loss of ventricular myocyte lineage specification leads to progressive cardiomyopathy and complete heart block., *Cell* **117**, 373–86 (2004).

122. M. Müller *et al.*, Selection of ventricular-like cardiomyocytes from ES cells in vitro., *FASEB journal : official publication of the Federation of American Societies for Experimental Biology* **14**, 2540–8 (2000).

123. H.-S. Cho, M. Takano, A. Noma, The electrophysiological properties of spontaneously beating pacemaker cells isolated from mouse sinoatrial node., *The Journal of physiology* **550**, 169–80 (2003).

124. C. Wiese *et al.*, Formation of the sinus node head and differentiation of sinus node myocardium are independently regulated by Tbx18 and Tbx3., *Circulation research* **104**, 388–97 (2009).

125. W. Shi *et al.*, Distribution and Prevalence of Hyperpolarization-Activated Cation Channel (HCN) mRNA Expression in Cardiac Tissues, *Circulation Research* **85**, e1–e6 (1999).

126. G. Krapivinsky *et al.*, The G-protein-gated atrial K+ channel IKACh is a heteromultimer of two inwardly rectifying K(+)-channel proteins., *Nature* **374**, 135–41 (1995).

127. J. M. B. Anumonwo, A. N. Lopatin, Cardiac strong inward rectifier potassium channels., *Journal of molecular and cellular cardiology* **48**, 45–54 (2010).

128. S. L. Paige *et al.*, Endogenous Wnt/beta-catenin signaling is required for cardiac differentiation in human embryonic stem cells., *PloS one* **5**, e11134 (2010).

129. J. C. Moore *et al.*, Distinct cardiogenic preferences of two human embryonic stem cell (hESC) lines are imprinted in their proteomes in the pluripotent state., *Biochemical and biophysical research communications* **372**, 553–8 (2008).

130. S. D. Lundy, W.-Z. Zhu, M. Regnier, M. A. Laflamme, Structural and Functional Maturation of Cardiomyocytes Derived from Human Pluripotent Stem Cells., *Stem cells and development* **22** (2013), doi:10.1089/scd.2012.0490.

131. S. C. Barry *et al.*, Lentivirus vectors encoding both central polypurine tract and posttranscriptional regulatory element provide enhanced transduction and transgene expression., *Human gene therapy* **12**, 1103–8 (2001).

132. S. Li *et al.*, Stable transduction of myogenic cells with lentiviral vectors expressing a minidystrophin., *Gene therapy* **12**, 1099–108 (2005).

133. E. Drouin, F. Charpentier, C. Gauthier, K. Laurent, H. Le Marec, Electrophysiologic characteristics of cells spanning the left ventricular wall of human heart: evidence for presence of M cells., *Journal of the American College of Cardiology* **26**, 185–92 (1995).

134. R. Morin *et al.*, Profiling the HeLa S3 transcriptome using randomly primed cDNA and massively parallel short-read sequencing., *BioTechniques* **45**, 81–94 (2008).

135. D. Weisbrod *et al.*, SK4 Ca2+ activated K+ channel is a critical player in cardiac pacemaker derived from human embryonic stem cells., *Proceedings of the National Academy of Sciences of the United States of America* (2013), doi:10.1073/pnas.1221022110.

136. Y. Shiba *et al.*, Human ES-cell-derived cardiomyocytes electrically couple and suppress arrhythmias in injured hearts., *Nature* **489**, 322–5 (2012).

Vita

Jay Gantz was born and raised as a Hawkeye Fan in Iowa City, Iowa. Jay graduated as Valedictorian from Iowa City West High School in 2002.

In 2006, Jay graduated as a member of the first class from the Franklin W. Olin College of Engineering with a Bachelor of Science in Engineering with a concentration in Bioengineering. During his undergraduate years, Jay pursued engineering research in both academic and corporate settings. Jay spent the summer after his freshman year as a research intern at a medical device company where he had daily contact with patients. Jay grew to love his interaction with patients and started to seriously consider a career integrating engineering and medicine.

Jay accepted a Fulbright Scholarship in 2006 and spent the year after his undergraduate studies at the Swiss Federal Institute of Technology in Lausanne, Switzerland. Jay worked with Professor Jeff Hubbell to deliver healing compounds to injured cardiac blood vessels using polymeric microparticles. This work piqued Jay's interest in the regenerative potential of the cardiac system.

In 2007, Jay decided Seattle was the next best place to Switzerland and he moved to Seattle to join the Medical Scientist Training Program at the University of Washington. Outside of his studies, Jay continued his long-standing passions for playing the cello, woodworking and exploring mountains by ski and by foot.

Jay earned a Doctor of Philosophy from the University of Washington's Department of Bioengineering in 2013. He completed his dissertation work in the laboratory of Dr. Michael A. Laflamme where he studied the pacemaking potential of subpopulations of cardiomyocytes derived from human embryonic stem cells. Jay plans to pursue a career in academic medicine with the scientific goal of regenerating damaged tissues with cell-based therapies.